NASA Contractor Report 178030

NASA-CR-178030
19860015864

Guidance Studies for Curved, Descending Approaches Using the Microwave Landing System (MLS)

J. B. Feather

McDonnell Douglas Corporation
Douglas Aircraft Company
Long Beach, California 90846

Contract NAS1-16202
May 1986

National Aeronautics and
Space Administration

Langley Research Center
Hampton, Virginia 23665

TABLE OF CONTENTS

TABLE OF CONTENTS (Continued)

LIST OF FIGURES

LIST OF FIGURES (Continued)

LIST OF FIGURES (Continued)

LIST OF TABLES

Page

LIST OF SYMBOLS

A	Angle defining the arc length of the turn, rad.
C_1, C_2, C_3	Difference equation coefficients for the vertical complementary filter, ND
D_{TG}	Distance to go to origin, Measured in ground plane, ft.
d	Distance from AZ/DME transmitter to coordinate origin, ft.
$G_h, G_{\dot{h}}$	Vertical guidance gains on altitude error and error rate, respectively, deg/ft, deg/fps
G_{hI}	Vertical guidance gain on integral term, deg/ft. sec
g	Gravity constant, ft/sec^2
h	Altitude, ft.
Δh	Altitude deviation from desired value, ft.
$\Delta\hat{h}$	Computed vertical tracking error signal, ft.
$\hat{\dot{h}}$	Computed vertical tracking error rate signal, ft./sec.
$\hat{\ddot{h}}$	Vertical acceleration, ft./sec.^{2}
$\dot{h}_F$	Filtered altitude rate, ft./sec.
h_G	Altitude at which glide slope is to change, ft.
h_m	Altitude derived from MLS angles and range signals, ft.
ℓ	Length from MLS antenna to aircraft CG, ft.
R	Radius of circular turn, ft.
R_{DME}	Range from DME-P antenna to aircraft., ft.
S_1, S_2	Linear steering signal commands for lateral guidance, deg.
S_I	Signal used in vertical guidance to determine time to pitch over to first glide slope, deg.
S_{L1}	Signal used to determine switch time to second glide slope during first lateral segment, deg.
S_{L2}	Signal used to determine switch time to second glide slope during second lateral segment, deg.
S_x, S_y, S_z	Wind magnitude at 33 ft. altitude in earth coordinates, KT
T_A	Turn anticipation time, sec

LIST OF SYMBOLS

ΔT	Digital computer simulation integration interval, sec.
u_g, v_g, w_g	Turbulence levels along x-y-z axes, KT
V_G	Ground speed, ft./sec.
V_{Gx}	X-axis component of ground speed, ft./sec.
W	Wind factor as a function of altitude, ND
W_X, W_Y, W_Z	Wind magnitudes at altitude h in earth coordinates, KT
W_{TX}, W_{TY}, W_{TZ}	Total winds (including turbulence), KT
x_2, y_2	Coordinates of the point at which the turn begins, ft.
x_A, Y_A	Coordinates at which turn anticipation starts, ft.
x_C, y_C	Coordinates of the center of the turn circle, ft.
X_F	Coordinate of final approach fix point, ft.
x_m, y_m, z_m	Aircraft CG position coordinate, ft.
x'_m, y'_m, z'_m	Aircraft MLS antenna coordinates derived from MLS angles and range signals, ft.
x', y'	Coordinates of entry point to MLS coverage, ft.
Δy	Computed lateral tracking error signal during linear segments, ft.
$\Delta \dot{y}$	Computed lateral track error rate during circular segment, ft./sec.
Δz_1	Component of computed vertical tracking error rate derived from vertical acceleration, ft./sec.
Δz_2	Component of computed vertical tracking error rate derived from vertical tracking error, ft./sec.
γ	Vertical flight path angle, deg.
Δ	Distance between segmented glide slope ground intercepts, ft.
$\Delta\psi$	Course angle error, deg.
ε_{EL}	Glide slope angular error, deg.
ε_R	Lateral tracking error during turn, ft.
$\dot{\varepsilon}_R$	Lateral tracking error rate during turn, ft./sec.
$\varepsilon_x, \varepsilon_y$	Lateral tracking errors during linear segments, ft.

LIST OF SYMBOLS

$\dot{\varepsilon}_x, \dot{\varepsilon}_y$	Lateral tracking error rates during linear segments, ft./sec.
θ	Aircraft pitch angle, deg.
θ_{1C}, θ_{2C}	Components of pitch predict angle, deg.
θ_{AZ}	MLS azimuth angle, deg.
θ_{CI}	Integral component of pitch steering command, deg.
θ_{EC}	Glide slope command angle, deg.
θ_{ED}	First desired glide slope angle, deg.
θ_{EF}	Second desired glide slope angle, deg.
θ_{EL}	Computed glide slope angle, deg.
θ_P	Pitch predict angle, deg.
θ_{STR}	Pitch steering command, deg.
τ	Time constant, sec.
ϕ	Bank angle, deg.
ϕ_{STR}	Bank steering command, deg.
ϕ_{LIM}	Autopilot command rate limit, deg./sec.
ψ_D	Desired course angle, deg.
ψ_G	Ground track angle, deg.
ψ_R	Reference course angle, deg.

SUMMARY AND INTRODUCTION

Results of the MLS guidance studies presented in this report are discussed using the following topic format:

- o Basic MLS Operation
- o Approach Path Definition
- o Guidance Algorithm Development
- o Simulation Results

A brief discussion of MLS operations is given with a comparison to the existing Instrument Landing System (ILS). Added capability using an MLS for terminal area guidance are highlighted, and transformation of angle/range data to aircraft position coordinates are discussed.

Each of the approach paths simulated in the study are defined mathematically. These definitions are used in developing the guidance algorithms that provide steering signals to the autopilot. The lateral guidance algorithm developed here is similar to the one in Reference 1, but with specific modifications to accommodate the MD-80 autopilot. Also, only signals available in the MD-80 hardware were considered for computational purposes. This consideration required developing complementary filters to derive the necessary signals. The vertical guidance algorithm is a linear law using vertical position and rate. Complementary filters are required here also to provide the desired steering signals.

Simulation results for 10 different cases are presented in the form of computer-generated plots, including tracking errors, bank and pitch angles, and acceleration levels. Three basic types of approach paths were simulated:

- o 180° Turn with a Single Glide Slope
- o 180° Turn with a Segmented Glide Slope
- o Laterally Segmented Turn with a Single Glide Slope

From these three types of paths, 10 cases were considered that included MLS noise, winds and turbulence, a light-weight case, and speed change during descent. Comparison of tracking accuracy are made between these cases to assess the guidance system performance.

Although the simulation uses the MD-80 as the aircraft, the basic algorithm could be modified easily to accommodate other aircraft. Guidance gain adjustments and possible filter modifications would probably be the only required changes. The MD-80 was selected because of the proposed flight demonstration at Burbank to collect data on MLS approaches.

CONCLUSIONS AND RECOMMENDATIONS

Initial development of vertical and lateral guidance algorithms for MLS operations has been started using a batch MD-80 simulation program. These algorithms provide steering signals to the roll and pitch autopilot to guide the aircraft along desired approach paths. Reasonable tracking errors and acceleration levels result in all cases. Results for one particular approach which could be used at Burbank in a flight demonstration program indicate adequate tracking and acceptable performance.

A good deal more effort is required, however, to fully define guidance systems capable of operating real time in a flight test environment. Of particular importance is a fixed-base simulator evaluation with actual hardware in the loop. Tests using the simulator will help identify any interface problems when the guidance algorithms are integrated with the autopilot and performance management system. Specifically, the following tasks are recommended as candidates for future efforts:

- Refine the complementary filters to operate more effectively with turbulence.
- Include the lateral and vertical guidance algorithms in the fixed-base simulator and perform system evaluations.
- Define the interface requirements between the MLS guidance computer and existing airborne equipment.
- Revise the algorithms as necessary as a result of the above evaluations.
- Expand the study efforts to include equipment vendors that would be affected as the result of an MD-80 flight test program at Burbank.

BASIC MLS OPERATION

OVERVIEW

Microwave landing systems will allow more flexible and efficient procedures to be used in the terminal area than now possible with ILS installations. This improvement is due to the availability of accurate angle and range information to airborne computers for precision approaches. An MLS, operating at frequencies an order of magnitude higher than present ILS frequencies, can develop narrow, scanned beams covering a large volume. Coverage up to 15° in elevation and $\pm$ 60° in azimuth is possible out to 20 nm from the runway. While in this volume, aircraft can execute almost limitless approach paths that include obstacle avoidance, noise abatement, increased approach and departure traffic, and arrival time control.

TERMINAL AREA GUIDANCE

Several examples of the increased terminal area guidance possibilities using MLS are shown in the sketch of Figure 1. The ILS, characterized by its narrow beam, can provide approach guidance signals only over a relatively small volume as compared to the MLS. As depicted in the figure, both commercial transports as well as general aviation can use the MLS capability for a variety of different approaches and departures. Ground based transmitting equipment that provides this capability typically would consist of approach elevation, approach azimuth, back azimuth, and precision distance measuring equipment (DME-P).

Airborne equipment is comprised of an MLS angle receiver, MLS antennas, a precision DME interrogator, a guidance computer and appropriate controls and display. Software for the computer would be developed to derive guidance signals from the MLS angle and range data. These steering signals define an outer loop to the autopilot, which would send commands to the appropriate surfaces to complete the closed loop guidance system.

MLS GEOMETRY

Angle and range information, as output from the MLS receiver, is used by the guidance computer to calculate the present position of the aircraft. This position information is, in turn, used to compute the desired approach paths and establishes a reference for the guidance algorithms. The geometry used in the present study is shown in simplified form in Figure 2. Location of the elevation transmitter (EL) and the azimuth/distance measuring equipment (AZ/DME) are shown relative to the runway and the earth-fixed coordinate system.

The assumed geometry of Figure 2 leads to the following equations that define the rectangular coordinates (x'_m, y'_m, z'_m) of the aircraft given the MLS elevation and azimuth angles, and the DME range:

$$y'_m = -R_{DME} \sin \theta_{AZ} \tag{1}$$

$$x'_m = d \cos^2 \theta_{EL} - \left[\cos^2 \theta_{EL}(R^2_{DME} - d^2 \sin^2 \theta_{EL}) - y^2_m\right]^{\frac{1}{2}} \tag{2}$$

$$z'_m = -\left[x'^2_m + y'^2_m\right]^{\frac{1}{2}} \tan \theta_{EL} \tag{3}$$

The term d used above is the distance from the coordinate origin to the AZ/DME position (assumed to be 10,000 feet for this study). It is customary to use a positive value for altitude, so the variable h_m, defined as $h_m = -z'_m$, is used in subsequent equations in this report.

APPROACH PATH DEFINITIONS

For purposes of the present study contract, three final approach paths were chosen for guidance algorithm development and aircraft performance evaluation. These paths are a single glide slope trombone approach (180° turn to final), a segmented glide slope trombone approach, and a single glide slope laterally segmented approach specifically for the Burbank airport.

TROMBONE APPROACHES (180° TURN)

The desired ground track for the trombone approaches is shown in the sketch of Figure 3. The following assumptions for theses cases were made to fully define the lateral approach parameters:

- A constant turn rate of 1.5 deg/sec was selected
- Landing speed was set at 140 KT
- The final approach fix point was selected to correspond to an 800 ft altitude on a 3 deg glide slope
- A 40 deg azimuth coverage was selected

The resulting turn radius, nominal bank angle, final approach fix point, and MLS entry point for the above assumptions are given in the table below:

TROMBONE APPROACH PARAMETERS

$R = 9123.$ Ft.
$\emptyset_N = 10.8$ Deg.
$X_F = -15265.$ Ft.
$X' = -11737.$ Ft.

SINGLE GLIDESLOPE

Pitch over from level flight to a 3° glide slope during the 180° turn characterizes this trombone approach. Figure 4 represents the geometry for this particular case. As depicted in the figure, the initial point is outside the MLS coverage volume. Before entry into the MLS region, the pitch autopilot is in altitude hold and the roll autopilot is in heading hold mode. (The autothrottle remains in the IAS mode throughout the entire final approach). Upon entry, the autopilot is switched to the MLS vertical and lateral modes, where the signals generated by the appropriate guidance algorithms are used as outer loop commands.

A turn anticipation was found to be necessary in order to reduce tracking errors during the turn. The time to start the turn anticipation is computed using the nominal bank angle magnitude and the roll autopilot command rate limit.

Logic in the vertical guidance computer determines when pitchover is to occur. In this case, the aircraft has begun the turn when pitch over to a 3 degree glide slope begins. The turn-to-final logic is used to anticipate when the wings-level command is to be initiated. This logic allows a smooth transition in the command signal to the final straight-in portion of the approach.

SEGMENTED GLIDE SLOPE

For this case, pitch over to a steeper glide slope (4.5 degrees) occurs during the straight downwind portion of the approach, and a pitch up to a 3 degree glide slope occurs during the turn. Figure 5 depicts the events for this segmented glide slope case. Laterally, the desired ground track is the same as the previously described case.

SPEED CHANGE

The aircraft initial position is the same as shown in Figure 4, but the speed is 165 KT and the flaps are at 15 degrees. A programmed speed reduction to 140 KT occurs just after initiation to pitch over to 3 degrees. This program consists simply of a step flap setting command from 15 to 40 degrees at the same time the speed command is changed from 165 to 140 KT. The autothrottle in IAS mode commands the thrust change to execute this speed change.

LATERALLY SEGMENTED APPROACH (BURBANK)

A laterally-segmented approach is one containing two or more straight segments with undefined transitions. For purposes of system evaluation, the approach defined in Figure 6 was simulated and represents one possible approach for runway 15 at Burbank. The curved path between the two straight segments was computed in this study as a circular arc whose radius varies as needed for a pre-selected bank angle at the current ground speed. A nominal bank angle of 20 degrees and a speed of 140 KT results in the radius of 4772 ft. (.78 nm) as shown in the figure. The point x_F was fixed at 3.6 nm. Vertically, the aircraft is assumed to be on a constant 3.8 degree glide slope during the approach.

GUIDANCE ALGORITHM DEVELOPMENT

MLS/MD-80 AUTOPILOT INTERFACE CONSIDERATIONS

It was decided at the beginning of this study that the MLS guidance algorithms would be developed to be compatible with the existing MD-80 roll and pitch inner loops. No changes to the MD-80 autopilot would be made except to include a switch to allow either the MLS pitch and roll commands or the signals from the existing autopilot outer loop computations. This decision minimizes the modifications that must be made to existing hardware and software to implement the MLS guidance modes.

Figure 7 is a simplified block diagram showing the basic switching from existing modes of operation to the new MLS modes. Included in the MLS guidance computer are filters and other transformations that use only measurable quantities available from existing sources on the MD-80. Complementary filters that derive rate signals are used both in the roll and pitch computations. This technique allows use of available signals and also affords filtering of noisy signals.

LATERAL GUIDANCE EQUATIONS

There are three basic segments of operation for the lateral guidance system. Each approach path simulated for this study fits into one of these operational modes. The first lateral segment is a linear path displaced from the runway centerline. The second segment is a turn from this first path to the third segment, which is a linear path along the runway centerline. Logic in the computer program selects the appropriate coding for the particular approach path being simulated.

The following equations describe the lateral guidance algorithm that has been simulated using the MD-80 simulation program. Each block of equations is identified as to its function, and key equations are referenced in the lateral flow diagram of Figure 8.

LATERAL COMPLEMENTARY FILTERS

Lateral position coordinates from the MLS geometry, Equations (1) & (2), are processed using complementary filters. The outputs are estimates of both the position ($\hat{X}'_m$, $\hat{Y}'_m$) and rate variables ($\hat{\dot{X}}'_m$, $\hat{\dot{Y}}'_m$). These outputs are used in the lateral and vertical algorithms to generate steering commands.

$$\varepsilon_x = x'_m - \hat{x}'_m \qquad |\varepsilon_x| \leq 500 \text{ ft} \tag{4}$$

$$\varepsilon_y = y'_m - \hat{y}'_m \qquad |\varepsilon_y| \leq 500 \text{ ft} \tag{5}$$

$$\varepsilon_{\dot{x}} = \frac{1}{\Delta T}\left[x'_m - x'_{m-}\right] - \hat{\dot{x}}_{m-} \tag{6}$$

$$\varepsilon_{\dot{y}} = \frac{1}{\Delta T}\left[y'_m - y'_{m-}\right] - \hat{\dot{y}}_{m-} \tag{7}$$

$$\hat{x}'_m = \hat{x}'_{m-} + \Delta T\left[0.654\varepsilon_x + \hat{\dot{x}}'_{m-}\right] \tag{8}$$

$$\hat{y}'_m = \hat{y}'_{m-} + \Delta T\left[0.654\varepsilon_y + \hat{\dot{y}}'_{m-}\right] \tag{9}$$

$$\hat{\dot{x}}'_m = \hat{\dot{x}}'_{m-} + \Delta T\left[0.129\varepsilon_x + 0.125\varepsilon_{\dot{x}} + \ddot{x}\right] \tag{10}$$

$$\hat{\dot{y}}'_m = \hat{\dot{y}}'_{m-} + \Delta T\left[0.129\varepsilon_y + 0.125\varepsilon_{\dot{y}} + \ddot{y}\right] \tag{11}$$

In the above equations, the minus subscript denotes the first past value of the variable.

The ground track angle, $\hat{\psi}_G$, is computed from the rate estimates. The position estimates are corrected for the MLS antenna being displaced ℓ feet from the aircraft CG:

$$\hat{\psi}_G = \tan^{-1}(\hat{\dot{y}}_m/\hat{\dot{x}}_m) \qquad 0 < \hat{\psi}_G \leq 360^o \tag{12}$$

$$\hat{x}_m = \hat{x}'_m - \ell \cos \hat{\psi}_G \tag{13}$$

$$\hat{y}_m = \hat{y}'_m - \ell \sin \hat{\psi}_G \tag{14}$$

Linear steering command signals, S_1 and S_2, are generated for the first and third lateral segments. The desired course angle, ψ_D, is a constant for each segment and is an input to the guidance algorithm.

$$\Delta y = (\hat{y}_m - y_2) \cos \psi_D - (\hat{x}_m - x_2) \sin \psi_D \tag{15}$$

$$\Delta\psi = \hat{\psi}_G - \psi_D \tag{16}$$

$$\hat{V}_G = \left[\hat{\dot{x}}_m^2 + \hat{\dot{y}}_m^2\right]^{\frac{1}{2}} \tag{17}$$

$$\Delta\dot{y} = \hat{V}_G \sin \Delta\psi \tag{18}$$

$$S_1 = 0.0275(\Delta y + 18.18\Delta\dot{y}) \tag{19}$$

$$S_2 = 0.0275(\hat{y}_m + 18.18\hat{\dot{y}}_m) \tag{20}$$

Guidance gains appearing in Equations (19) & (20) were selected in a tradeoff study involving adequate system stability and tracking accuracy. The values shown give reasonable responses during the linear segments of the lateral approach paths.

FIRST LATERAL SEGMENT

During the first segment, the roll steering command, ϕ_{STR}, is set equal to the negative of the steering signal S_1:

$$\phi_{STR} = -S_1 \tag{21}$$

TURN ANTICIPATION

As noted briefly in an earlier section, a turn anticipation was employed to help reduce the tracking errors during the turn. This anticipation takes the form of computing a distance based on a turn anticipation time (T_A) and the x component of the ground speed. The point x_A in Figure 3 is calculated from

$$x_A = x_2 - T_A V_{Gx}$$

where T_A is an input parameter and V_{Gx} is the computed ground speed component. The roll autopilot command rate limit, $\dot{\phi}_{LIM}$, is used to compute the steering command ramp signal that is used between the first and second lateral segments:

$$\phi_{STR} = \dot{\phi}_{LIM}\, t, \qquad 0 \leq t \leq T_A \tag{22}$$

A limit is placed on ϕ_{STR} so that it does not exceed the nominal bank angle (ϕ_N) for the speed and turn radius being used. Switching to the turn anticipation occurs when the point x_A is reached. Switching to the second lateral segment occurs when the point x_2 is reached.

SECOND LATERAL SEGMENT

A steering command is generated which is composed of a calculated bank angle plus two errors signals. The bank angle component is a function of calculated ground speed and desired turn radius. The error components are the radial position and rate error signals that allow proper tracking of the desired ground paths.

For the circular turn, the position error, ε_R, is calculated using the equation

$$\varepsilon_R = R - \left[(\hat{x}_m - x_c)^2 + (\hat{y}_m - y_c)^2 \right]^{\frac{1}{2}} \tag{23}$$

The reference course angle, ψ_R, is defined during the turn and is used to generate the rate error signal $\dot{\varepsilon}_R$:

$$\psi_R = 180. + \tan^{-1} \frac{x_c - \hat{x}_m}{\hat{y}_m - y_c} \tag{24}$$

$$\dot{\varepsilon}_R = \hat{V}_G \sin(\psi_G - \psi_R) \tag{25}$$

Finally, the roll steering angle during the turn is computed from

$$\phi_{STR} = \tan^{-1} \frac{\hat{V}_G^2}{gR} - 0.01\varepsilon_R - 0.1\dot{\varepsilon}_R \tag{26}$$

Switching to the third segment occurs when the lateral coordinate, $\hat{y}_m$, is less than a fixed value

$$|\hat{y}_m| \leq 100 \text{ FT}$$

and when the steering signal, S_2, is less than ϕ_{STR} as computed from Equation (26):

$$|S_2| \leq |\phi_{STR}| \tag{27}$$

THIRD LATERAL SEGMENT

Similar to the first segment equations, the roll steering command is set to the negative of the second linear command signal:

$$\phi_{STR} = -S_2 \tag{28}$$

VERTICAL GUIDANCE EQUATIONS

Vertical guidance as defined in this study consisted of glide slope changes during both straight-in approaches as well as during turns. Because of this guidance philosophy, the vertical algorithm must have knowledge of which lateral segment is being tracked. The linear guidance law requires a distance to go to touch down, and this distance is a function of the lateral path being flown. Equations and logic required to track a desired vertical path are therefore more complicated than the lateral guidance algorithm.

Figure 9 is a block diagram of the vertical guidance law showing how the various signals are summed to form the vertical steering signal, θ_{STR}. This signal is input to the MD-80 pitch autopilot to command the desired vertical flight path.

The following sections describe the equations and logic required to generate θ_{STR}. The vertical flow diagram of Figure 10 references these equations in the various branches of the program flow.

VERTICAL COMPLEMENTARY FILTER

Generation of the vertical rate error, $\Delta\hat{\dot{h}}$, is implemented in a complementary filter whose inputs are vertical acceleration and vertical position error (Figure 9). The acceleration is generated by differentiating the rate signal (which exists in the MD-80 autopilot). The position error comes from the vertical guidance algorithm and is a function of the vertical angular tracking error, ε_{EL}. Digital implementation of this filter is described in the following equations.

$$\hat{\ddot{h}} = -\left[\dot{h}_F - \dot{h}_{F-}\right]/\Delta T \tag{29}$$

$$\Delta z_1 = C_1\,\Delta z_{1-} + C_3\,\hat{\ddot{h}} \tag{30}$$

$$\Delta z_2 = C_1\,\Delta z_{2-} + C_2\left[\Delta\hat{h} - \Delta\hat{h}_-\right] \tag{31}$$

$$\Delta\hat{\dot{h}} = \Delta z_1 + \Delta z_2 \tag{32}$$

$$C_1 = e^{-\Delta T/\tau} \qquad (\tau = 4.0 \text{ sec})$$

$$C_2 = \tau\left(1 - e^{-\Delta T/\tau}\right)$$

$$C_3 = \left(1 - e^{-\Delta T/\tau}\right)/\Delta T$$

$$\gamma = -\tan^{-1}\frac{\dot{h}_F}{\hat{V}_G} \tag{33}$$

The ground track distance to go, D_{TG}, is calculated for the first lateral segment from

$$D_{TG} = -x_F + R \cdot A - \Delta + \left[(x_2 - \hat{x}_m)^2 + (y_2 - \hat{y}_m)^2\right]^{\frac{1}{2}} \tag{34}$$

and for the second lateral segment from the expression

$$D_{TG} = -x_F + R\left[\pi - \tan^{-1}\frac{x_c - \hat{x}_m}{\hat{y}_m - y_c}\right] \tag{35}$$

For curved path finals, the angle A used above is computed from

$$A = \pi \text{ rad} \tag{36}$$

and for laterally segmented final, A is given by

$$A = \pi - \tan^{-1} \frac{x_c - x_2}{y_2 - y_c} \text{ rad} \tag{37}$$

The term Δ is the difference in distance to go for segmented glide slope finals. It is computed from

$$\Delta = h_G \left(\frac{1}{\tan \theta_{EF}} - \frac{1}{\tan \theta_{ED}} \right) \tag{38}$$

where h_G is the altitude at which the glide slope changes value, θ_{ED} is the first glide slope angle, and θ_{EF} is the second glide slope angle.

GLIDE SLOPE SWITCHING LOGIC

The following parameters are used in switching to the first glide slope:

$$\varepsilon_{EL} = \theta_{ED} - \tan^{-1} \frac{h_m}{D_{TG}} \tag{39}$$

$$\Delta\hat{h} = D_{TG}\, \varepsilon_{EL}/57.3 \tag{40}$$

Δz_1, Δz_2, $\Delta\hat{\dot{h}}$ from Eqn. (30)-(32)

$$S_I = G_h\, \Delta\hat{h} + G_{\dot{h}}\, \Delta\hat{\dot{h}} \tag{41}$$

Switching to the first glide slope occurs when S_I changes sign.

FIRST LATERAL SEGMENT

If the present path is on the first glide slope, then the following parameters are used to establish the time to switch to the second glide slope:

$$\varepsilon_{EL} = \theta_{EF} - \tan^{-1} \frac{h_m}{D_{TG} + \Delta} \tag{42}$$

$$\Delta\hat{h} = D_{TG} \cdot \varepsilon_{EL}/57.3 \tag{43}$$

$$\Delta z_1,\ \Delta z_2,\ \Delta\hat{\dot{h}} \text{ from Eqn. (30)-(32)} \tag{44}$$

$$S_{L1} = G_h\, \Delta\hat{h} + G_{\dot{h}}\, \Delta\hat{\dot{h}} \tag{45}$$

Switching to the second glide slope occurs when S_{L1} changes sign.

For the first glide slope, the distance to go and the pitch steering command components are computed from

$$D_{TG} = -x_F + R \cdot A - \Delta + \left[(x_2 - \hat{x}_m)^2 + (y_2 - \hat{y}_m)^2\right]^{\frac{1}{2}} \tag{46}$$

$$\theta_{1C} = \gamma - \theta_{ED} \tag{47}$$

$$\theta_{EC} = \theta_{ED} \tag{48}$$

and for the second glide slope they are

$$D_{TG} = -x_F + R \cdot A + \left[(x_2 - \hat{x}_m)^2 + (y_2 - \hat{y}_m)^2\right]^{\frac{1}{2}} \tag{49}$$

$$\theta_{1C} = \gamma - \theta_{EF} \tag{50}$$

$$\theta_{EC} = \theta_{EF} \tag{51}$$

Switching to the second lateral segment for curved path approaches occurs when

$$\hat{x}_m < x_2 \tag{52}$$

and switching for laterally-segmented approaches occurs when

$$\hat{x}_m > x_2 \tag{53}$$

SECOND LATERAL SEGMENT

For first glide slope tracking, the following quantities are computed to establish switching to the second glide slope:

$$\varepsilon_{EL} = \theta_{EF} - \tan^{-1} \frac{h_m}{D_{TG}} \tag{54}$$

$$\Delta\hat{h} = D_{TG} \cdot \varepsilon_{EL}/57.3 \tag{55}$$

Δz_1, Δz_2, $\Delta\hat{\dot{h}}$ from Eqn. (30)-(32)

$$S_{L2} = G_h \Delta\hat{h} + G_{\dot{h}} \Delta\hat{\dot{h}} \tag{56}$$

Switching occurs to the second glide slope when S_{L2} changes sign.

For the first glide slope, D_{TG} and the steering components are computed from

$$D_{TG} = -x_F + R \left[\pi - \tan^{-1} \frac{x_c - \hat{x}_m}{\hat{y}_m - y_c} \right] - \Delta \tag{57}$$

$$\theta_{EC} = \theta_{ED} \tag{58}$$

and for the second glide slope they are

$$D_{TG} = - x_F + R \left[\pi - \tan^{-1} \frac{x_c - \hat{x}_m}{\hat{y}_m - y_c} \right] \tag{59}$$

$$\theta_{2C} = \gamma - \theta_{EF} \tag{60}$$

$$\theta_{EC} = \theta_{EF} \tag{61}$$

Switching to the third lateral segment occurs when

$$\hat{x}_m > x_F \tag{62}$$

THIRD LATERAL SEGMENT

The distance to go for the third lateral segment is simply

$$D_{TG} = -\hat{x}_m \tag{63}$$

PITCH STEERING COMMAND

Four components comprise the steering command (θ_{STR}) that is input to the pitch autopilot. Two terms are composed of the altitude error, $\Delta\hat{h}$, and the altitude rate error, $\Delta\hat{\dot{h}}$. In addition, an integral term, θ_{CI}, on the error signal is included. A pitch predict term, θ_P, is used to increase the speed of response when abrupt pitch changes are commanded (as in initial pitch over from level flight).

Equations that represent the pitch guidance law implementation for simulation purposes are given in the following expressions:

$$\theta_{EL} = \tan^{-1} \frac{h_m}{D_{TG}} \tag{64}$$

$$\varepsilon_{EL} = \theta_{EC} - \theta_{EL} \tag{65}$$

$$\Delta\hat{h} = D_{TG}\, \varepsilon_{EL}/57.3 \tag{66}$$

Δz_1, Δz_2, $\Delta\hat{\dot{h}}$ from Eqn. (30)-(32)

$$\theta_{CI} = \theta_{CI-} + G_{hI}\, \Delta\hat{h}\, \Delta T \tag{67}$$

$$\theta_P = \theta_{1C} + \theta_{2C} \tag{68}$$

$$\theta_{STR} = \theta_{CI} + \theta_P + G_h\, \Delta\hat{h} + G_{\dot{h}}\, \Delta\hat{\dot{h}} \tag{69}$$

Guidance gains for the pitch steering command are numerically defined in Figure 9.

SPEED CONTROL

Programmed speed and flap changes have been simulated for the trombone approaches. The guidance algorithm for speed control is simply a step flap change to the flap servo, and a step speed change to the autothrottle. All existing logic and limits in the MD-80 associated with speed changes remain unaltered. The result is a flap change to the desired setting at the max rate and a speed change to the target speed within autothrottle limits.

Logic to initiate the speed change is controlled by the pitch over logic. Speed switching used the variable S_I of Equation (41) with a 5 second time delay. This delay allows initial pitch-over transients to settle before the speed begins to decrease. The case selected to evaluate performance during varying speed conditions was the trombone approach where pitch over to 3° occurs during the 180° turn.

SIMULATION DESCRIPTION

MD-80 SIMULATION

The MD-80 nonlinear simulation, a batch program with large flight envelope equations of motion, was used to evaluate performance of various MLS approaches. Guidance algorithms were coded into the appropriate routines with no changes to the roll and pitch autopilot or the autothrottle. Basically, the diagram of Figure 7 describes the system, where outer loop closures are simulated using the aircraft dynamics and aerodynamics.

MLS NOISE MODELS

Angle and range signals as output from the MLS receiver will contain noise in practice. For simulation purposes, additive noise has been included in the azimuth, elevation, and DME range variables, θ_{AZ}, θ_{EL}, and R_{DME}, respectively. The variables, as used in Equation (1) - (3), were modified to include this additive noise:

$$\theta_{AZ} = \theta_{AZ(TRUE)} + \theta_{AZ(NOISE)}$$

$$\theta_{EL} = \theta_{EL(TRUE)} + \theta_{EL(NOISE)} \qquad (70)$$

$$R_{DME} = R_{DME(TRUE)} + R_{DME(NOISE)}$$

Each noise component above was simulated using the model shown in Figure 11. Gains and frequencies for the International Civil Aviation Organization (ICAO) spec values were based on ICAO-defined control motion noise and path following error levels.

The ICAO-specified noise levels, if actually present in the MLS signals,

would result in unacceptable aircraft activity when coupled to flight control systems capable of accurate path control. Flight measurements indicate that the noise is somewhat less. A similar discrepancy is observed for ILS between ICAO-specified values and the noise actually experienced. Consequently, assumed levels of reduced value were simulated as well. These reduced levels were based on actual flight test data performed in France in 1983 (Reference 2). Results of these tests were used to define the gains and frequencies shown in the figure. Azimuth and elevation levels are significantly lower than the ICAO values, whereas the DME level remained unchanged.

During the course of the present study, baseline cases were run with the ICAO and the reduced noise levels for comparison. All other cases contained the reduced noise only. For certification purposes, the ICAO values must be used. However, it was felt that noise models, based on actual flight test data, would yield results representing levels encountered in actual practice.

WINDS AND TURBULENCE

Included in the simulation are options for winds, whose magnitudes are a function of altitude, and for turbulence as additive terms to the winds. The factor that is a function of altitude is denoted W and is defined by

$$W = 0.43 \log h + 0.35 \tag{71}$$

where h is the altitude in feet. Input values for S_x, S_y, and S_z (the wind values, earth axes, in knots) when the airplane is on the ground are used to compute the three wind components at altitude:

$$\begin{aligned} W_x &= W\, S_x \\ W_y &= W\, S_y \\ W_z &= W\, S_z \end{aligned} \tag{72}$$

Turbulence is a random variable that may be added to the above winds. White noise is passed through a first order filter whose parameters are functions of the wind components as shown in Figure 13. Outputs of the filter are denoted U_g, V_g, and W_g and are used to form the total simulated winds:

$$W_{Tx} = W_x + U_g$$

$$W_{Ty} = W_y + V_g$$

$$W_{Tz} = W_z + W_g$$

Aircraft performance characteristics limit wind components at touchdown to maximum values of 25 knot headwinds, 10 knot tailwinds, and 15 knot crosswinds.

TROMBONE FINALS

Results for the trombone final approaches are presented for several different cases. Table 1 shows the parameters for the trombone finals (Cases 1-9), and also for the laterally segmented final (Case 10). The baseline case consists of pitchover to a 3 degree glide slope during the turn at constant speed and with no MLS noise or winds. Performance results for this case show the basic aircraft responses to the steering commands. Comparison to cases with noise and winds shows the effects of these disturbances.

Cases 2 and 3 provide comparison of the ICAO noise and reduced MLS noise levels. All following cases have the reduced noise levels. Cases 4-6 are with winds and turbulence. Case 7 is the trombone approach but with a minimum landing weight (90000 lb.) and lower speed. Case 8 contains a speed change from 165 to 140 KT during the turn and pitch over to the 3 degree glide slope. Case 9 is the segmented glide slope trombone approach, and Case 10 is the laterally segmented approach at a constant 3.8 degree glide slope.

SINGLE GLIDE SLOPE CASES

Case 1.

Bank angle and lateral tracking error responses are shown in Figure 13 for Case 1 (Baseline). The intervals at which the three lateral segments occur are noted on the bank angle figure. Segments 1 and 3 represent the linear track mode, and segment 2 is the circular turn. The distances to go are noted on the lateral tracking error plot that correspond to these lateral segments. Turn anticipation occurs at 20 seconds with the overshoot due to existing filtering in the roll inner loop of the MD-80 autopilot. Better transient behavior could be obtained if this filter were removed, but no changes to the inner loops were made during this study. Some oscillation does occur after the wings-level command is initiated (at 137 seconds), and this transient is due to an integrator in the roll inner loop. Improvement could be realized if the inner loops could be modified to accommodate the MLS guidance algorithms. The nominal bank angle of 10.8° was attained, however, after the response had settled.

Lateral tracking error, Figure 13B is composed of two superimposed traces plotted as a function of distance to go, D_{TG}. The run starts at 50,000 ft., and the lateral error (Δy, Equation 15) is less than 0.1 ft. until the 180° turn starts at 44,300 ft. The track error during the turn is ε_R, and is computed from Equation (23). (No Δy is computed during the turn so the trace for it is zero during that time). The values of ε_R during the turn represent the errors due to aircraft dynamics and roll inner loop characteristics. At the turn to final point, D_{TG} = 16,100 ft., $_R$ is set to zero and the track error is $\hat{y}_m$ as computed from Equation (14). The discontinuity in the trace here is due to the two definitions of track error, one being relative to the circular arc and the other being relative to the extended runway centerline. Errors on the order of 10-30 ft. exist near the end of this 150 second run.

Pitch angle and vertical tracking error are shown in Figure 14. The aircraft pitches up to 6.0 degrees from its trim of 5.5 degrees to maintain altitude during the turn. At 40 seconds, pitch change for a 3 degree glide slope occurs, as noted by point A in the figures. At the end of the turn (137 seconds), there is a small pitch transient as a result of the bank angle returning to zero.

Vertical tracking error, as shown in Figure 14B, is calculated from Equation (40). Pitch over at 40 seconds corresponds to a distance of 39,500 ft. The initial error of 73 ft. at this distance is determined by the switching logic of Equation (41). The aircraft is below the desired glide slope of 3 degrees, and Equation (41) has just changed sign. At this point, the steering command in Equation (69) will be the correct polarity to pitch over to intercept the 3° path. Overshoot of 12 ft., with a steady state tracking error of a few feet, characterize this baseline trombone approach case.

Lateral and normal acceleration responses are shown in Figure 15. The lateral acceleration at turn entry is 0.007 g, and during the turn it is within 0.003 g. These levels are well below the established limits for passenger comfort (0.02 g and 0.01 g, respectively). The normal acceleration deviation from trim value does not exceed 0.04 g. Acceptable maximum value for normal acceleration is 0.2 g.

Lateral tracking errors (which are ground track deviations) are graphically displayed in Figure 16. The dashed line is the desired path and the solid line is the actual path. The dotted line represents the 40° azimuth coverage of the azimuth transmitter. The peak error of 100 ft. is just discernible during the first part of the turn. The errors will be more easily seen on this scale when winds and turbulence are present.

A three-dimensional representation of this case is shown in Figure 17. Descent during the turn can be visualized, and tracking of the 3° glide slope line (in the vertical plane containing the runway) is apparent.

Performance at the final approach fix point (800 ft. altitude) for all cases is summarized in Table 2. Lateral, vertical, and heading errors are shown in addition to the pitch and roll angles that occur at 800 ft. altitude.

Cases 2 and 3.

Two cases with MLS noise were run with the same conditions given in Case 1. Case 2 contained the ICAO noise levels. Figure 18 shows the pitch response and vertical tracking error as compared to the noise-free response of Case 1. The large excursion in pitch would be unacceptable. The ICAO-specified noise levels are higher than actual MLS signals as discussed in the section on MLS noise models.

Case 3 uses the practical reduced noise levels which are believed to be more representative of actual MLS signals. The results in Figure 19 show more reasonable excursions. Statistics (mean and variance) cannot be ascertained from just one run, but both Cases 2 & 3 have the same starting number for the random number generator. Hence, the two cases have the same random sequence for MLS noise, the only difference being the RMS levels of the receiver output (Figure 11).

Other variables for Case 3 are compared with Case 1 in Figures 20-22. In Figure 21 the lateral tracking error is separated into two parts, one for the first and third (linear) segments, and one for the second (circular) segment. Lateral and normal acceleration traces are shown in Figure 22.

Cases 4-6.

Two cases with winds, and one with added turbulence, were executed to determine performance in such an environment. Case 4 was set up to have a 25 KT headwind and a 15 KT crosswind at touchdown. Equation (71) was used to compute these winds at the 2000 ft. initial altitude for all the single glide slope cases. The result is a 44 KT tailwind and a 27 Kt crosswind at the beginning of the run.

Figure 23 compares the Case 4 roll response with this wind level with the no-wind case. A higher bank angle initially is required to compensate for the crosswind, but the angle is less than the no wind case as the aircraft completes the 180° turn. The lateral tracking error in Figure 24A peaks about 100 ft. higher than when no wind is present (Figure 24B). At the end of the run, the tracking error is comparable to the no wind case.

Lateral and normal accelerations are shown in Figure 25. Both accelerations initially are higher with the wind, but tend to the same general magnitudes during the turns.

The ground track error is shown in Figure 26 for Case 4. In order to avoid an initial step transient, the aircraft starts with a crab angle to compensate for the wind. The larger track error is evident when compared to the baseline case of Figure 16.

Case 5 is similar to Case 4 except the direction of the winds are reversed, and the magnitude of the tailwind at touchdown is 10 knots. The opposite direction of the crosswind causes the roll response to have the characteristic shape shown in Figure 27. The lateral track error is comparable to the baseline case as shown in Figure 28. Lateral and normal accelerations for Case 5 are compared to the baseline case in Figure 19. Both these accelerations are well within established guidelines which are based on passenger comfort. Laterally, during turn entry this acceleration should be less than $\pm$ 0.6 ft./sec.^{2} and during the turn the value is $\pm$ 0.3 ft./sec.^{2}. Normal acceleration deviation should be less that $\pm$ 0.2g throughout the turn and during pitch-over to the desired glide slope. The wind direction and magnitude for this case cause a small ground track deviation as shown in Figure 30.

Case 6 contains the turbulence (as defined by Equation (73) and Figure 12) added to the winds of Case 5. Numerical values for the winds (Sx and Sy) for this case yield the following RMS levels on the longitudinal, lateral, and vertical turbulence components:

RMS Turbulence Levels

	Longitudinal	Lateral	Vertical
ALT = 2000 Ft.	2.65 KT	3.98 KT	1.5 KT
ALT = 33 Ft.	1.5 KT	2.25 KT	1.5 KT

A statistical evaluation of the turbulence response was not performed. Figure 31 (A) and (B) compares one particular turbulence run with no turbulence of Case 5. The tracking errors are comparable in both cases. Accelerations, both lateral and normal, exceeded the guideline levels a few times during the run, Figure 31 (C) and (D). These exceedences are to be expected since this case represents relatively high turbulence levels.

Case 7.

Tracking errors for the light weight, low speed case are shown in Figure 32 and 33. Comparison with the 140 KT case shows tracking errors are nearly the same. The lateral and vertical guidance algorithms designed for a 140 KT speed appear to work well at other than nominal speeds.

SPEED CHANGE

Case 8.

Programmed speed changes from 165 KT to 140 KT result in increased peak tracking errors on the order of 20 ft. laterally and 50 ft. vertically as compared to the constant speed case. After the 140 KT speed has been reached, the errors become the same as the 140 KT case. Figure 34 shows the bank angle histories for this case and Case 3. About 5 degrees of additional bank angle resulted during transition to the lower speed. Speed transient is smooth (Figure 35) and takes about 30 seconds to settle out. The flap changes at its rate limit and reaches 40 degrees in about 13 seconds (Figure 36). Thrust changes are shown in Figure 37. Case 8 thrust approaches a minimum of about 3000 pounds during the speed reduction period. The guidance algorithms appear to work well for programmed speed changes.

SEGMENTED GLIDE SLOPE

Case 9.

Figure 5 shows the segmented glide slope geometry for Case 9. The pitch profile for this case is shown in Figure 38. Pitch over to 4.5 degrees occurs at 14.5 seconds with a pitch up to the 3 degree glide slope at 38 seconds. These points are denoted as A and B in the figures. The turn starts at 20 seconds and ends at 137 seconds. Vertical tracking errors are plotted in Figure 39 as a function of distance to go. Pitch over occurs at 45700 feet and pitch up occurs at 40000 feet. These events show as discontinuities due to the way the vertical guidance switching logic works. Steady state tracking for this case is the same as the single glide slope approach (Case 3). Lateral tracking is not affected by including a segmented glide slope in the vertical approach path. Deviations in normal acceleration at the pitch over point is about 0.1 g and is within the 0.2 g guideline (Figure 40).

LATERALLY SEGMENTED FINAL

Case 10.

The laterally segmented approach geometry is shown in Figure 6. The same guidance laws were used for this case with only the initial conditions being different than the trombone finals. Transition between the two straight segments is arbitrary, but was selected to be a circular arc based on a 20 degree bank angle at the current ground speed. The actual bank angle history is shown in Figure 41A. The overshoot is due to the inner loop filters as discussed in the trombone results section. The short time the aircraft is in the turn prevents a steady state bank to be established before it is time to turn to the final leg. Consequently, overshoot of about 8 degrees is experienced in roll at that time. Lateral tracking errors (Figure 41B) are nearly the same as the Case 3 trombone approach. The three lateral segments are identified in the figure at the distance to go corresponding to the times in Figure 41A. Vertical errors (Figure 42) are also comparable to Case 3 results. Acceleration levels in Figure 43 are within established guidelines.

Ground track for this case is shown in Figure 44 using an expanded scale. The lateral overshoot at $\dot{x}$ = -22000 ft. is less than 90 ft., and the error at x = -17000 ft. is 40 ft. These errors decrease to 20 ft. at the end of this 100 second run.

REFERENCES

1. J. E. Dieudonne, R. D. Grove, and G. G. Steinmetz: A Simulation Study of Curved, Descending, Decelerating, Landing Approaches for Transport Aircraft, NASA TN D-8190, April 1976.

2. Aviation Week and Space Technology, April 8, 1985/Volume 122, No. 14, page 79.

TABLE 1 - CASE SUMMARY FOR TROMBONE AND LATERALLY SEGMENTED FINALS

CASE NUMBER	GLIDESLOPE DEG.	SPEED KNOTS	WIND KNOTS (Sx/Sy)	TURB.	MLS NOISE	NOTES
1	0-3	140	NO	NO	NO	BASELINE
2					ICAO	ICAO NOISE LEVELS
3			NO		REDUCED	REDUCED NOISE LEVELS
4			-25/15			INITIAL TAIL/CROSS WINDS
5			10/-15	NO		INITIAL HEAD/CROSS WINDS
6		140	10/-15	YES		WIND WITH TURBULENCE
7		116	NO	NO		LOW WEIGHT
8	0-3	165-140				SPEED CHANGE
9	0-4.5-3	140				SEGMENTED GLIDE SLOPE
10	3.8					LATERALLY SEGMENTED

TABLE 2

ERRORS AT FINAL APPROACH FIX POINT (800 FT. ALT)

CASE NO.	LATERAL ERROR, FT. (+ TO RIGHT OF RUNWAY)	LATERAL ERROR RATE, FT/SEC (+ TO RIGHT)	VERTICAL ERROR, FT. (+ LOW)	VERTICAL ERROR RATE, FT/SEC (+ DOWN)	VELOCITY ERROR,FT/SEC (+ FAST)	TRACKING ERROR, DEGREE (+ RIGHT)	PITCH ANGLE, DEG (+ NU)	ROLL ANGLE, DEG (+ RWD)
1	-30.3	-3.5	+2.0	-0.05	-0.2	-0.3	2.7	6.4
2	-9.9	-4.6	-15.5	-1.8	-0.7	-0.5	2.9	6.3
3	-18.5	-3.9	+2.1	-0.5	-0.3	-0.4	2.8	6.2
4	-32.8	-2.2	-3.8	-1.1	-0.4	-0.7	3.7	4.8
5	20.0	-8.4	1.7	-0.6	-0.2	0.9	1.9	9.0
6	0.6	-4.0	-6.5	-3.4	+19.8	0.2	1.1	8.7
7	-42.4	-2.1	+1.8	-1.6	-0.08	0.2	2.7	5.7
8	-22.0	-1.8	-11.1	-0.004	-0.1	0.03	2.5	5.6
9	-11.3	-4.2	2.0	-0.8	-0.3	-0.5	3.0	6.0
10	-36.0	0.6	-1.0	-16.8	-0.8	0.1	1.6	0.2

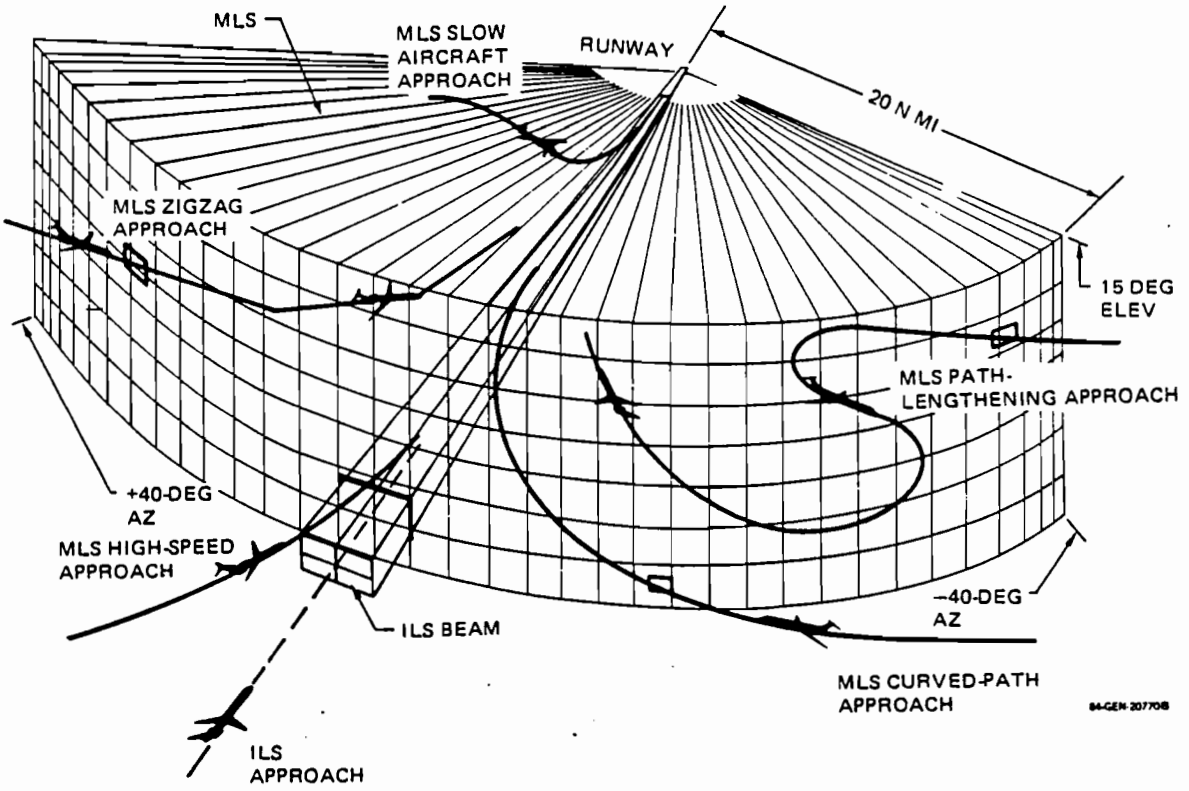

FIGURE 1. POSSIBLE APPROACHES IN THE MLS COVERAGE VOLUME

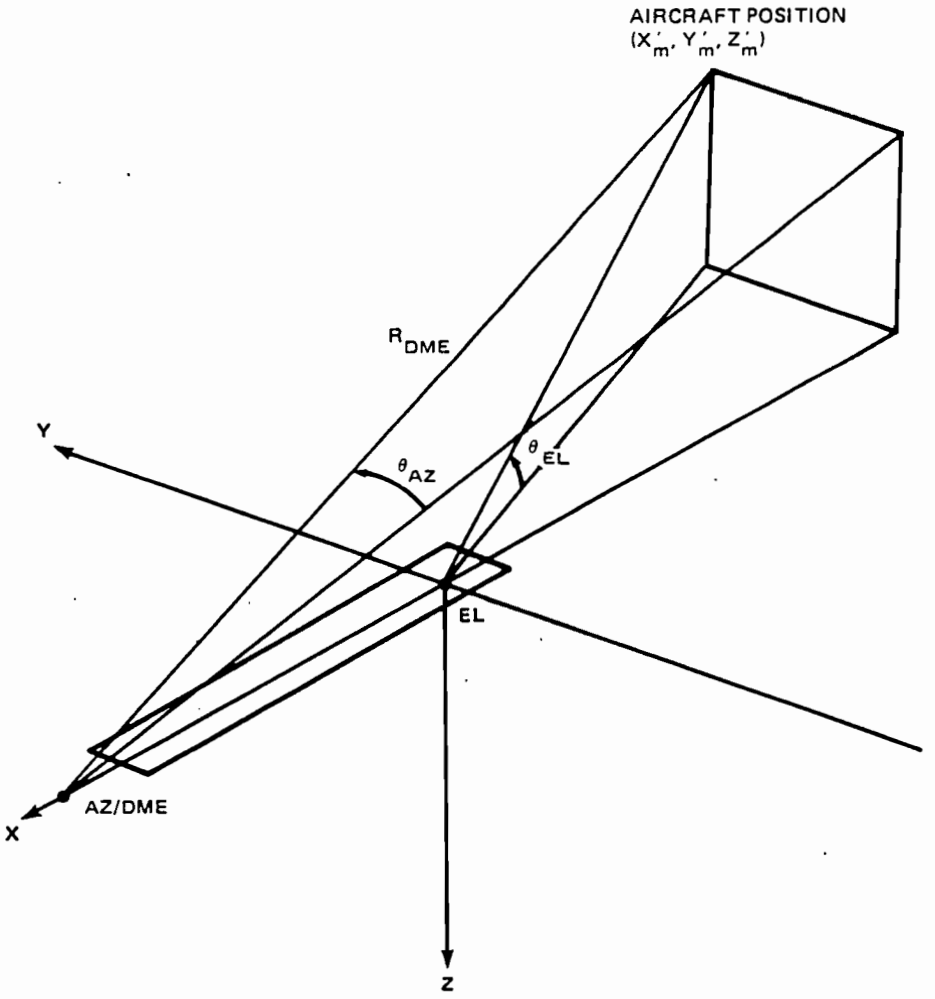

FIGURE 2. MLS GEOMETRY

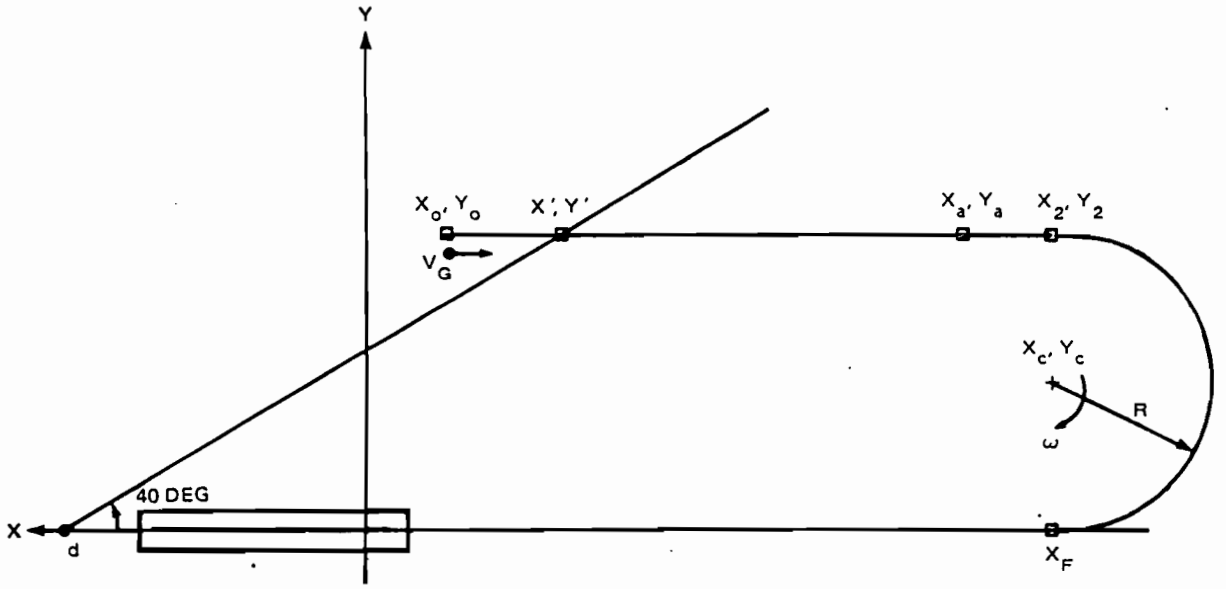

d = 10,000 FT		$X_2 = X_F$ = −15,265 FT	
X_o = −10,000 FT		X_A = −14,754 FT	
Y_o = Y' = Y_2 = 18,246 FT		R = 9,123 FT	
X' = −11,737 FT		ϕ_N = 10.8 DEG	
V_G = 140 KT		ω = 1.5 DEG/SEC	

FIGURE 3. DESIRED GROUND TRACK FOR THE TROMBONE APPROACHES

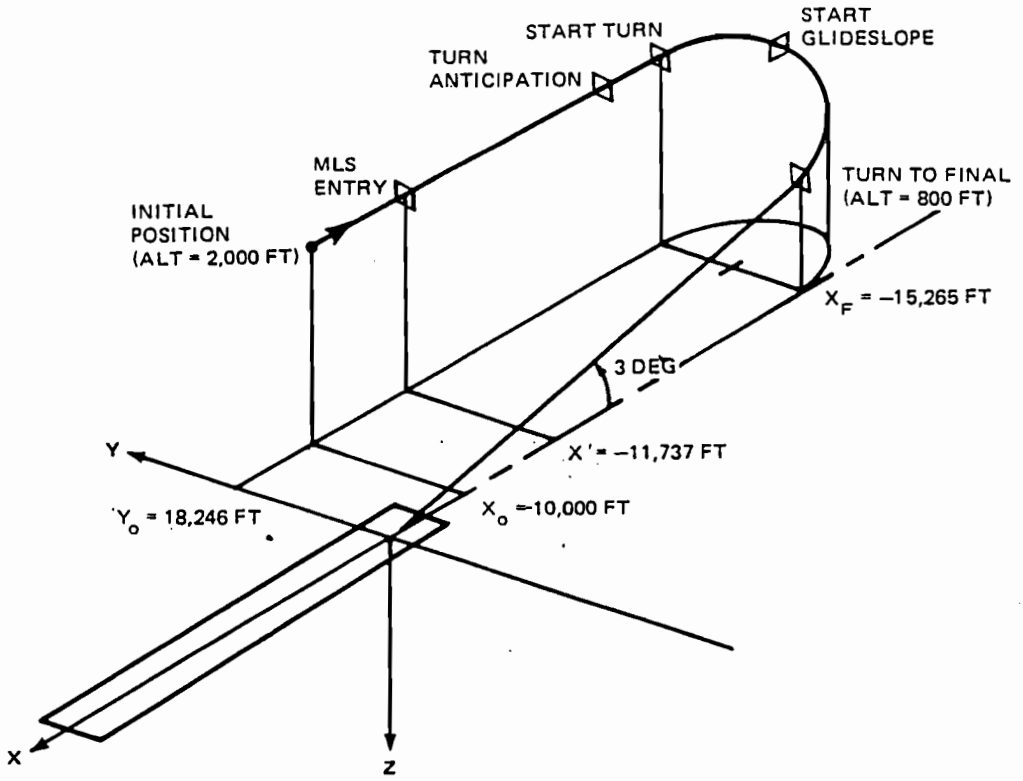

FIGURE 4. DESIRED PATH FOR THE SINGLE GLIDE SLOPE TROMBONE APPROACH

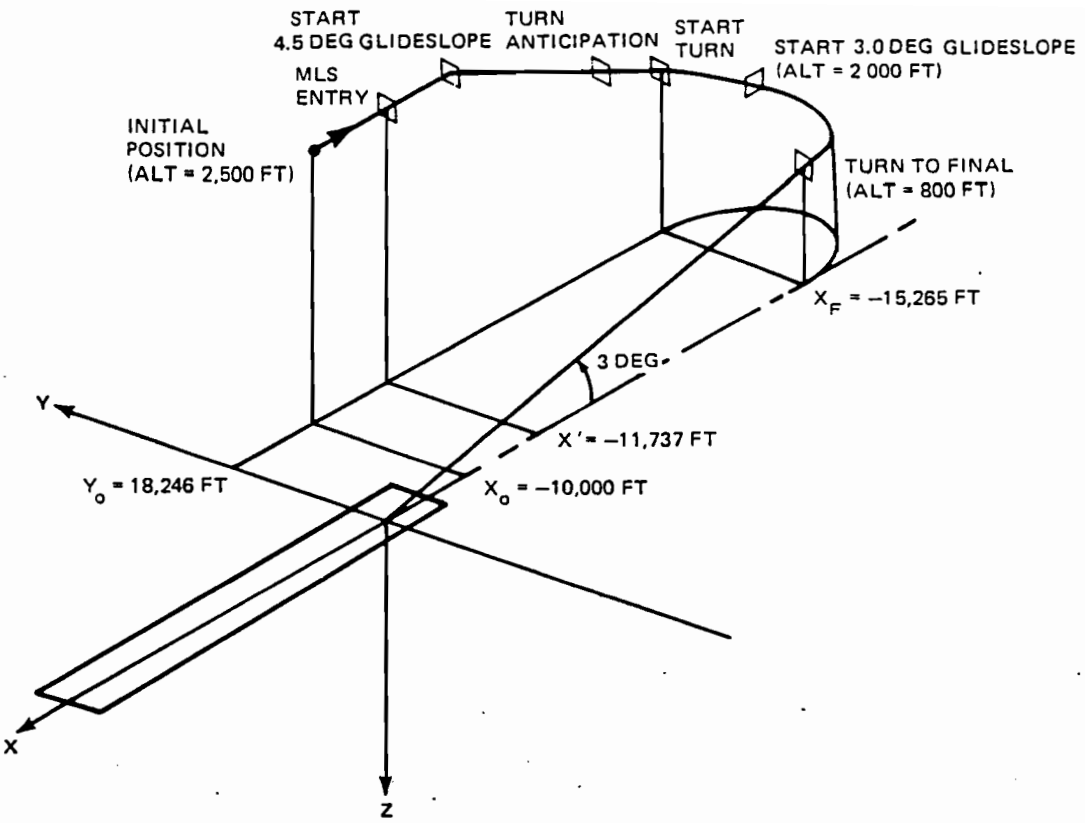

FIGURE 5. DESIRED PATH FOR THE SEGMENTED GLIDE SLOPE TROMBONE APPROACH

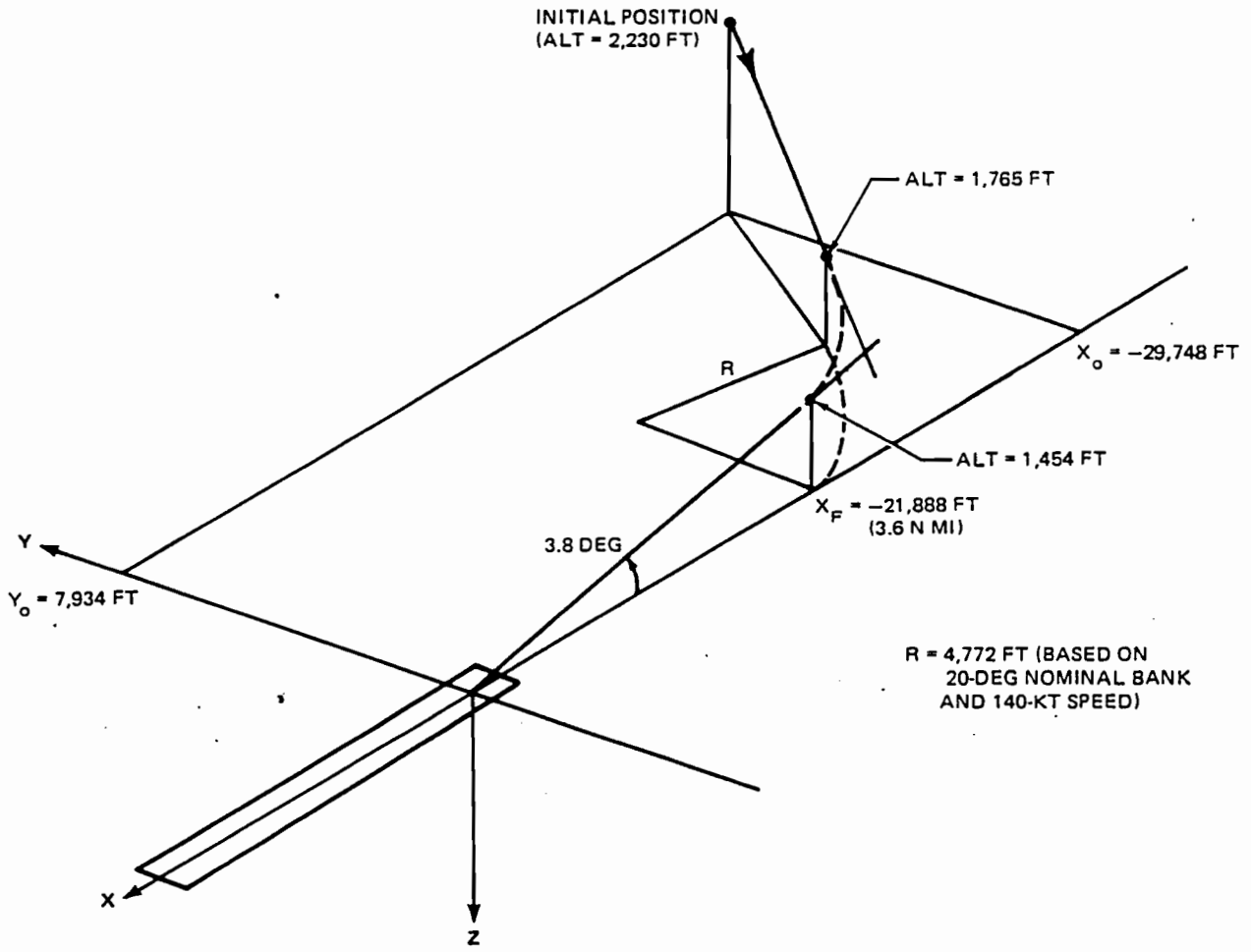

FIGURE 6. DESIRED PATH FOR LATERALLY SEGMENTED APPROACH

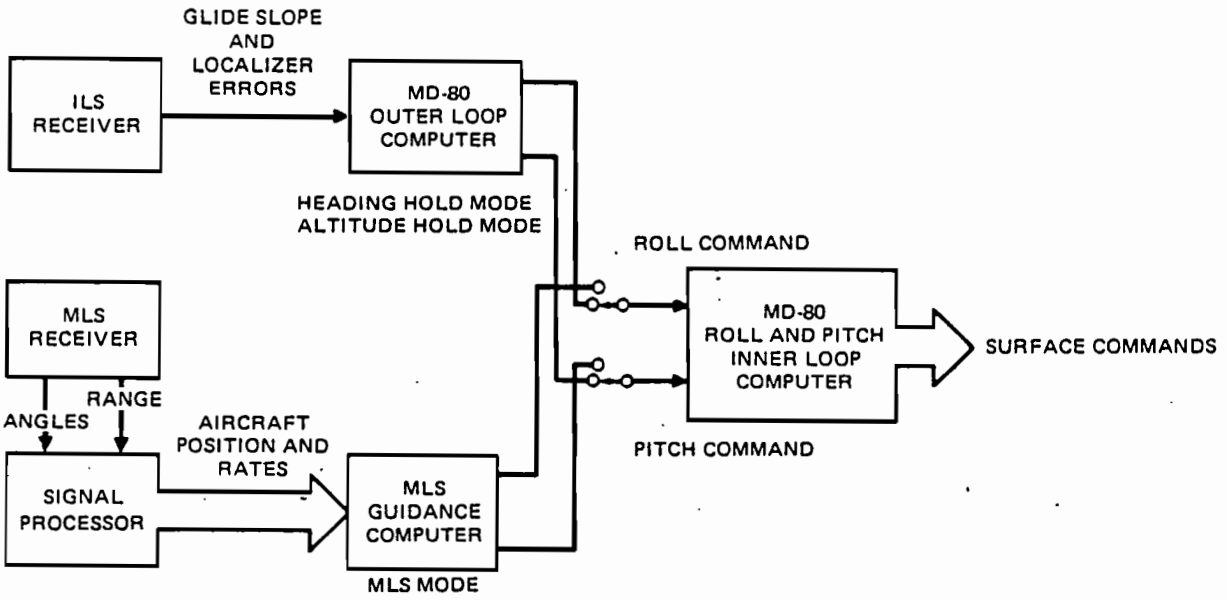

FIGURE 7. MLS/MD-80 AUTOPILOT INTERFACE BLOCK DIAGRAM

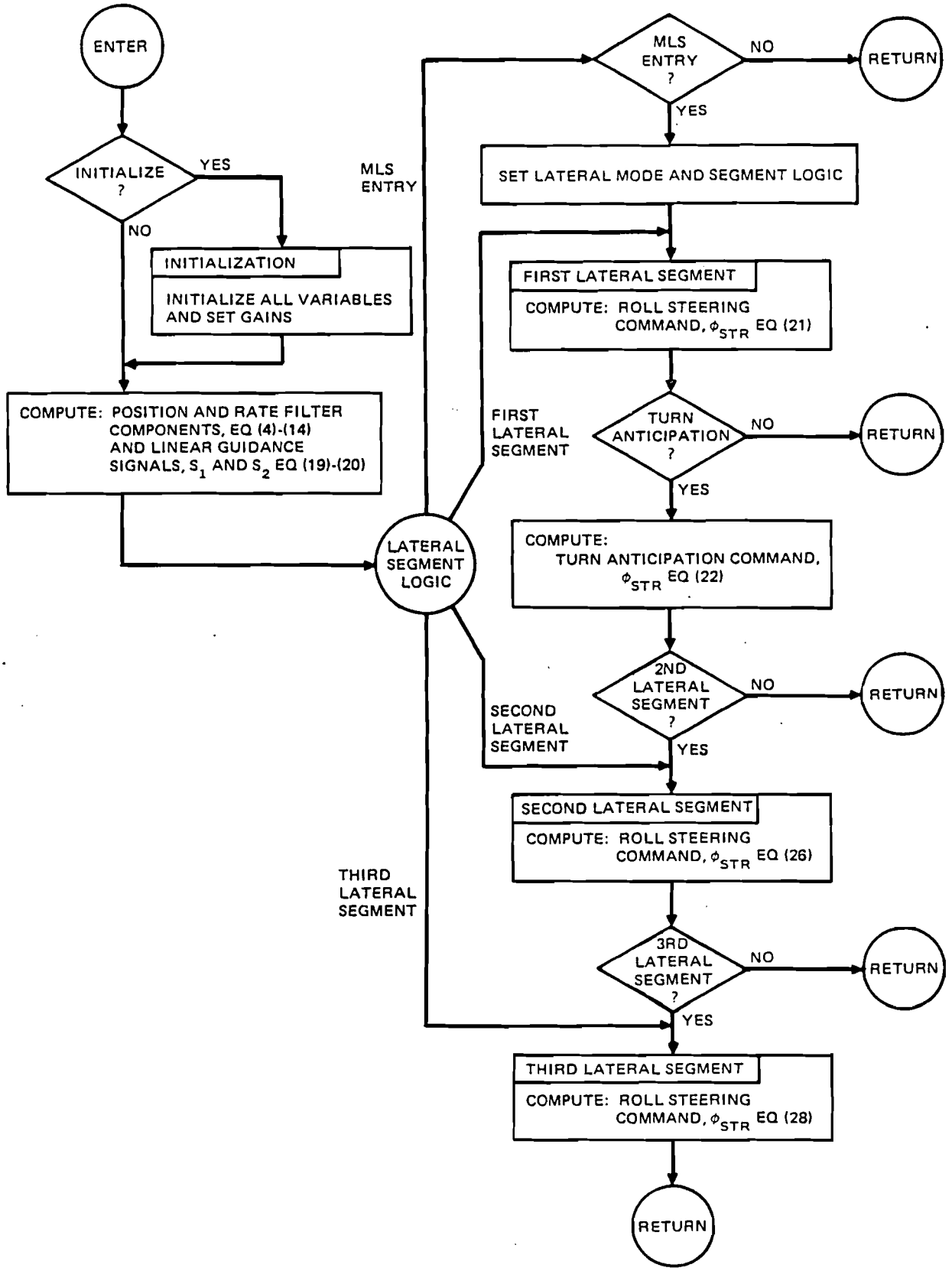

FIGURE 8. LATERAL GUIDANCE LAW FLOW DIAGRAM

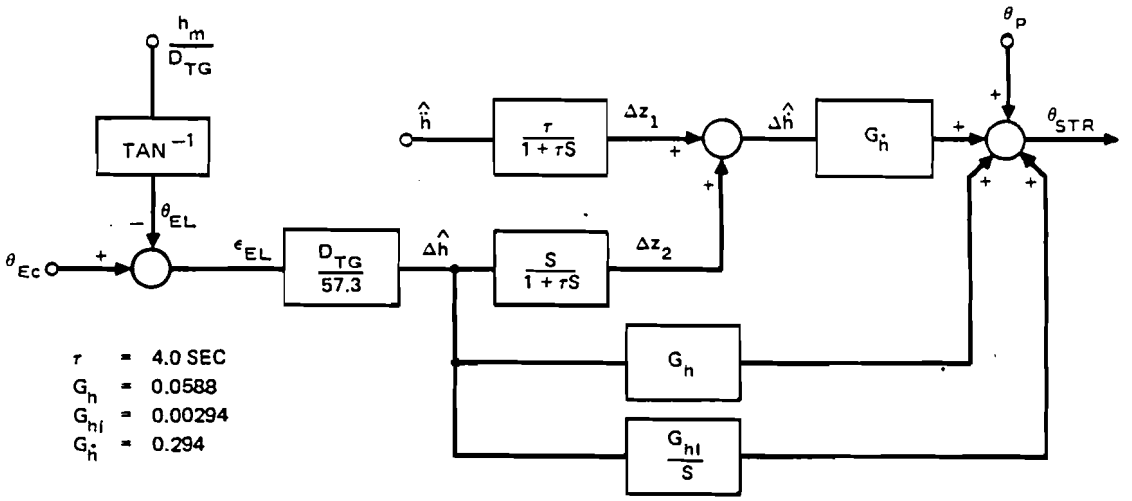

FIGURE 9. VERTICAL GUIDANCE LAW BLOCK DIAGRAM

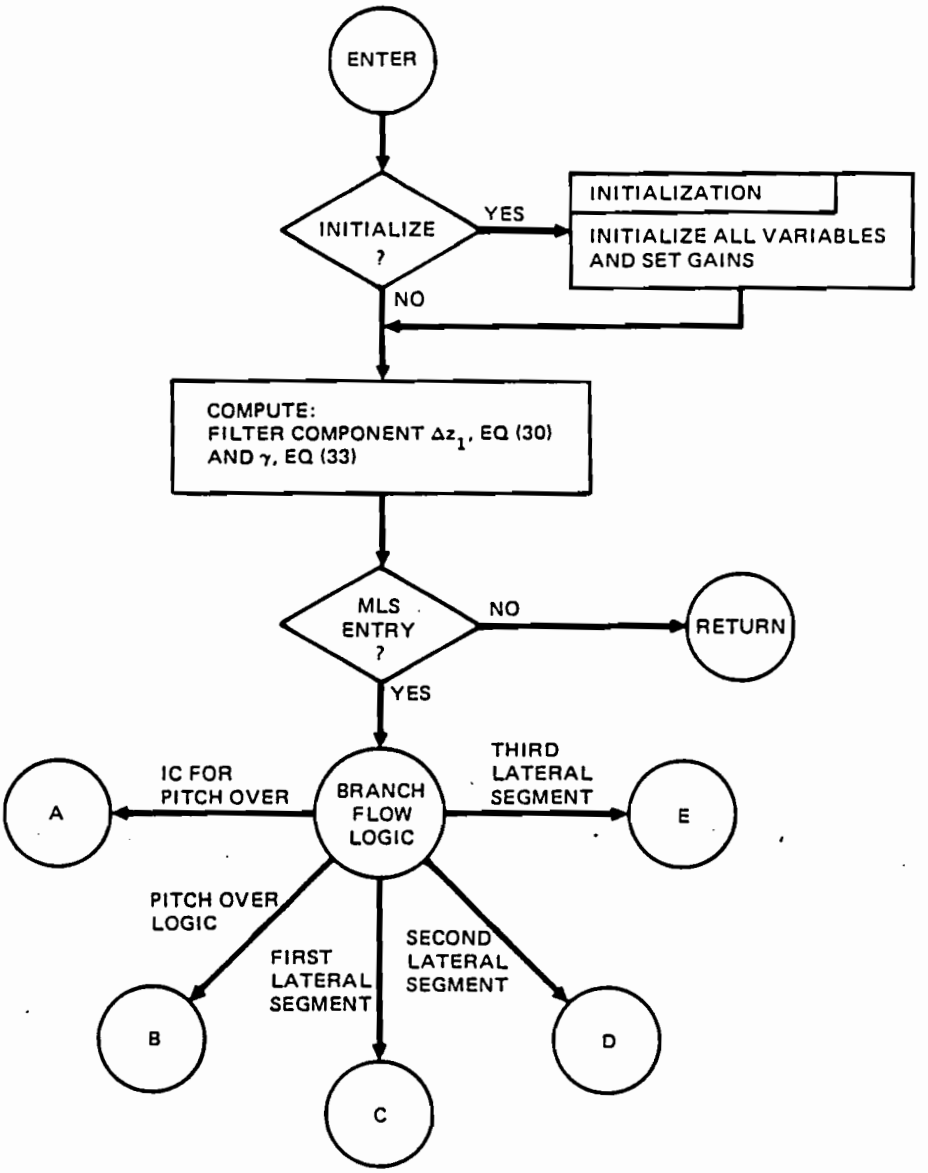

FIGURE 10. VERTICAL GUIDANCE LAW FLOW DIAGRAM (PART 1)

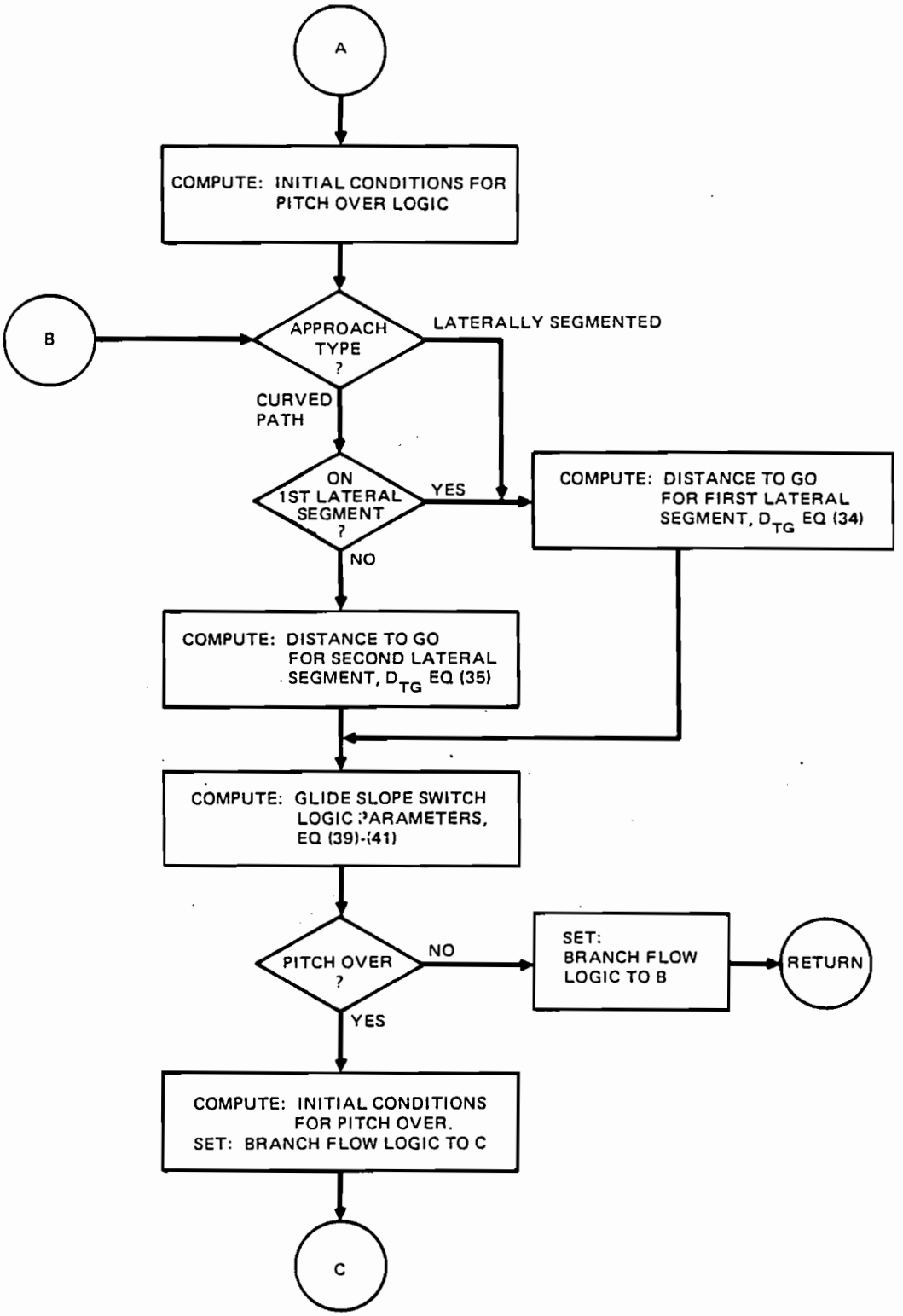

FIGURE 10. VERTICAL GUIDANCE LAW FLOW DIAGRAM (PART 2)

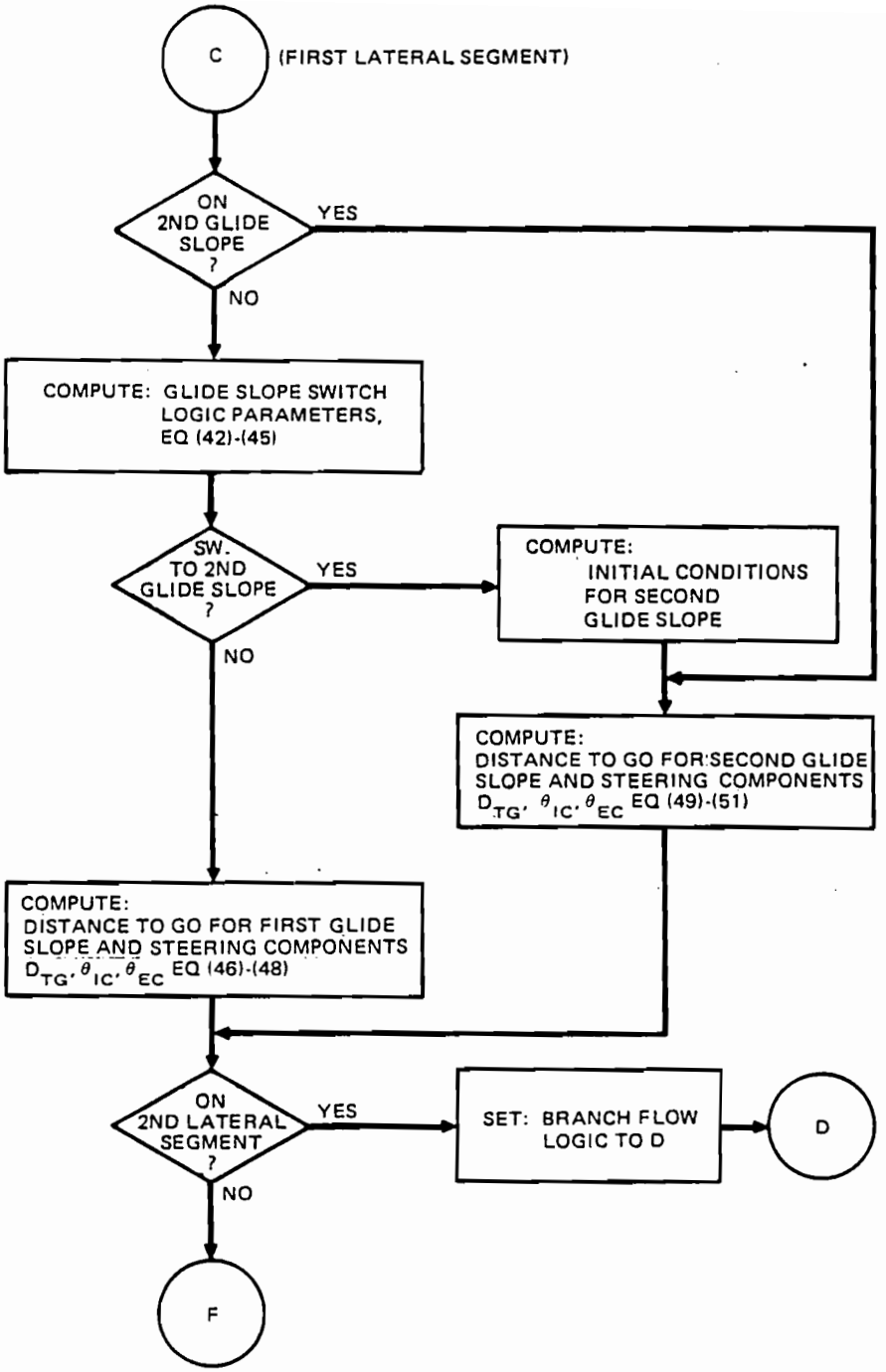

FIGURE 10. VERTICAL GUIDANCE LAW FLOW DIAGRAM (PART 3)

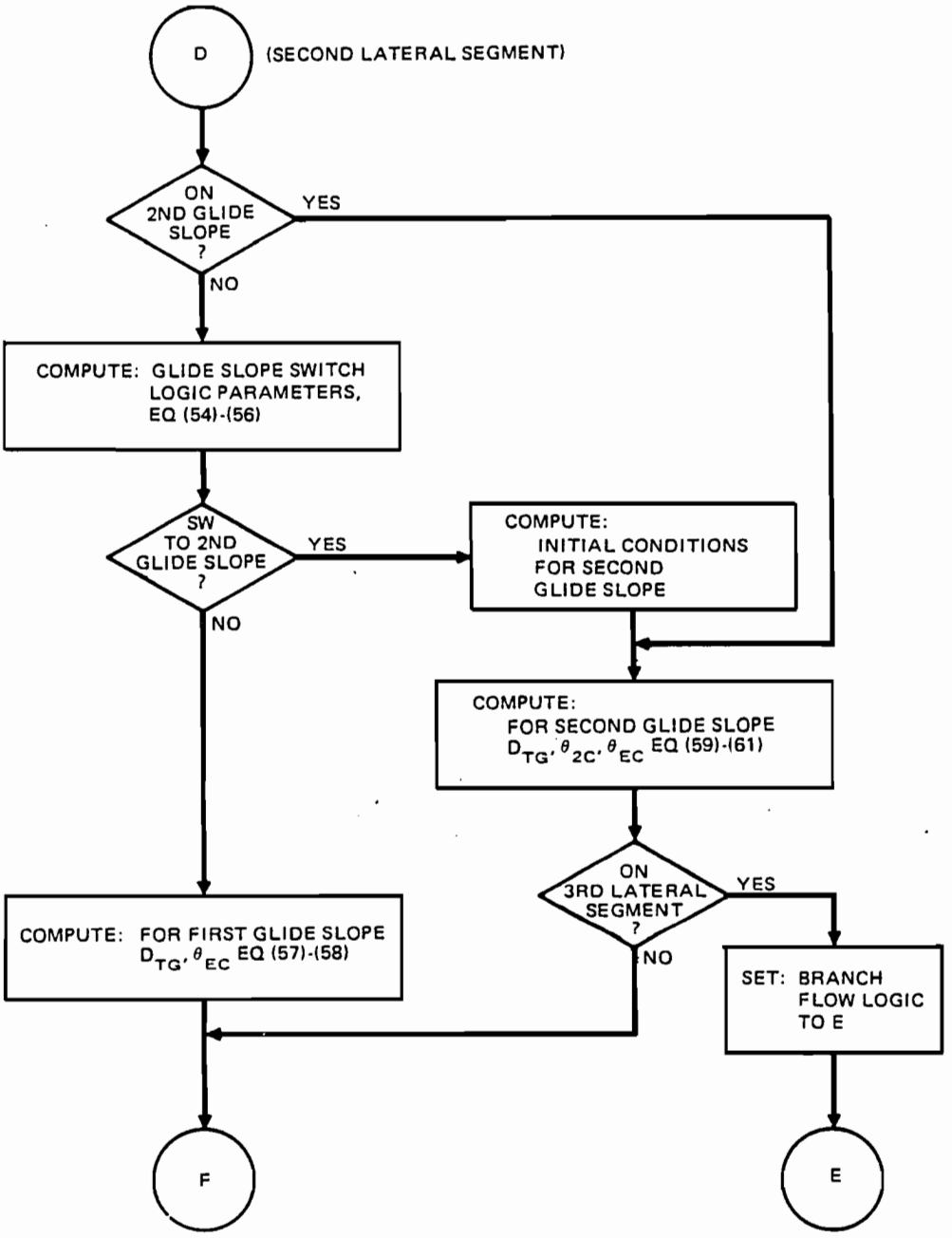

FIGURE 10. VERTICAL GUIDANCE LAW FLOW DIAGRAM (PART 4)

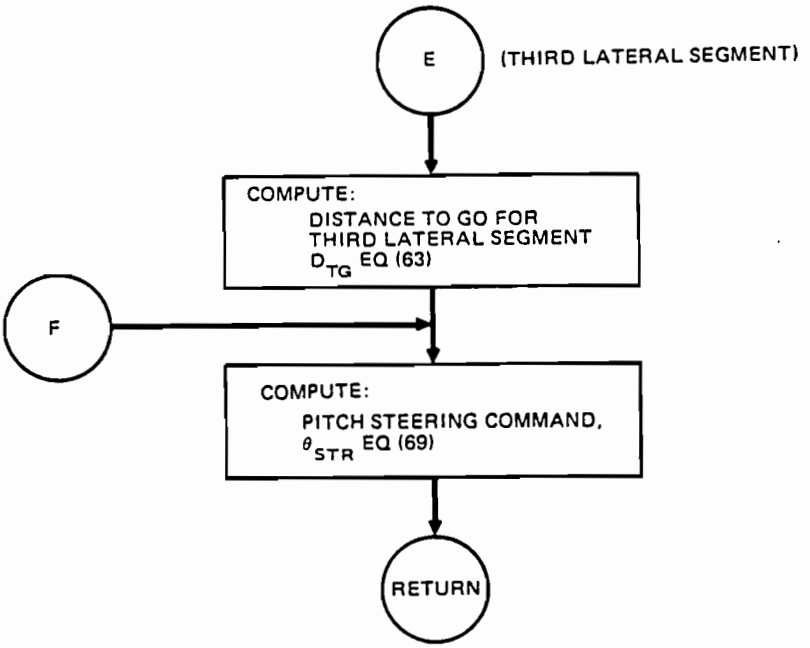

FIGURE 10. VERTICAL GUIDANCE LAW FLOW DIAGRAM (PART 5)

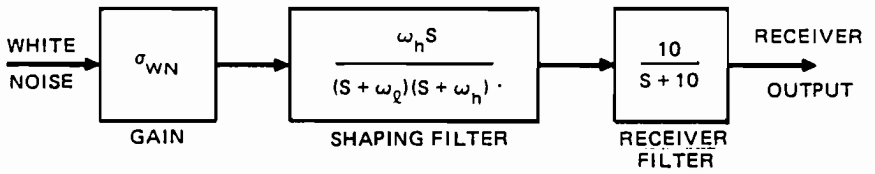

	AZIMUTH	ELEVATION	DME
	ω_ℓ = 0.001 RAD/SEC	ω_ℓ = 0.001 RAD/SEC	ω_ℓ = 0.001 RAD/SEC
ICAO SPEC VALUES	ω_h = 0.0942 RAD/SEC	ω_h = 0.1579 RAD/SEC	ω_h = 0.245 RAD/SEC
	σ_{WN} = 0.263	σ_{WN} = 0.2488	σ_{WN} = 154.7
	σ_{REC} = 0.057 DEG	σ_{REC} = 0.069 DEG	σ_{REC} = 53.4 FT
ASSUMED PRACTICAL VALUES	ω_h = 0.16 RAD/SEC	ω_h = 0.34 RAD/SEC	ω_h = 0.245 RAD/SEC
	σ_{WN} = 0.064	σ_{WN} = 0.024	σ_{WN} = 154.7
	σ_{REC} = 0.02 DEG	σ_{REC} = 0.0097 DEG	σ_{REC} = 53.4 FT

FIGURE 11. MLS ANGLE AND RANGE NOISE MODELS (AT THRESHOLD)

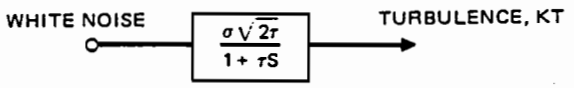

$\sigma_{WN} = 1.0$

FILTER PARAMETERS

	LONGITUDINAL	LATERAL	VERTICAL
τ(SEC)	$600/V_{TAS}$	$600/V_{TAS}$	$30/V_{TAS}$
σ(KT)	$0.15\|W_x\|$	$0.15\|W_y\|$	1.5

FIGURE 12. FILTER MODEL FOR SIMULATED TURBULENCE

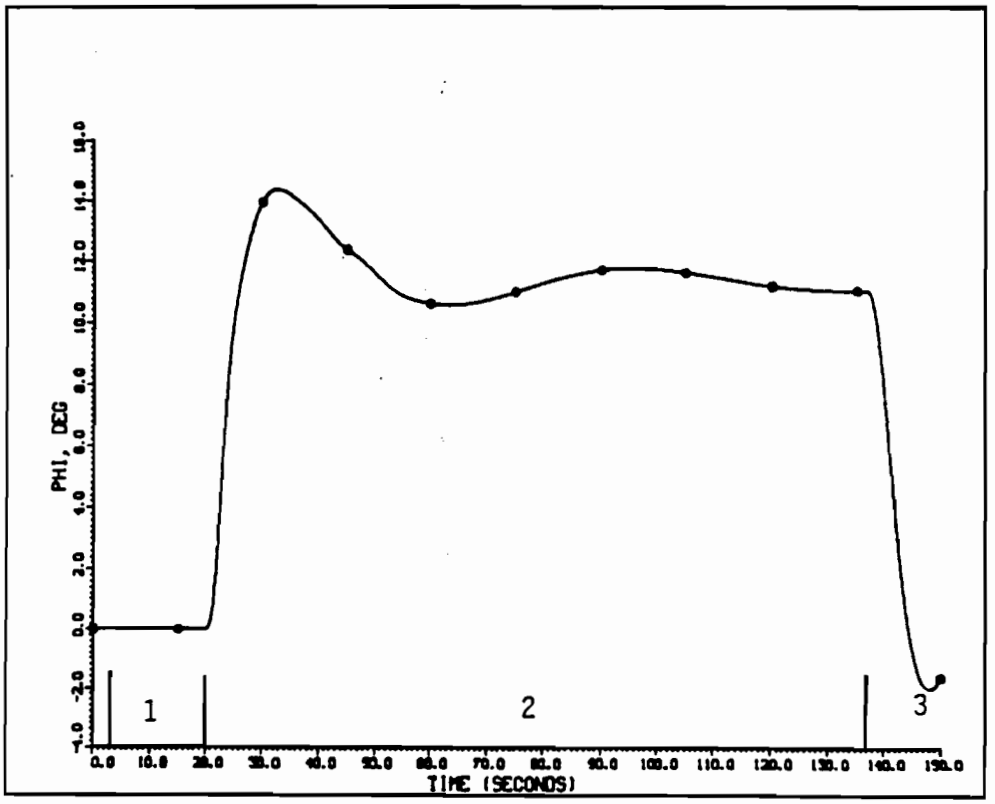

(A)

LEGEND

1 1st LAT SEG
2 2nd LAT SEG
3 3rd LAT SEG

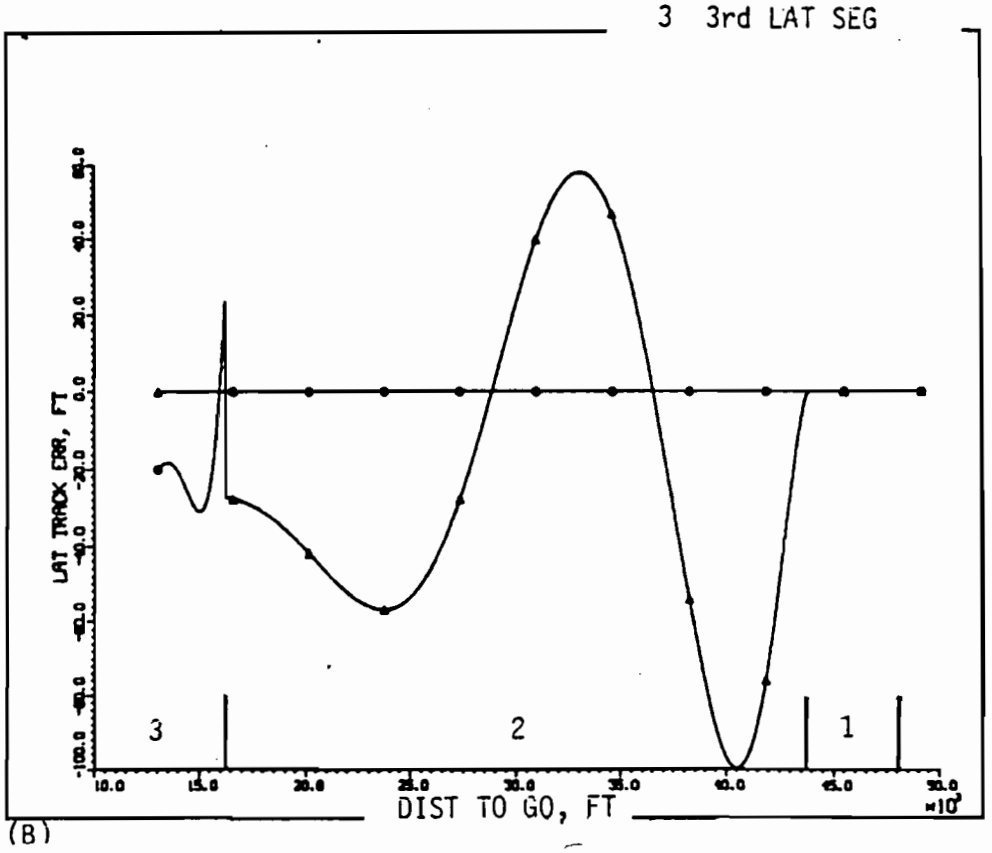

(B)

FIGURE 13 - BANK ANGLE AND LATERAL TRACKING ERROR FOR BASELINE (CASE 1)

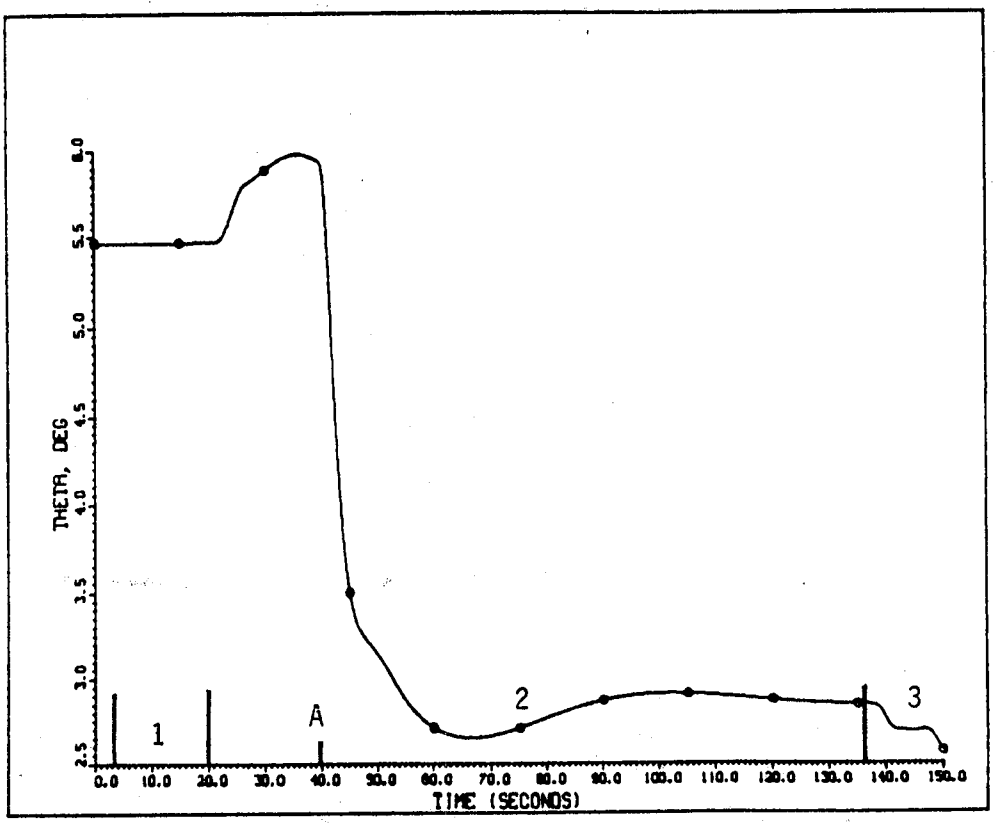

(A)

LEGEND

1 1st LAT SEG
2 2nd LAT SEG
3 3rd LAT SEG

A 1st GLIDE SLOPE

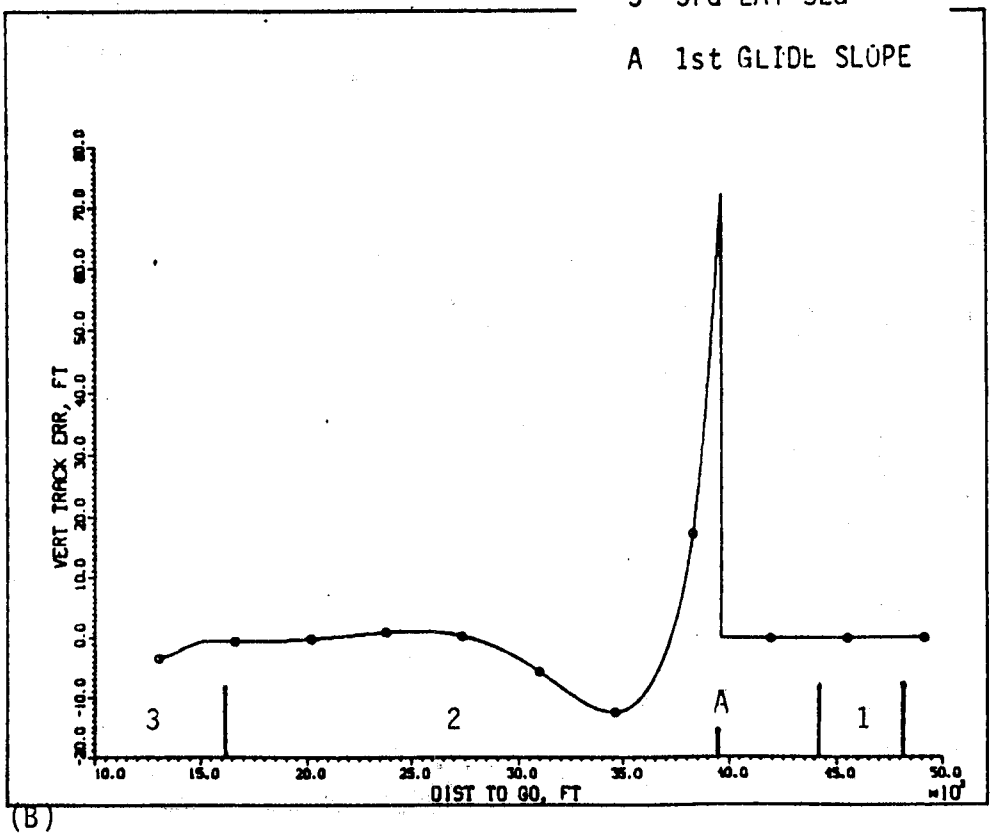

(B)

FIGURE 14 - PITCH ANGLE AND VERTICAL TRACKING ERROR FOR BASELINE (CASE 1)

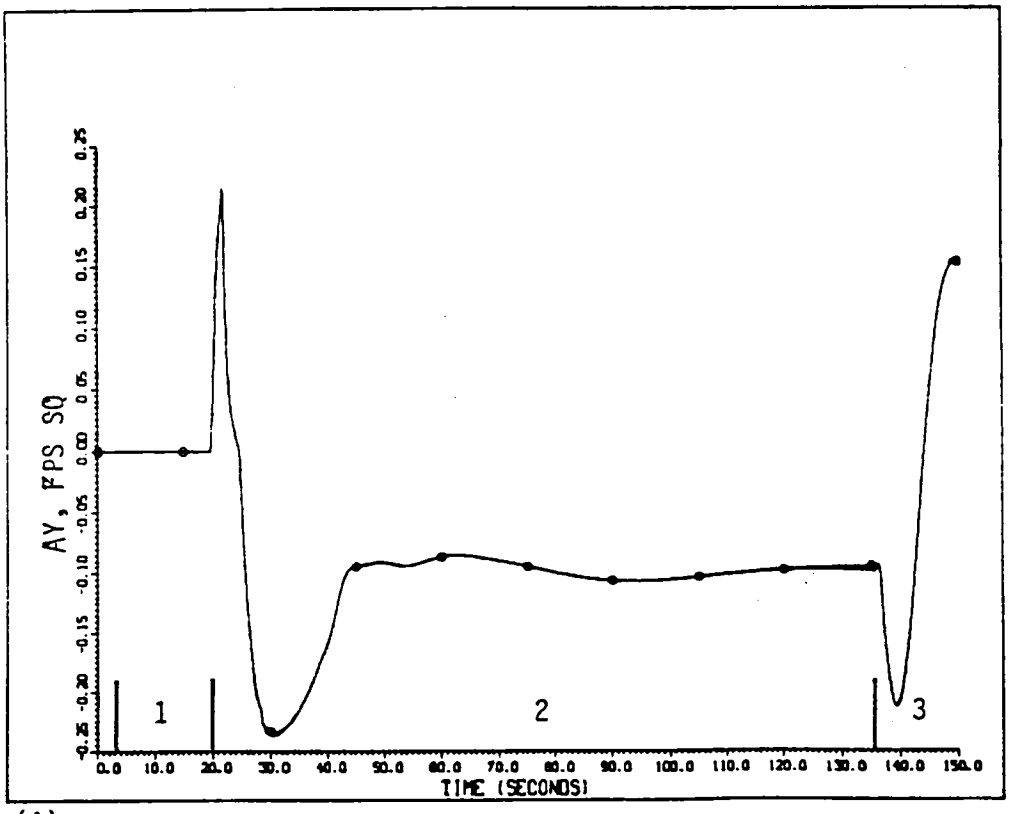

(A)

LEGEND

1 1st LAT SEG
2 2nd LAT SEG
3 3rd LAT SEG

A 1st GLIDE SLOPE

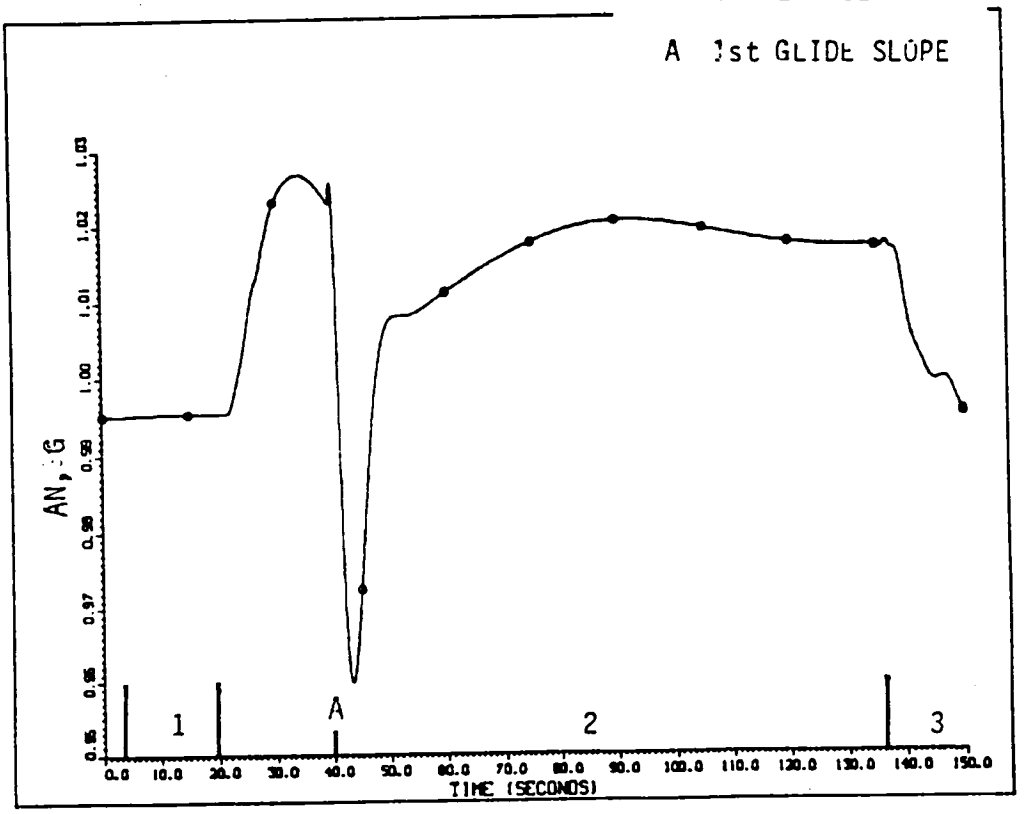

(B)

FIGURE 15 - LATERAL AND NORMAL ACCELERATION FOR BASELINE (CASE 1)

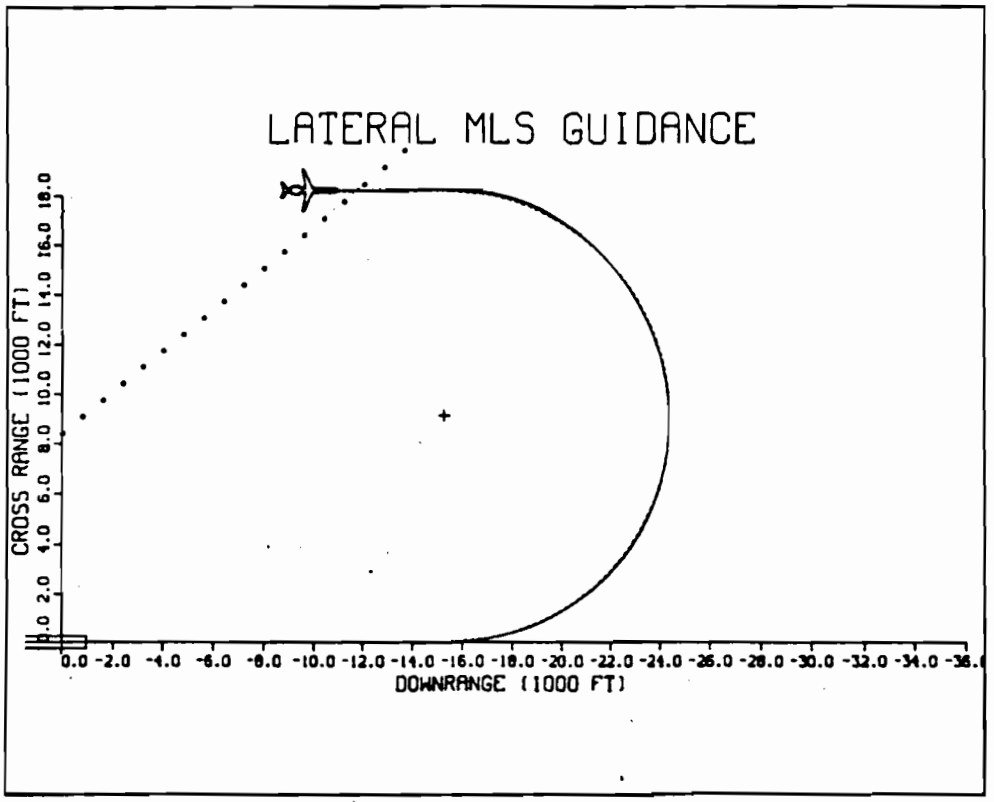

FIGURE 16 - GROUND TRACK FOR BASELINE (CASE 1)

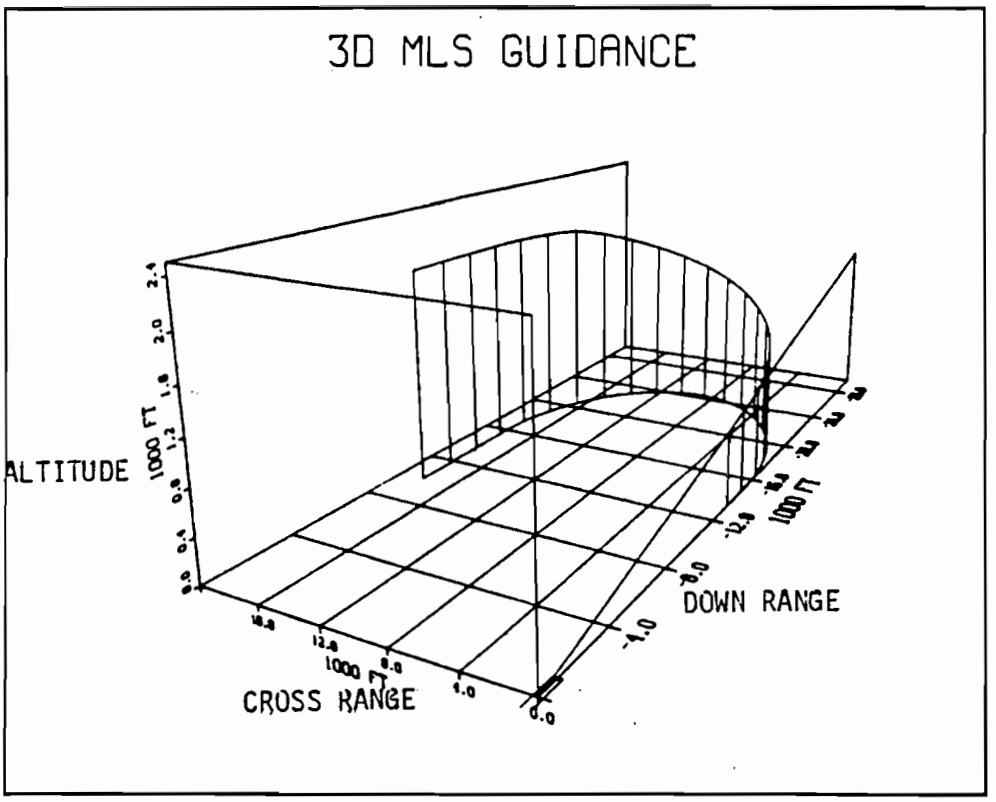

FIGURE 17 - TRAJECTORY FOR BASELINE (CASE 1)

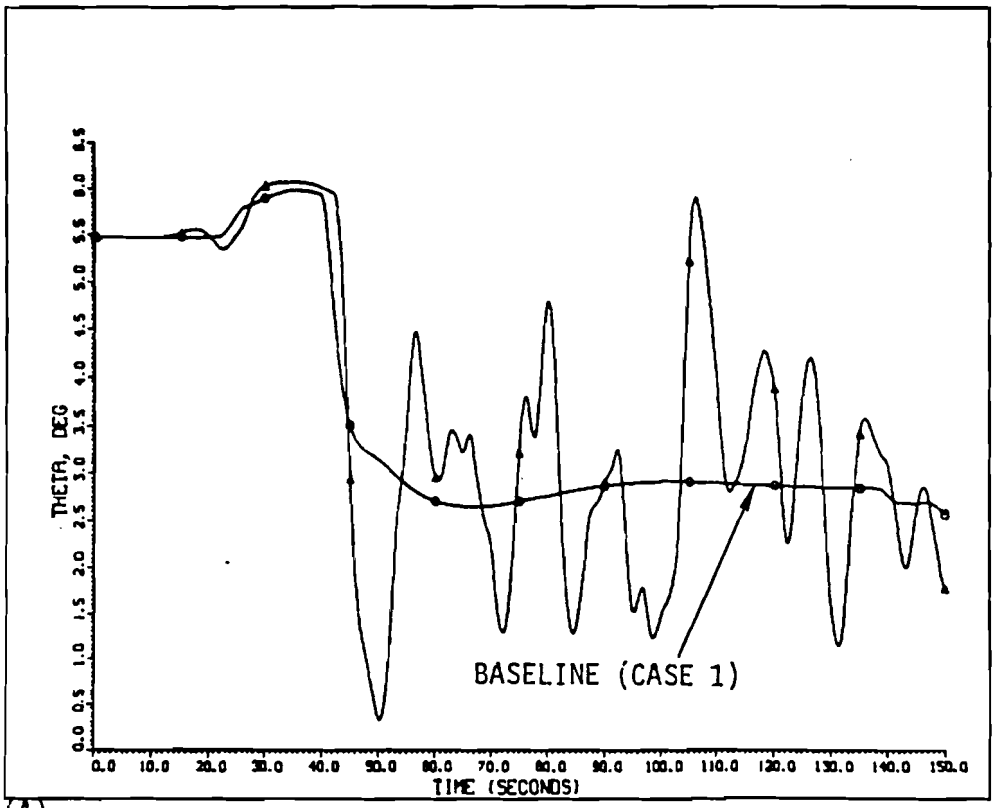

(A)

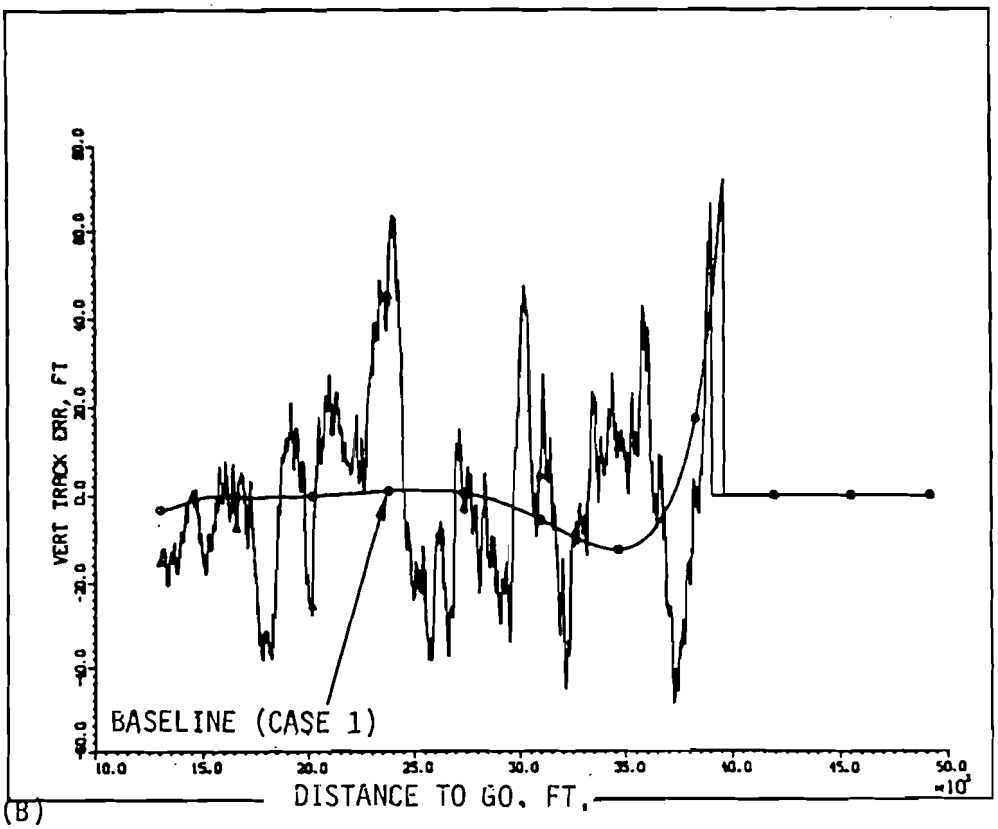

(B)

FIGURE 18 - PITCH ANGLE AND VERTICAL TRACKING ERROR FOR ICAO NOISE LEVELS (CASE 2)

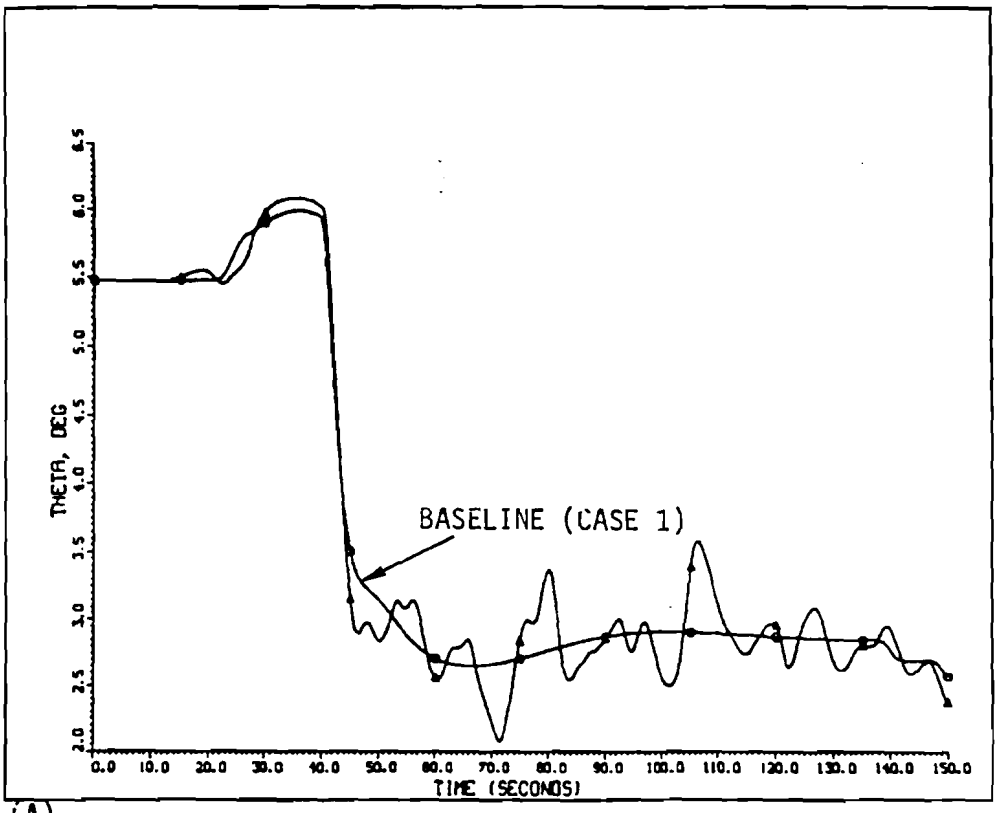

(A)

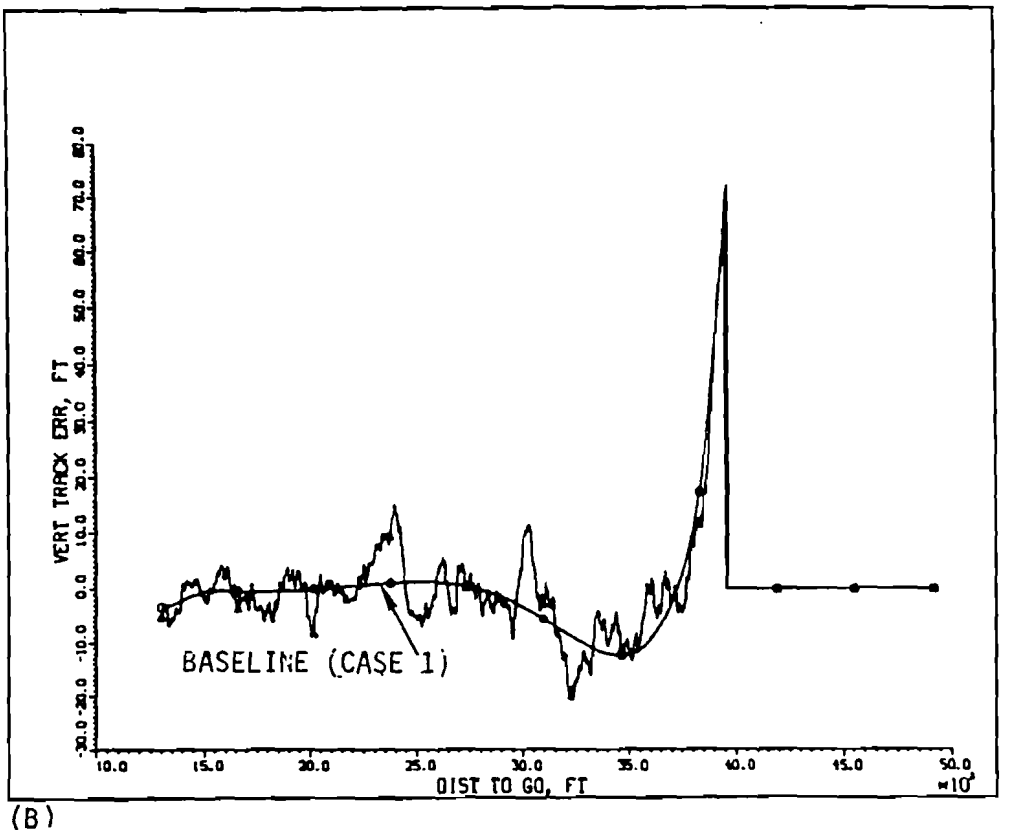

(B)

FIGURE 19 - PITCH ANGLE AND VERTICAL TRACKING ERROR FOR REDUCED NOISE LEVELS (CASE 3)

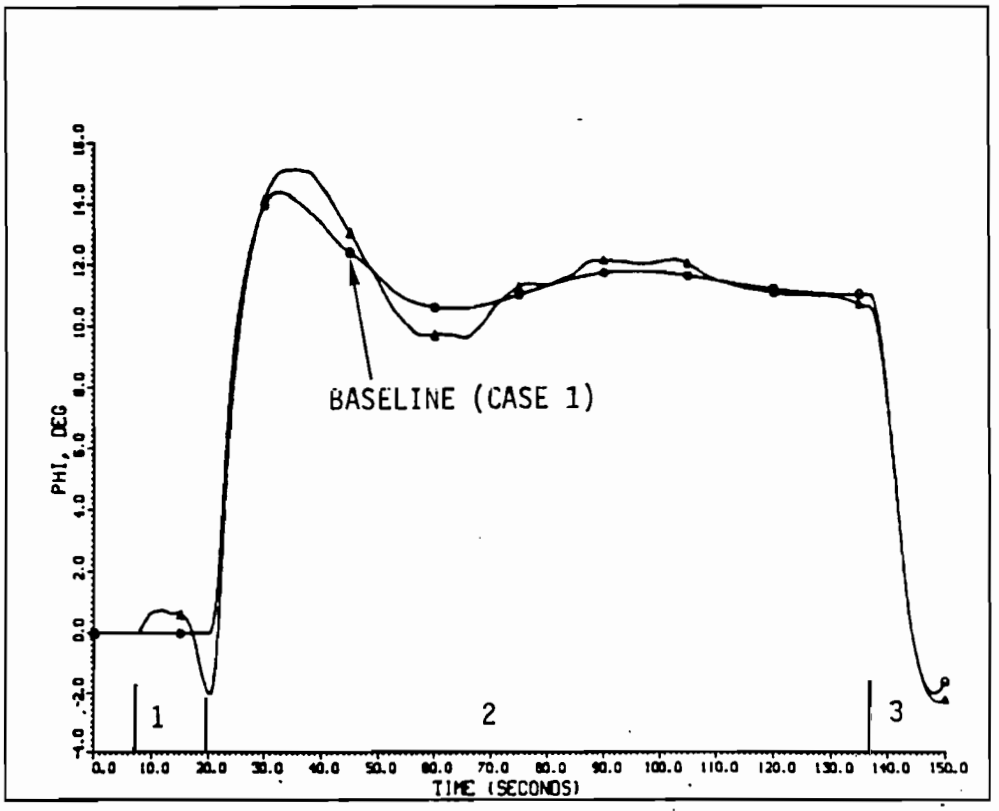

FIGURE 20 - BANK ANGLE FOR REDUCED NOISE (CASE 3)

LEGEND

1 1st LAT SEG
2 2nd LAT SEG
3 3rd LAT SEG

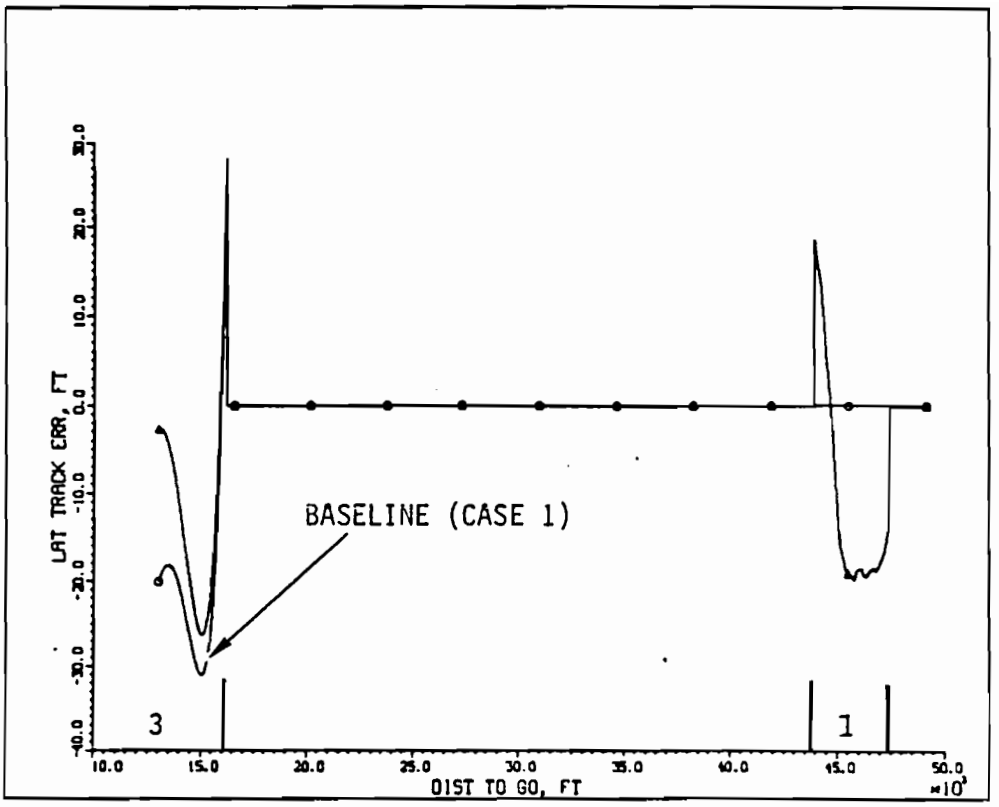

(A) FIRST AND THIRD LATERAL SEGMENTS (LINEAR TRACK)

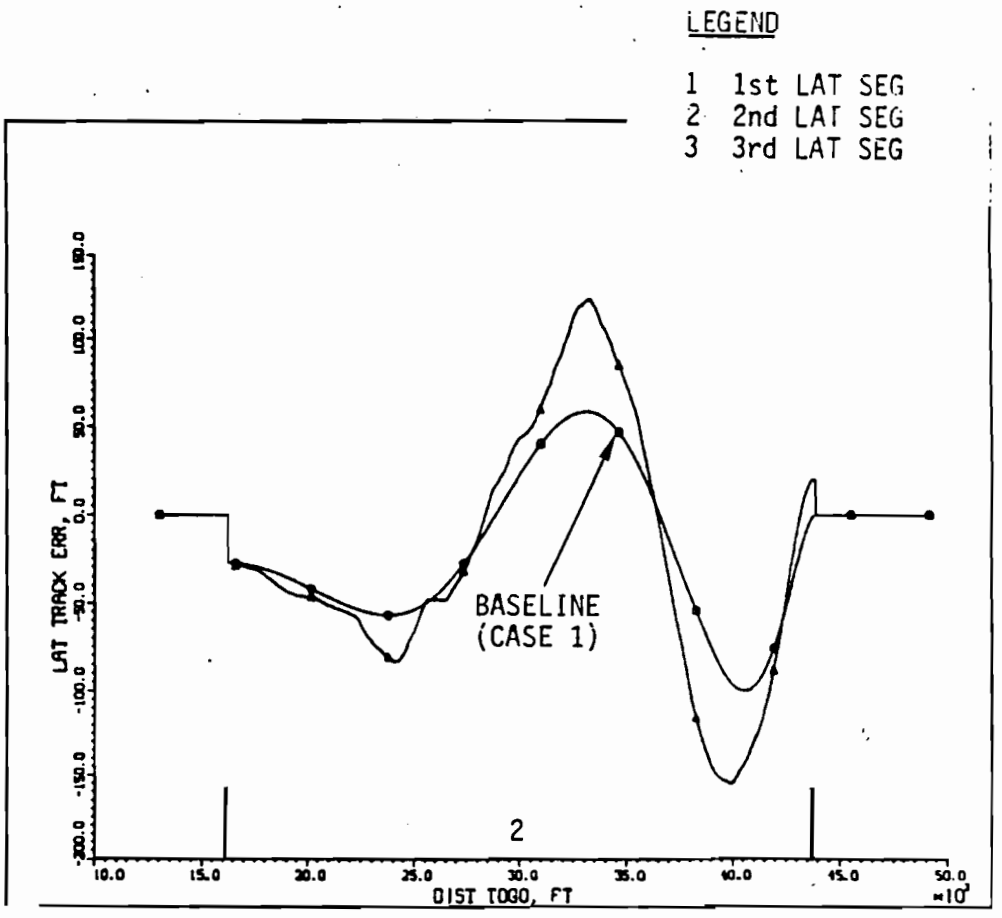

(B) SECOND LATERAL SEGMENT (CIRCULAR TRACK)

FIGURE 21 - LATERAL TRACKING ERRORS FOR REDUCED NOISE (CASE 3)

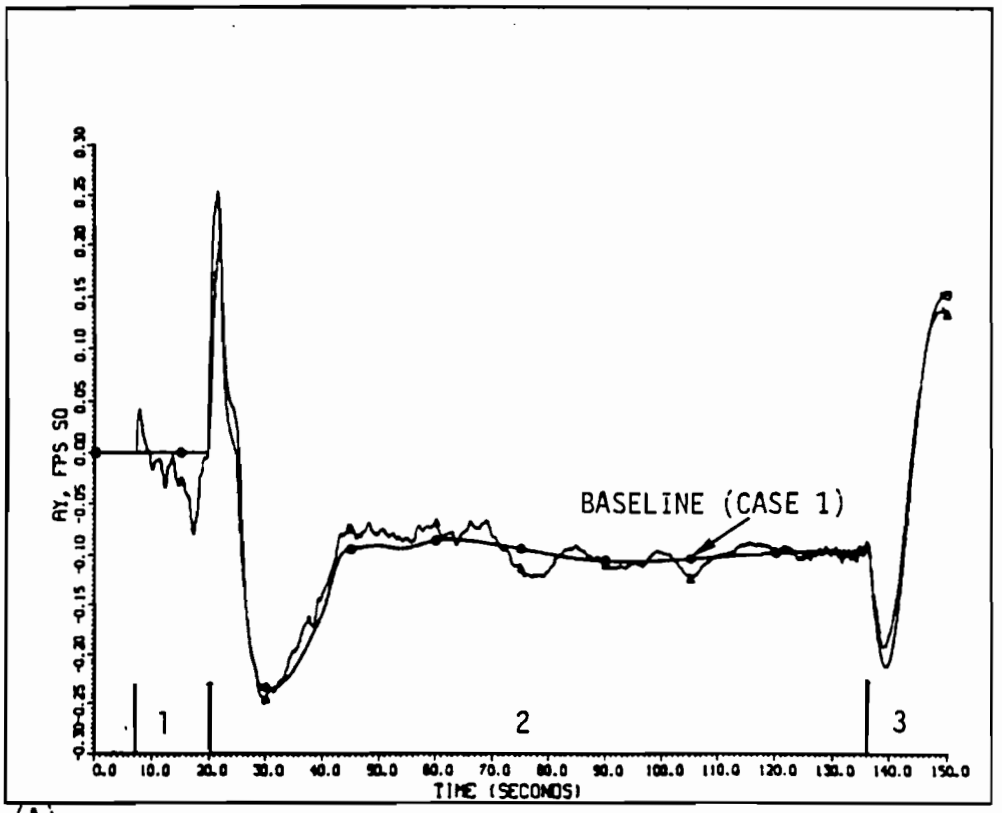

(A)

LEGEND

1 1st LAT SEG
2 2nd LAT SEG
3 3rd LAT SEG

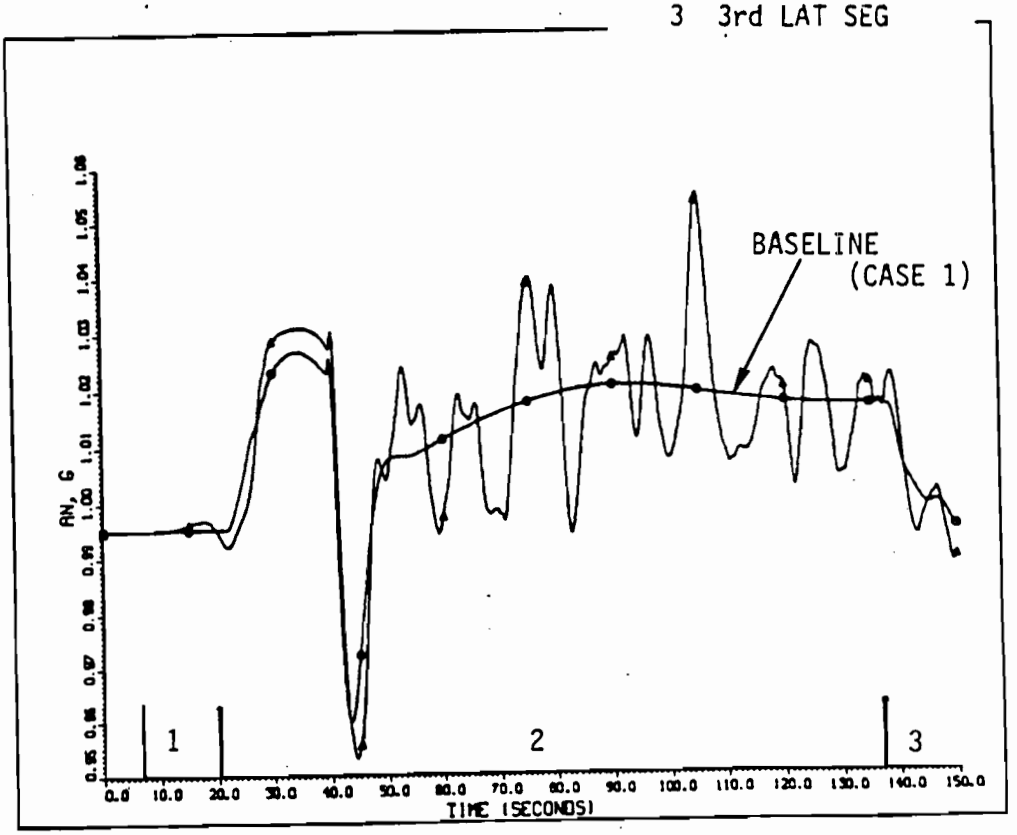

(B)

FIGURE 22 - LATERAL AND NORMAL ACCELERATIONS FOR REDUCED NOISE (CASE 3)

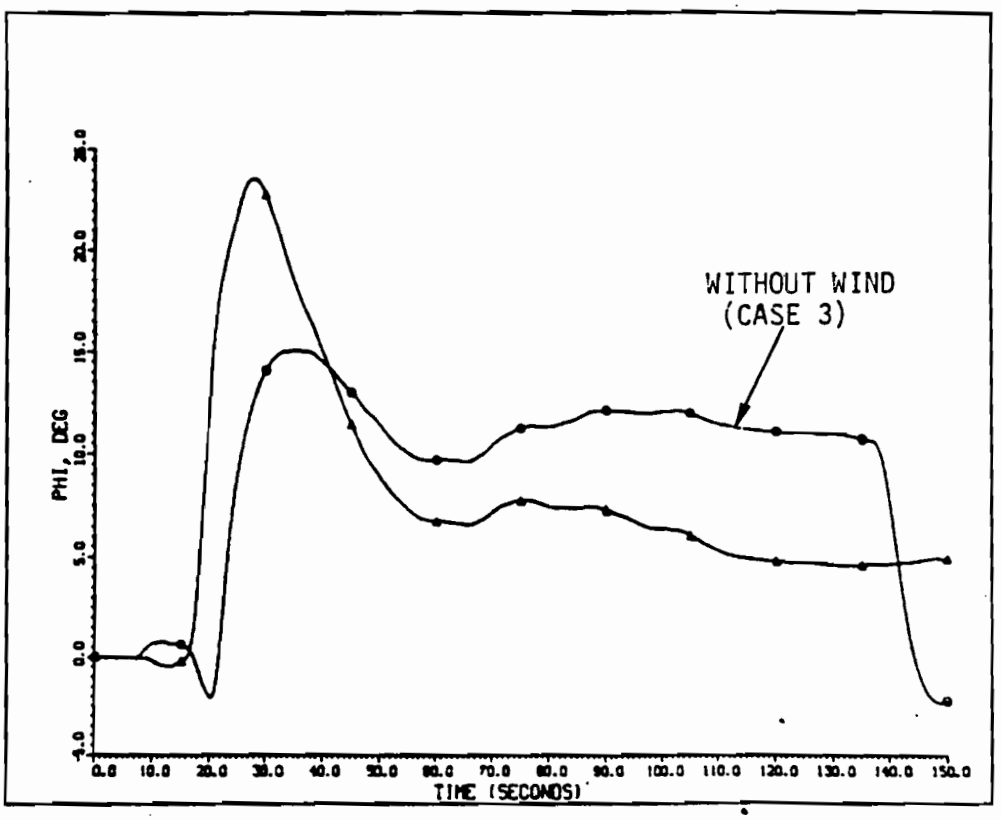

FIGURE 23 - BANK ANGLE WITH AN INITIAL TAIL WIND AND CROSS WIND (CASE 4)

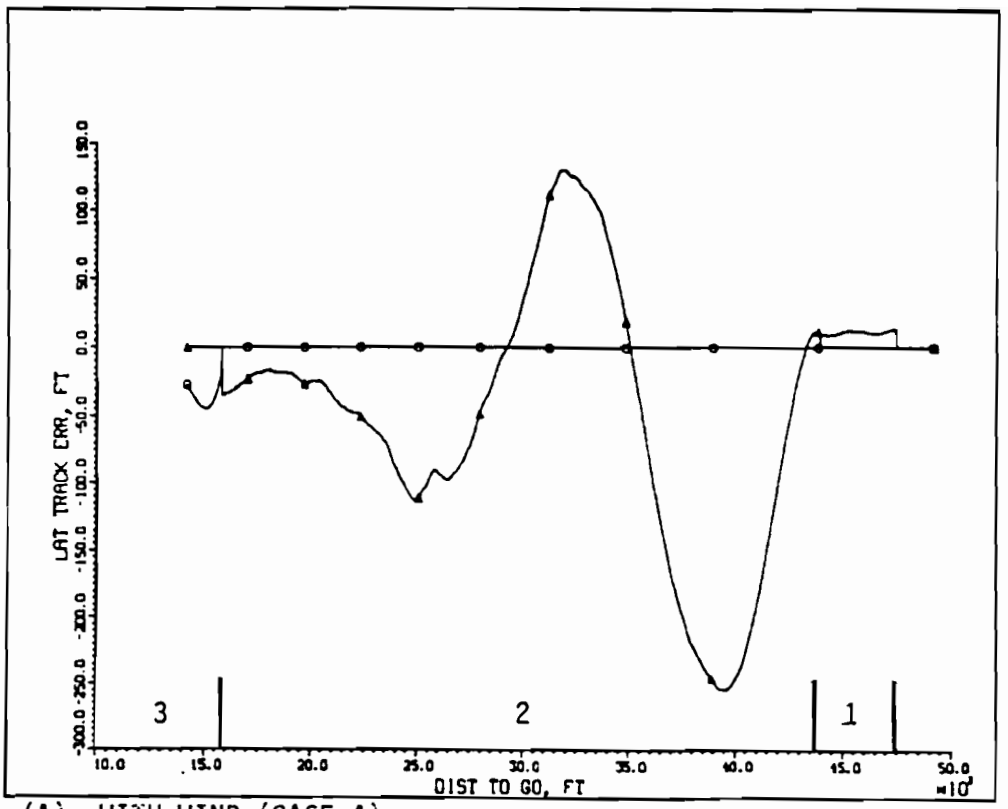

(A) WITH WIND (CASE 4)

LEGEND

1 1st LAT SEG
2 2nd LAT SEG
3 3rd LAT SEG

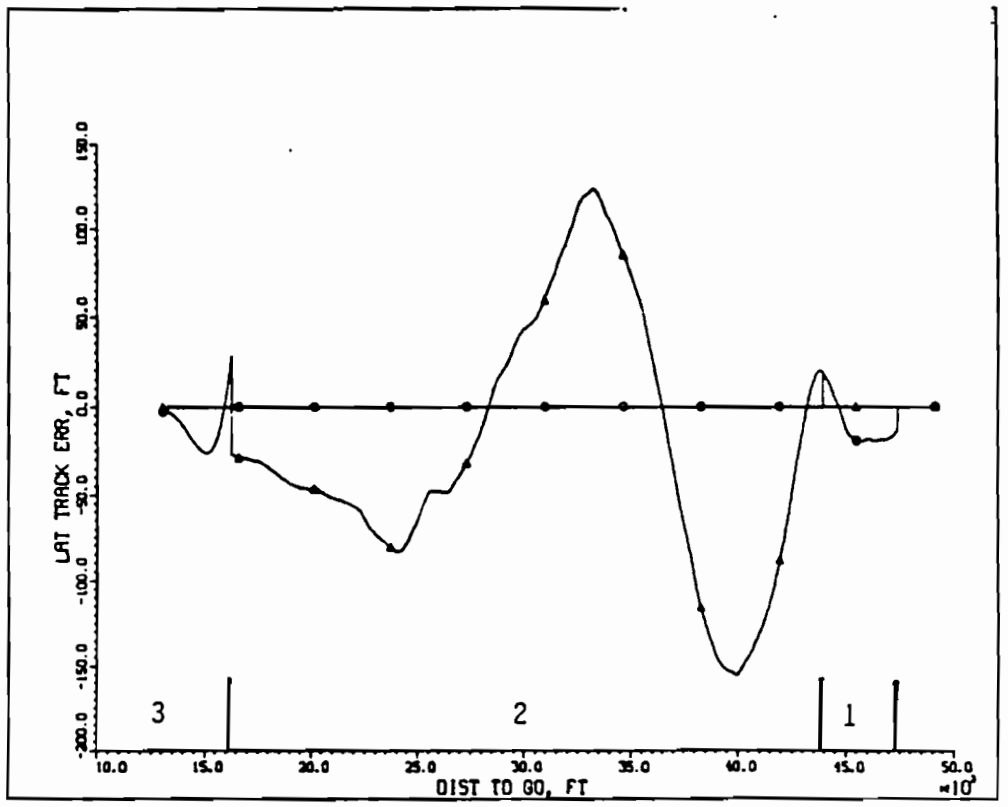

(B) WITHOUT WIND (CASE 3)

FIGURE 24 - LATERAL TRACKING ERRORS WITH AN INITIAL TAIL WIND AND CROSS WIND (CASE 4)

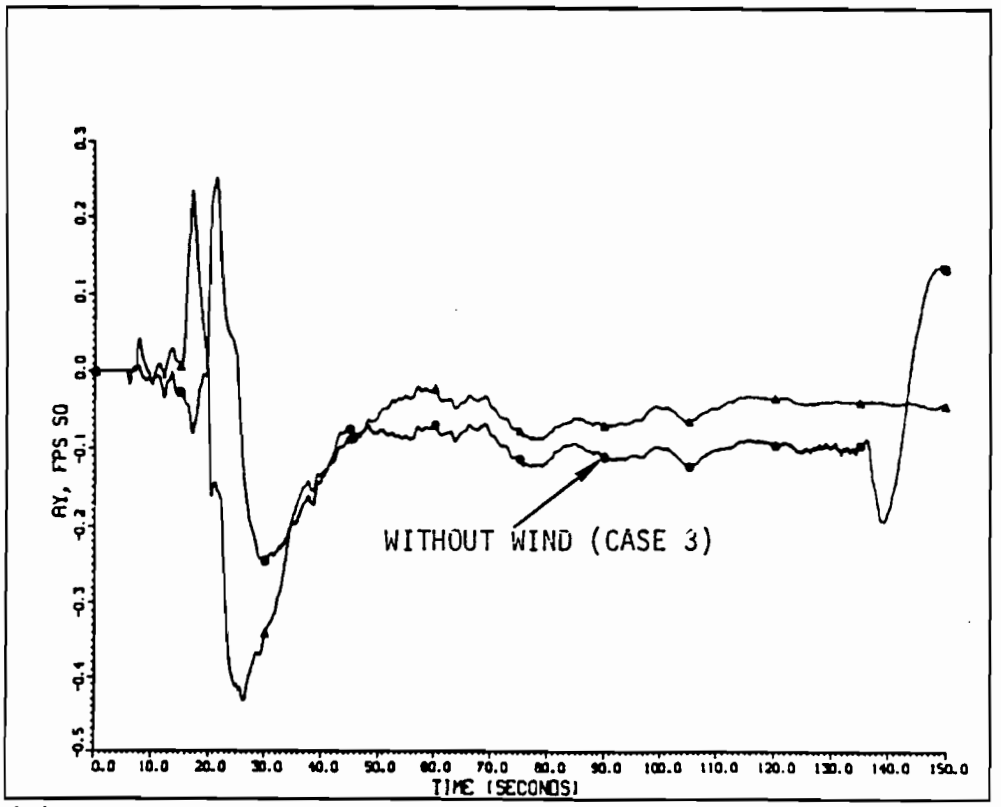

(A)

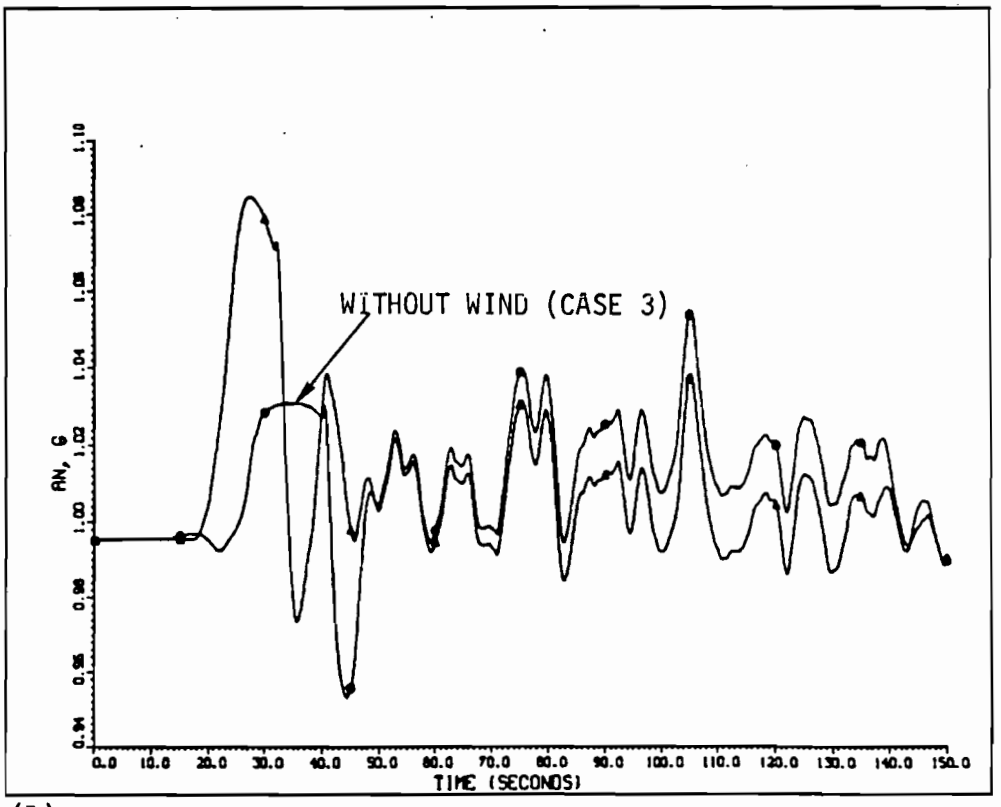

(B)

FIGURE 25 - LATERAL AND NORMAL ACCELERATIONS WITH AN INITIAL TAIL WIND AND CROSS WIND (CASE 4)

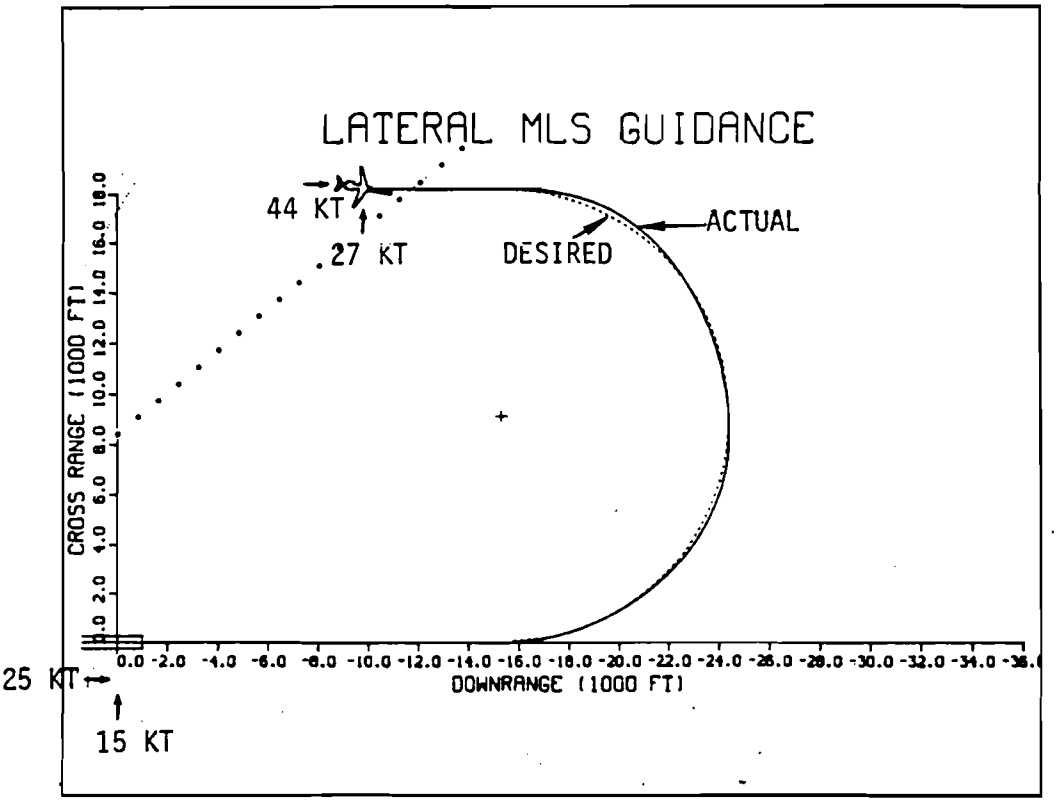

FIGURE 26 - GROUND TRACK WITH AN INITIAL TAIL WIND AND CROSS WIND (CASE 4)

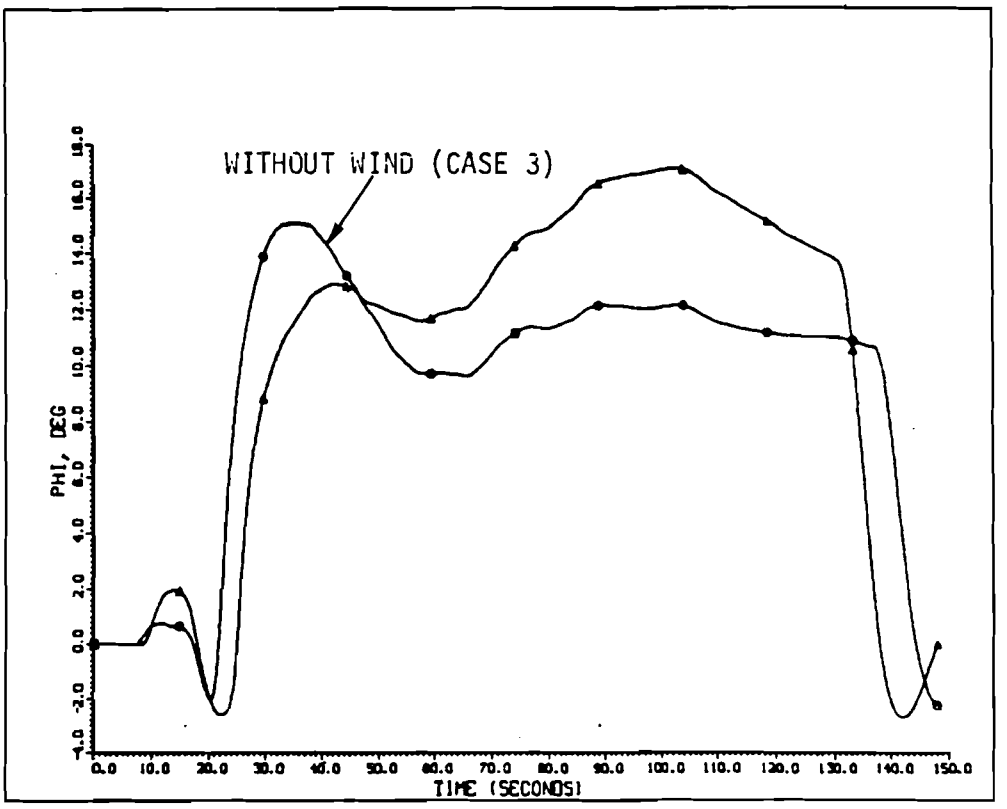

FIGURE 27 - BANK ANGLE WITH AN INITIAL HEAD WIND AND CROSS WIND (CASE 5)

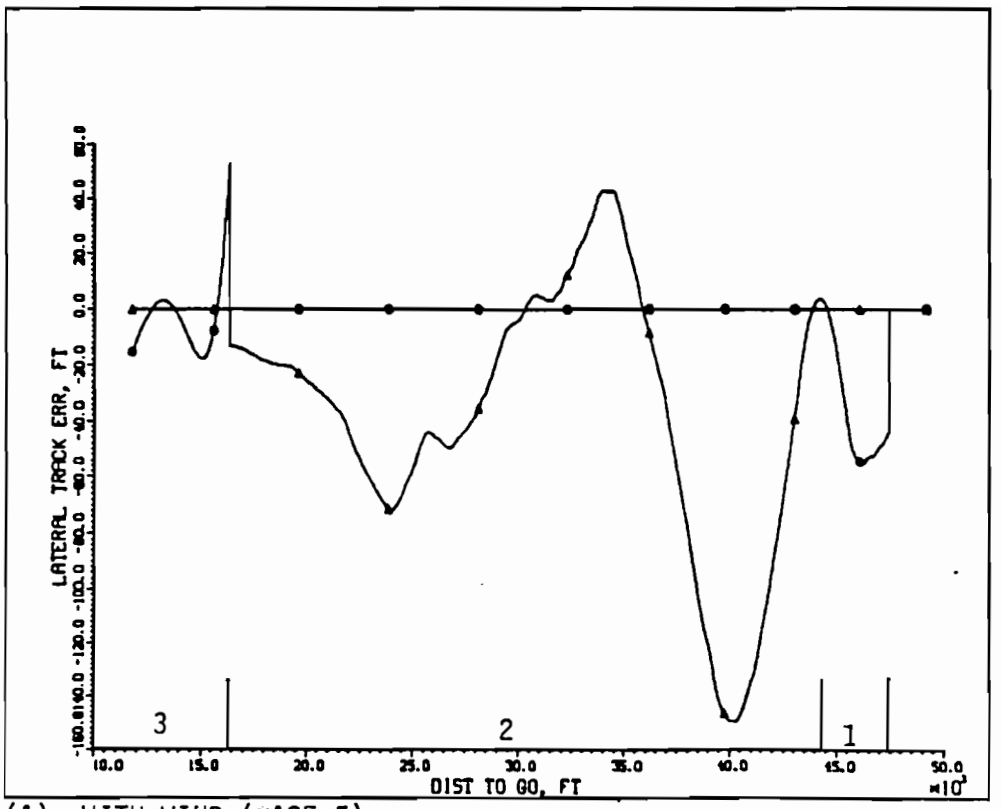

(A) WITH WIND (CASE 5)

LEGEND

1 1st LAT SEG
2 2nd LAT SEG
3 3rd LAT SEG

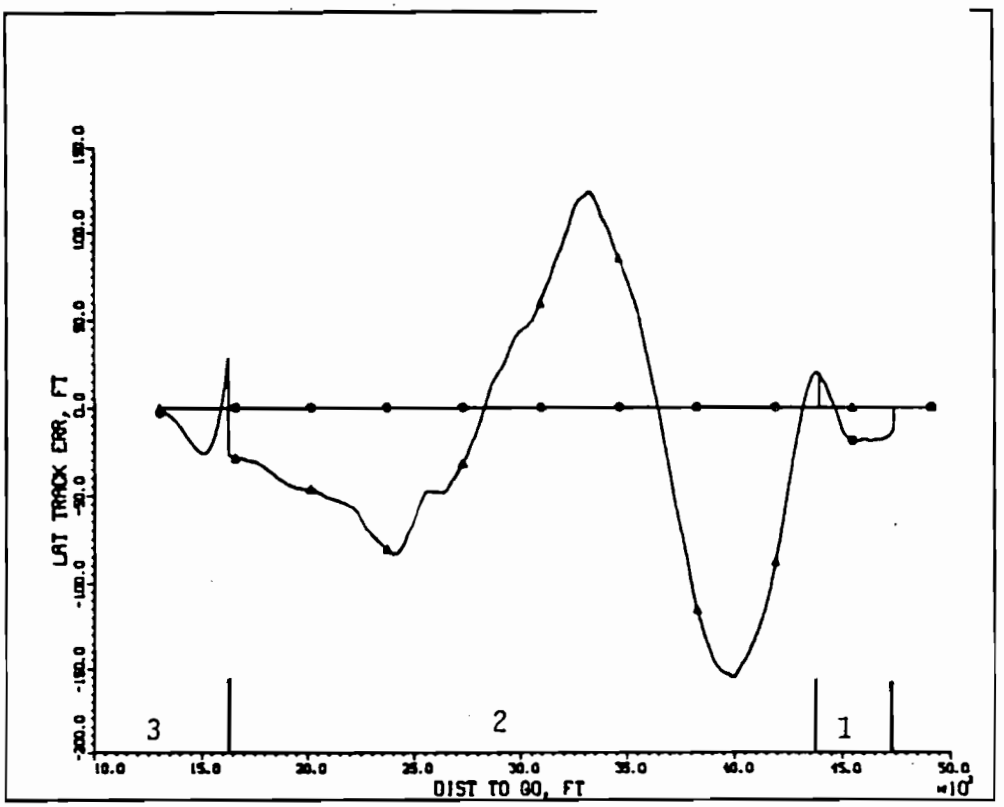

(B) WITHOUT WIND (CASE 3)

FIGURE 28 - LATERAL TRACKING ERRORS WITH AN INITIAL HEAD WIND AND CROSS WIND (CASE 5)

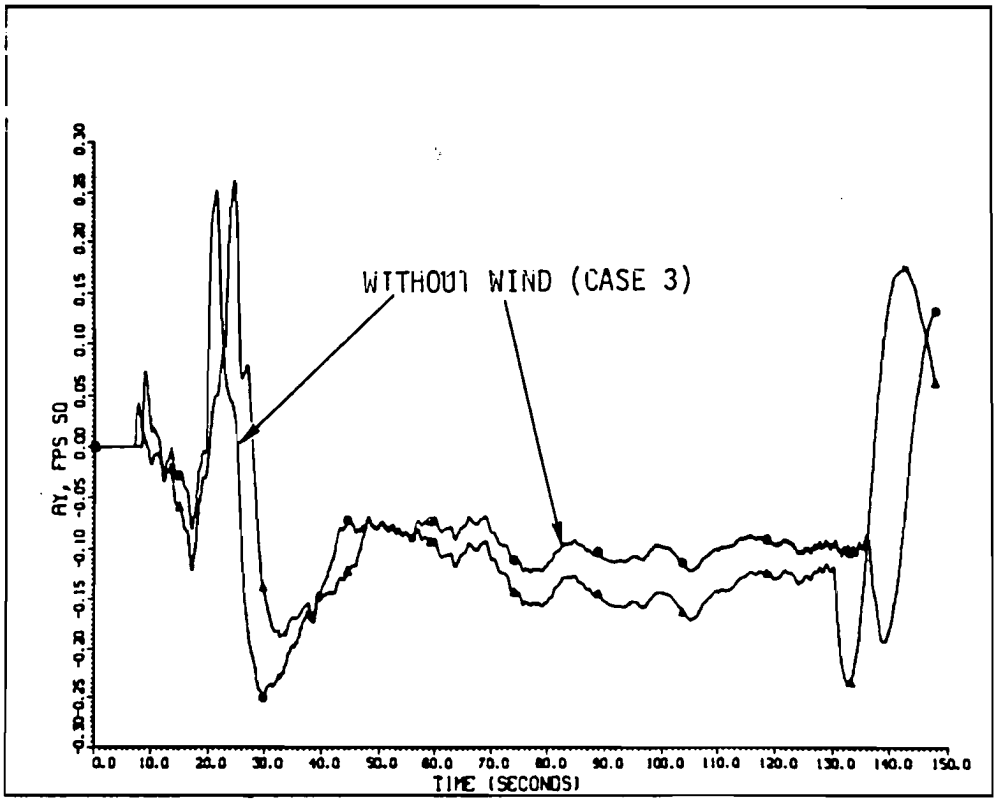

(A)

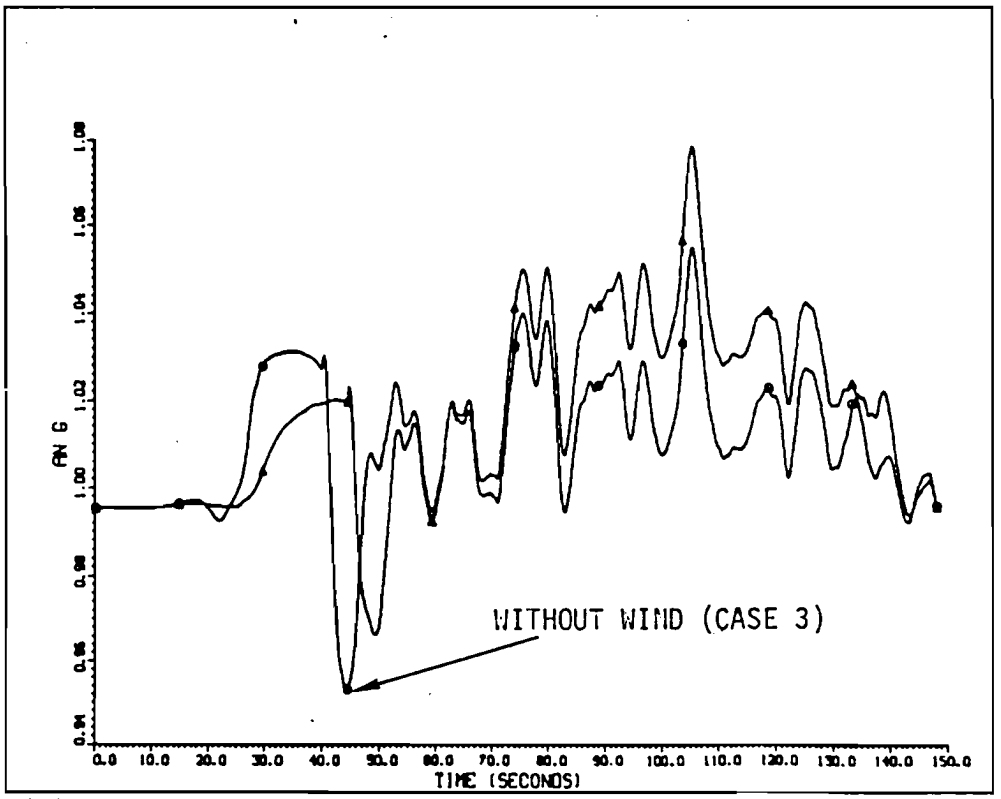

(B)

FIGURE 29 - LATERAL AND NORMAL ACCELERATIONS WITH AN INITIAL HEAD WIND AND CROSS WIND (CASE 5)

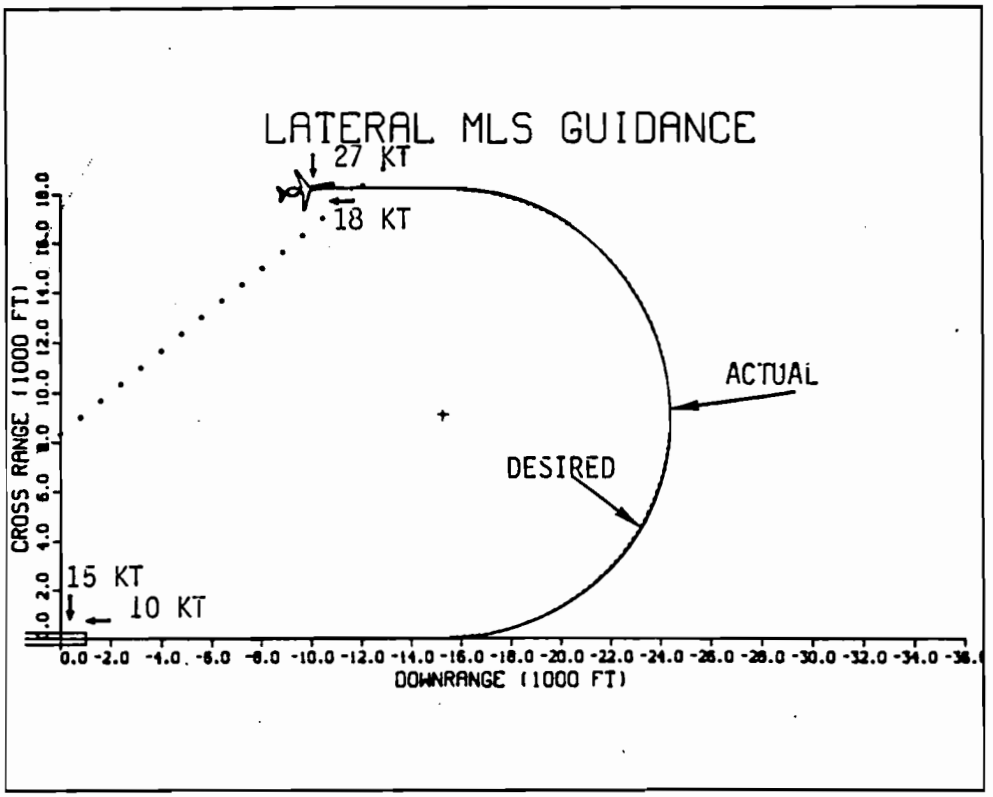

FIGURE 30 GROUND TRACK WITH AN INITIAL HEAD WIND AND CROSS WIND (CASE 5)

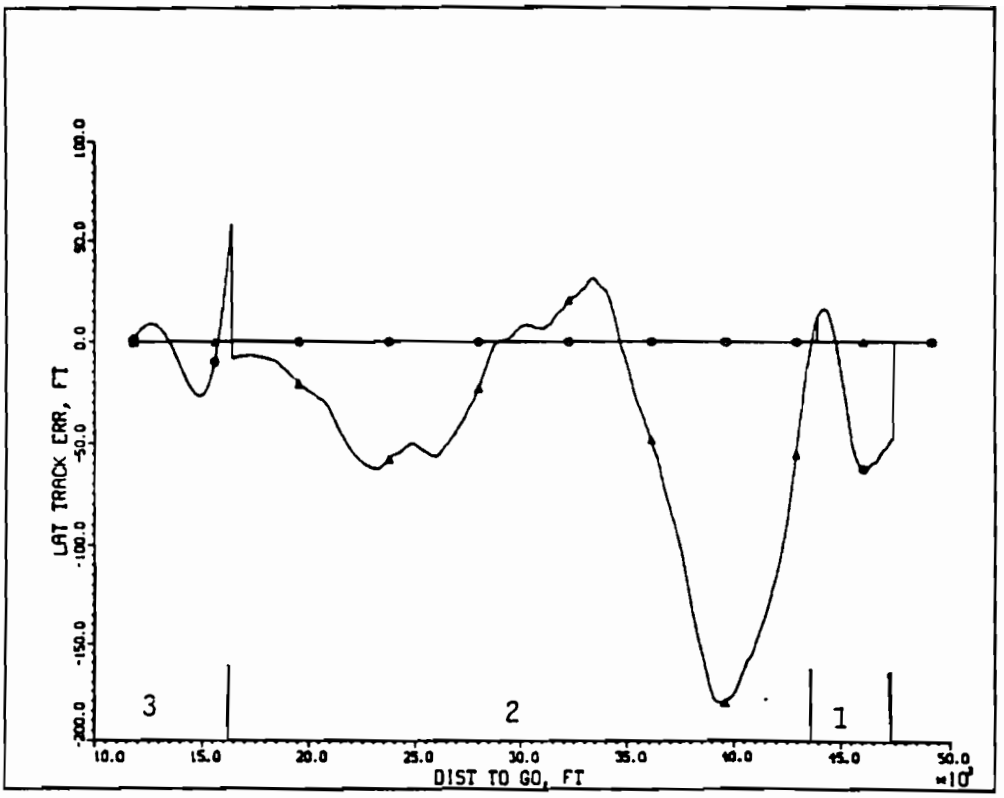

(A) WITH TURBULENCE (CASE 6)

LEGEND

1 1st LAT SEG
2 2nd LAT SEG
3 3rd LAT SEG

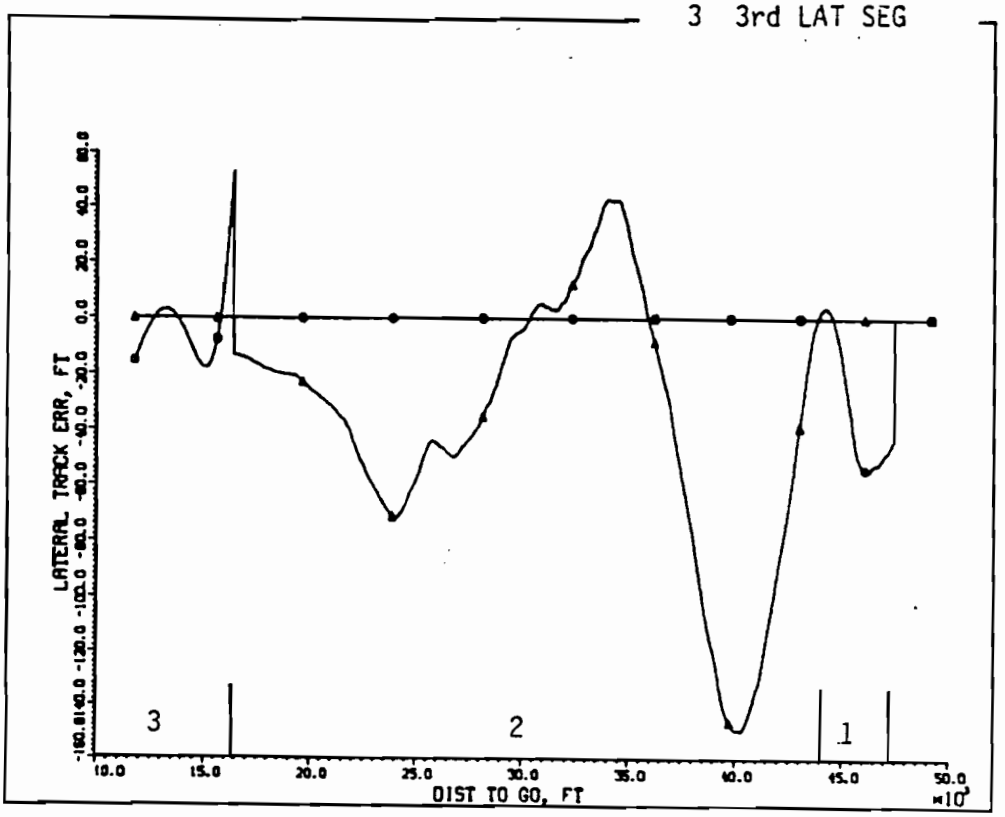

(B) WITHOUT TURBULENCE (CASE 5)

FIGURE 31 - LATERAL TRACKING ERRORS AND ACCELERATION LEVELS WITH TUBURLENCE (CASE 6)

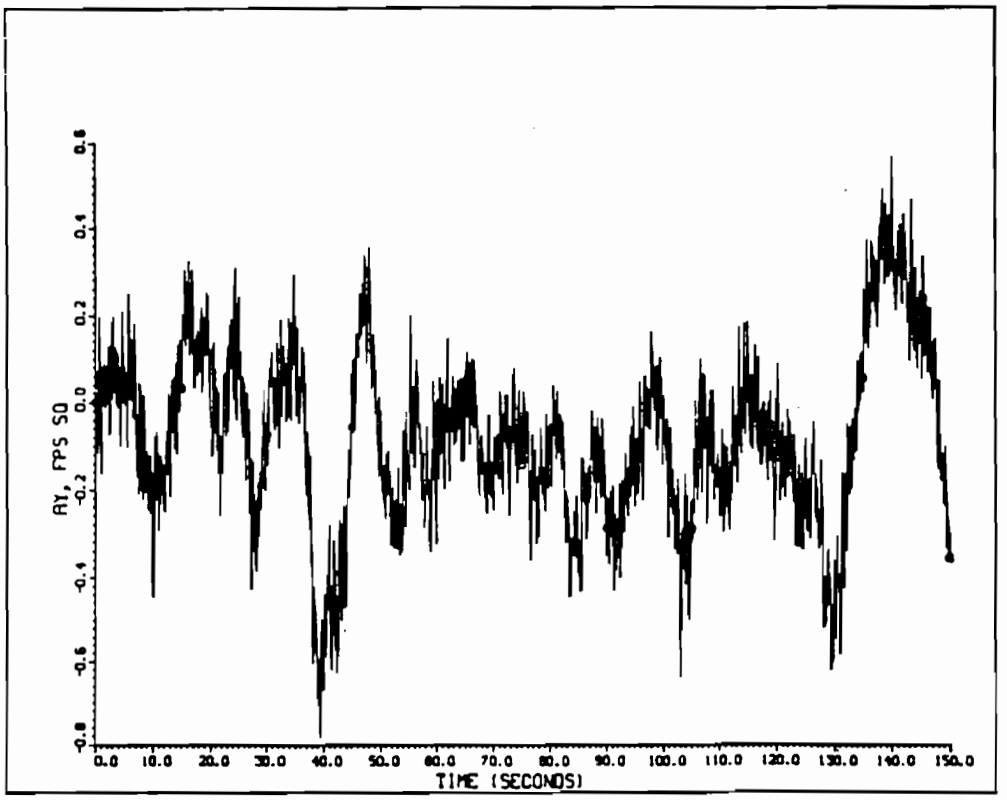

(C) LATERAL ACCELERATION

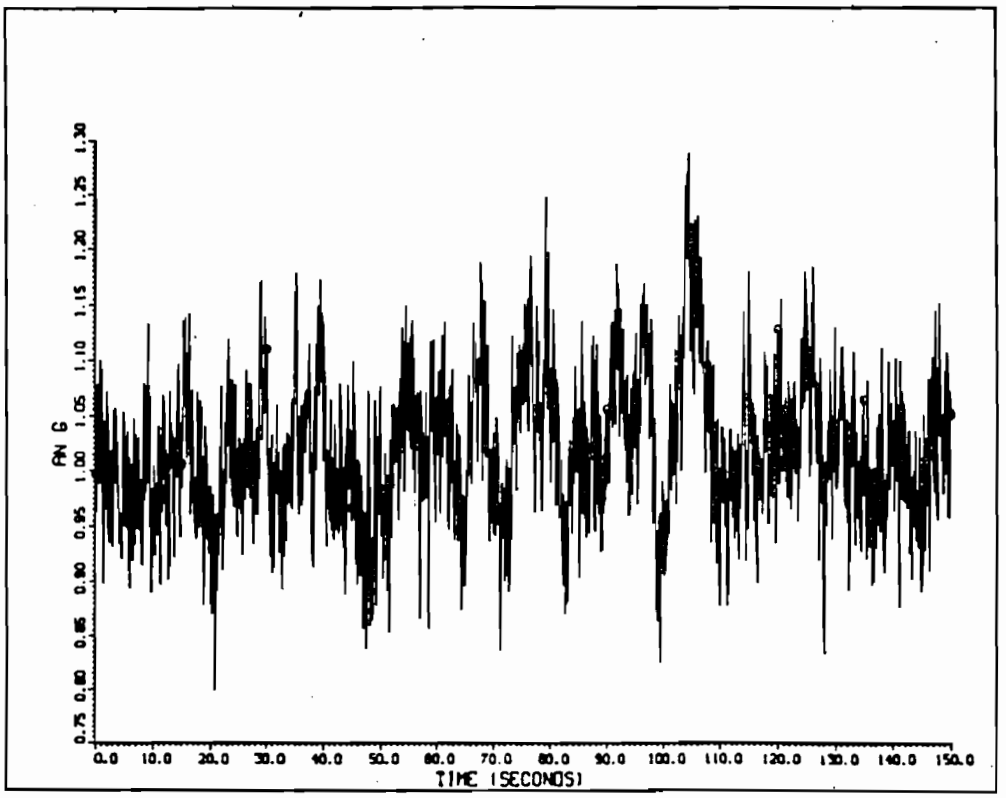

(D) NORMAL ACCELERATION

FIGURE 31 - LATERAL TRACKING ERROR AND ACCELERATION LEVELS WITH TURBULENCE (CASE 6)

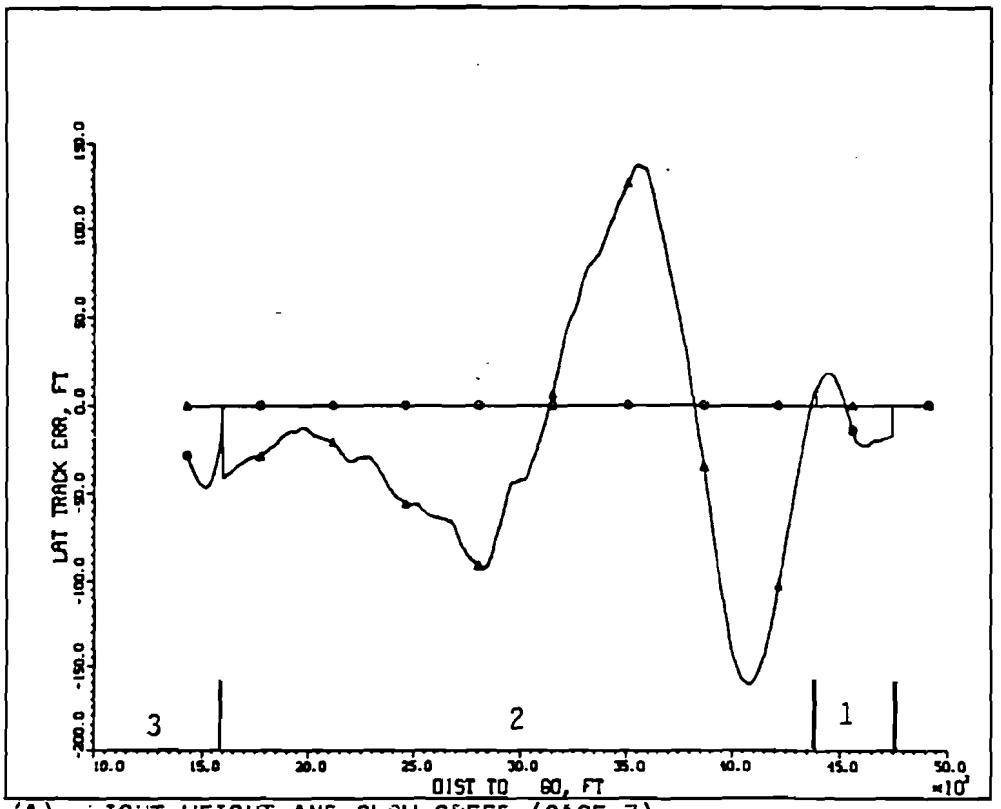

(A) LIGHT WEIGHT AND SLOW SPEED (CASE 7)

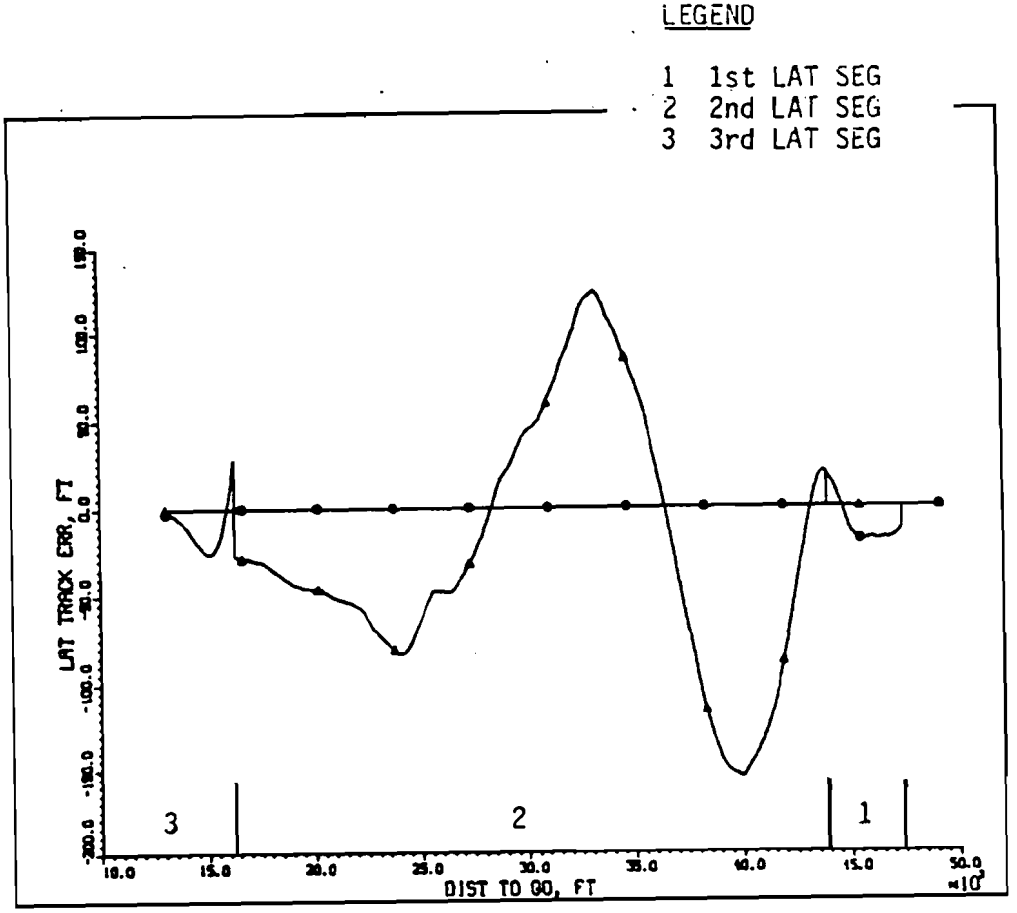

(B) FULL WEIGHT AND NOMINAL SPEED (CASE 3)

FIGURE 32 - LATERAL TRACKING ERRORS FOR LIGHT WEIGHT AND LOW SPEED (CASE 7)

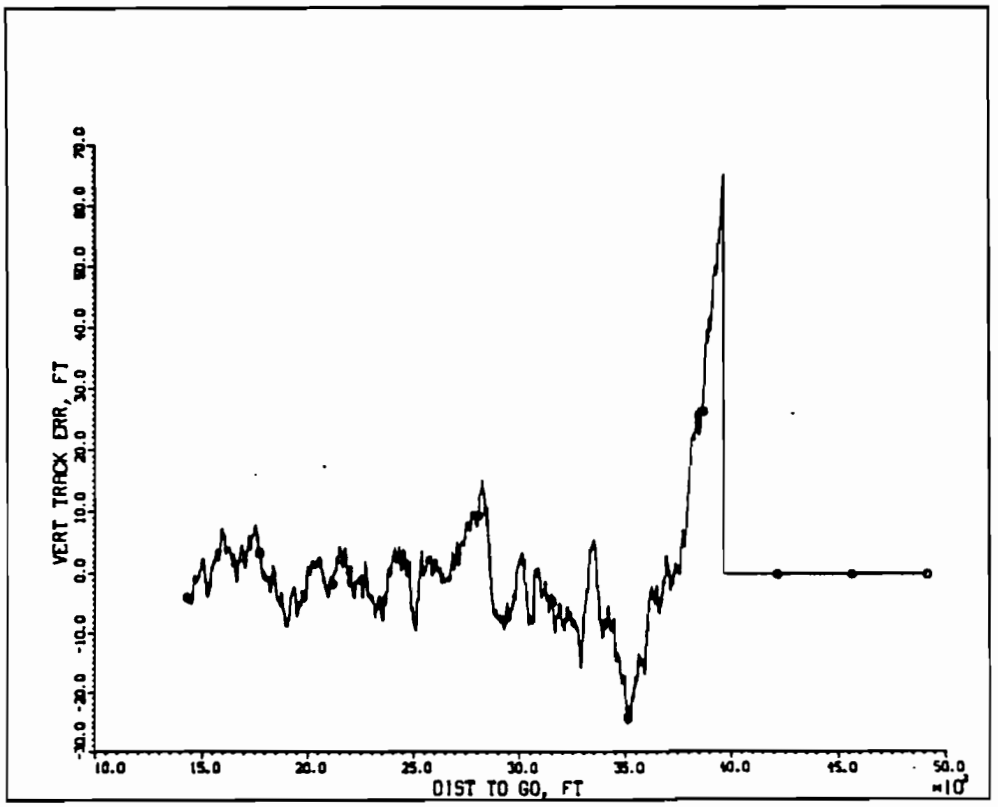

(A) LIGHT WEIGHT AND LOW SPEED (CASE 7)

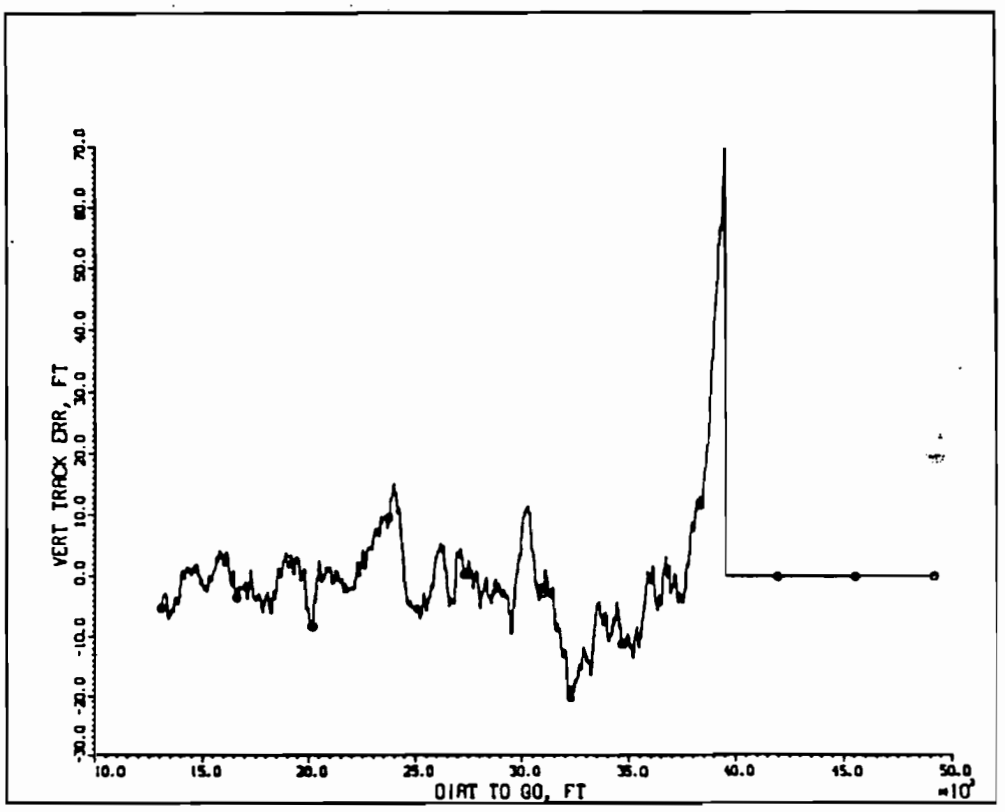

(B) FULL WEIGHT AND NOMINAL SPEED (CASE 3)

FIGURE 33 - VERTICAL TRACKING ERRORS FOR LIGHT WEIGHT AND LOW SPEED (CASE 7)

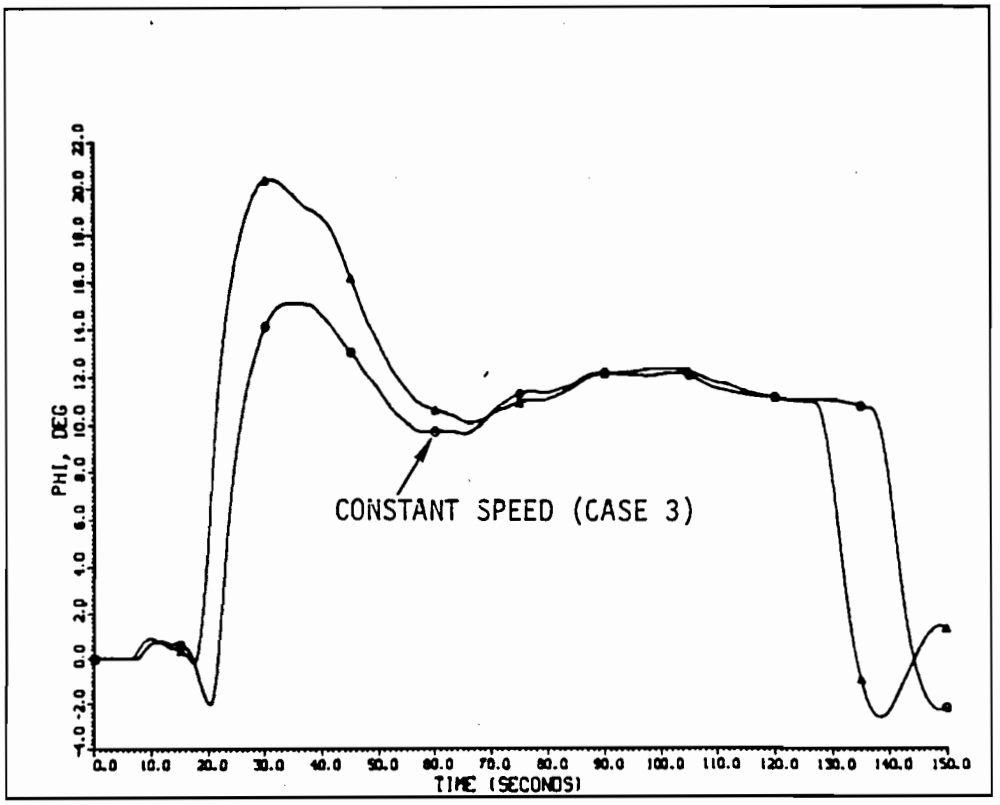

FIGURE 34 - BANK ANGLE FOR SPEED CHANGE (CASE 8)

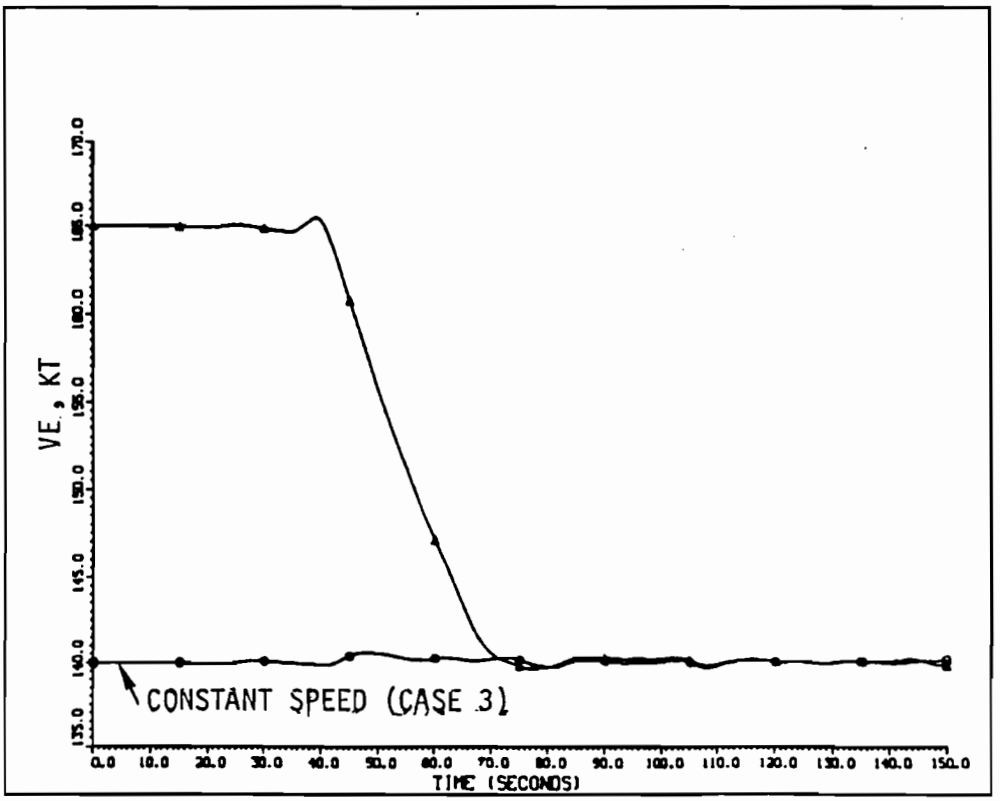

FIGURE 35 - VELOCITY FOR SPEED CHANGE (CASE 8)

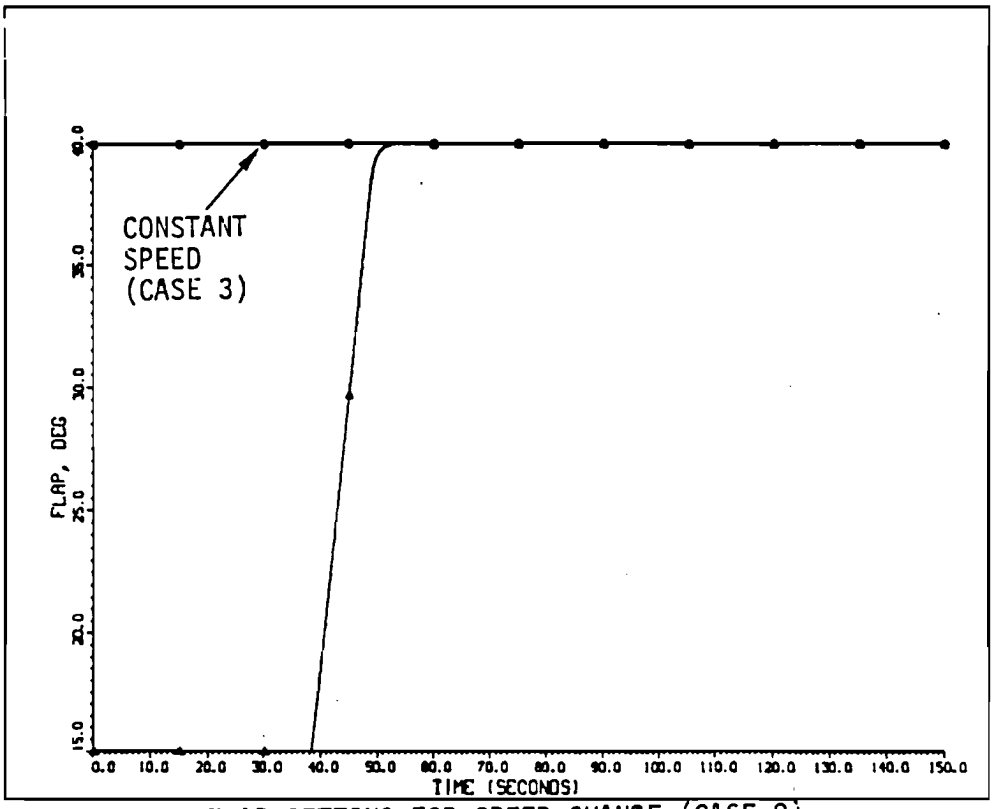

FIGURE 36 - FLAP SETTING FOR SPEED CHANGE (CASE 8)

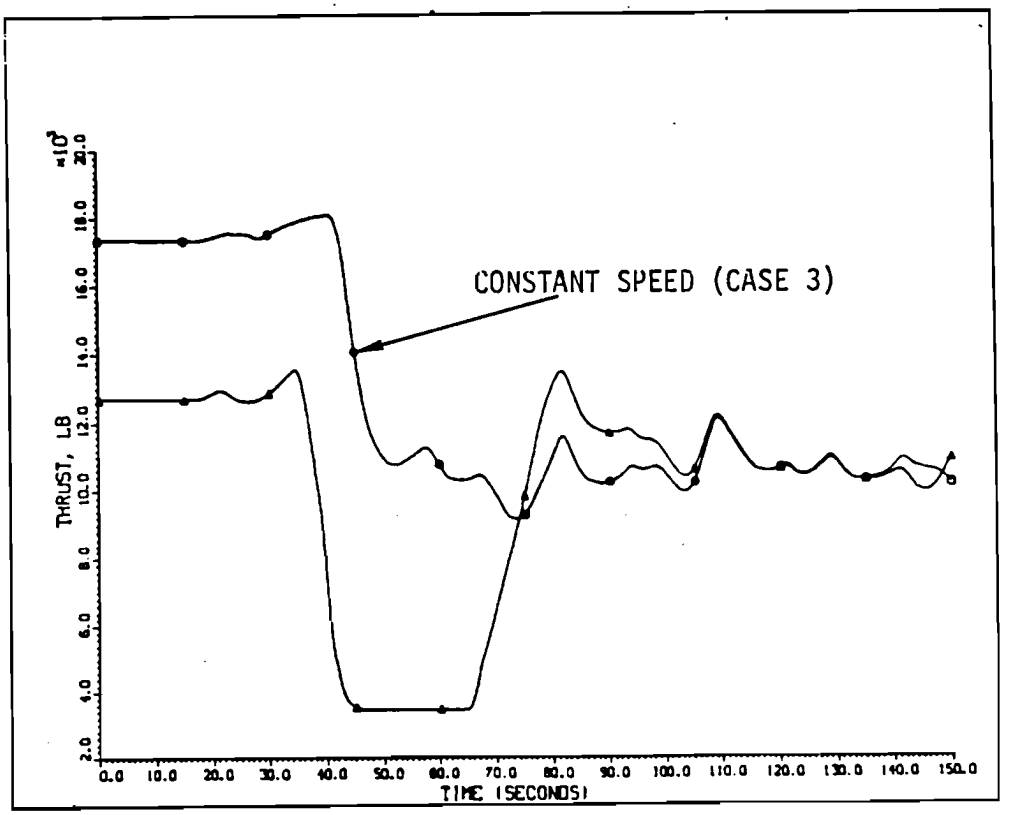

FIGURE 37 - THRUST LEVEL FOR SPEED CHANGE (CASE 8)

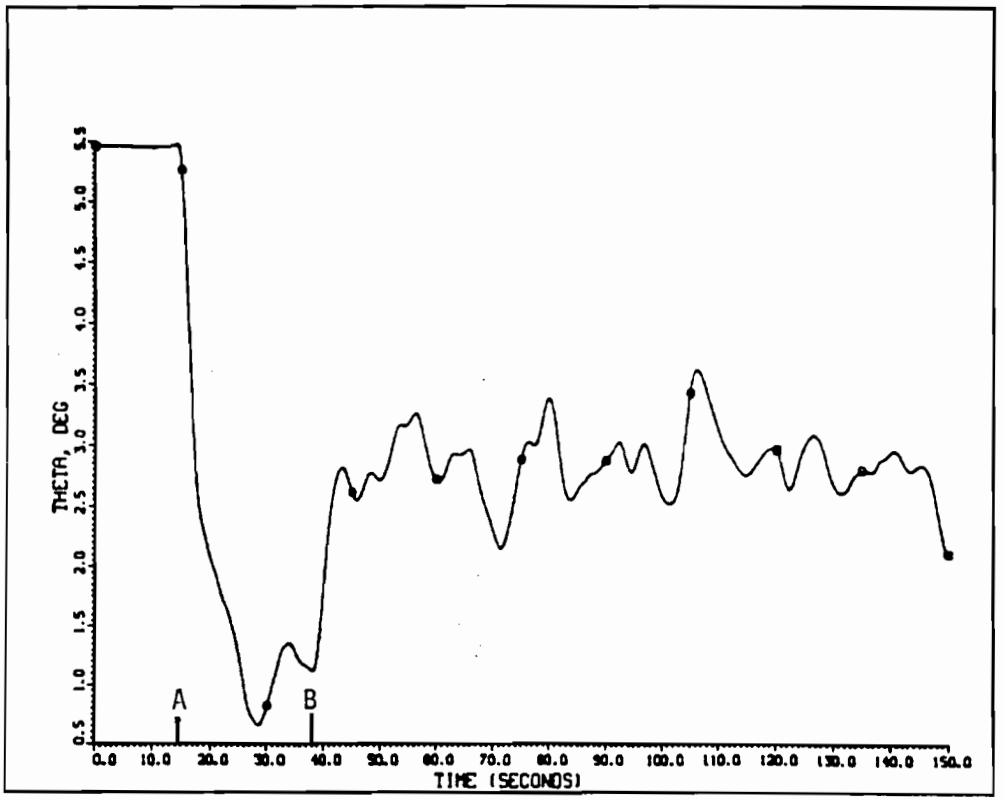

FIGURE 38 - PITCH ANGLE FOR SEGMENTED GLIDE SLOPE (CASE 9)

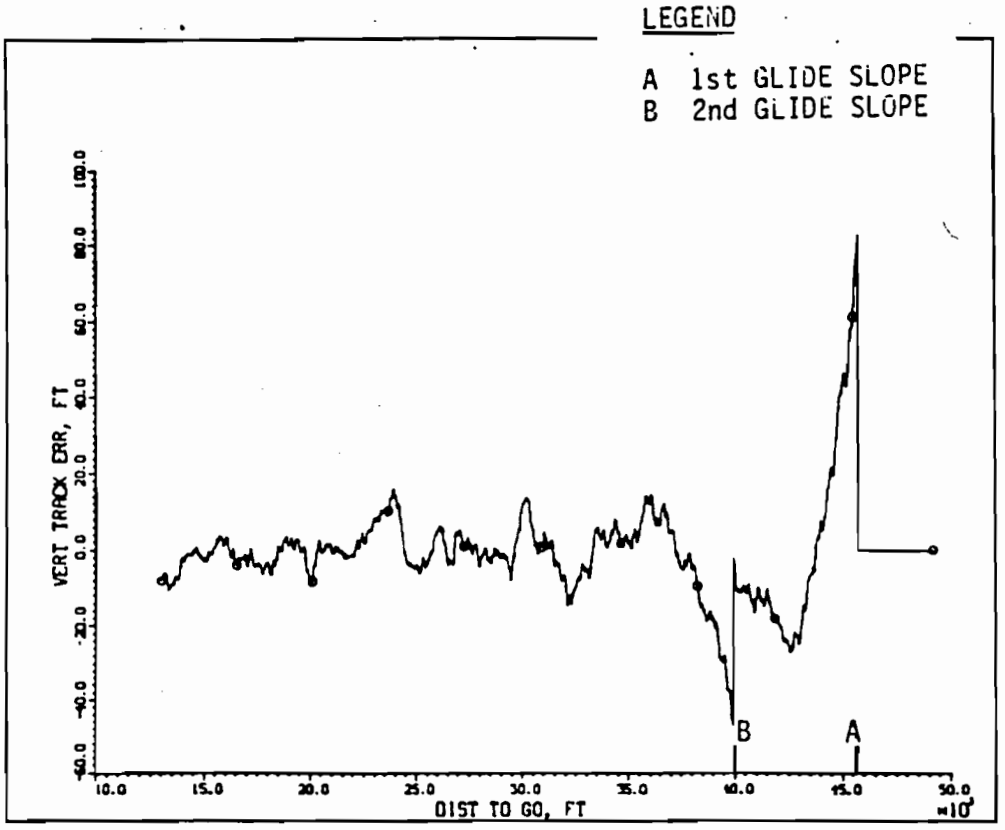

FIGURE 39 - VERTICAL TRACKING ERROR FOR SEGMENTED GLIDE SLOPE (CASE 9)

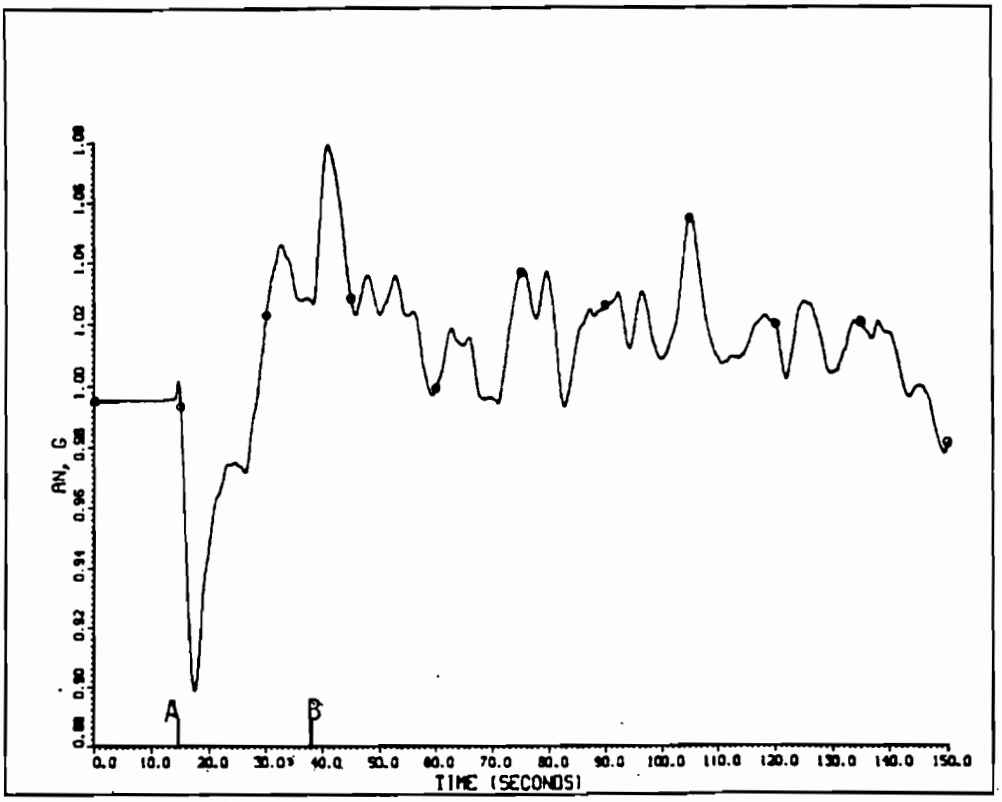

FIGURE 40 - NORMAL ACCELERATION FOR SEGMENTED GLIDE SLOPE (CASE 9)

LEGEND

A 1st GLIDE SLOPE
B 2nd GLIDE SLOPE

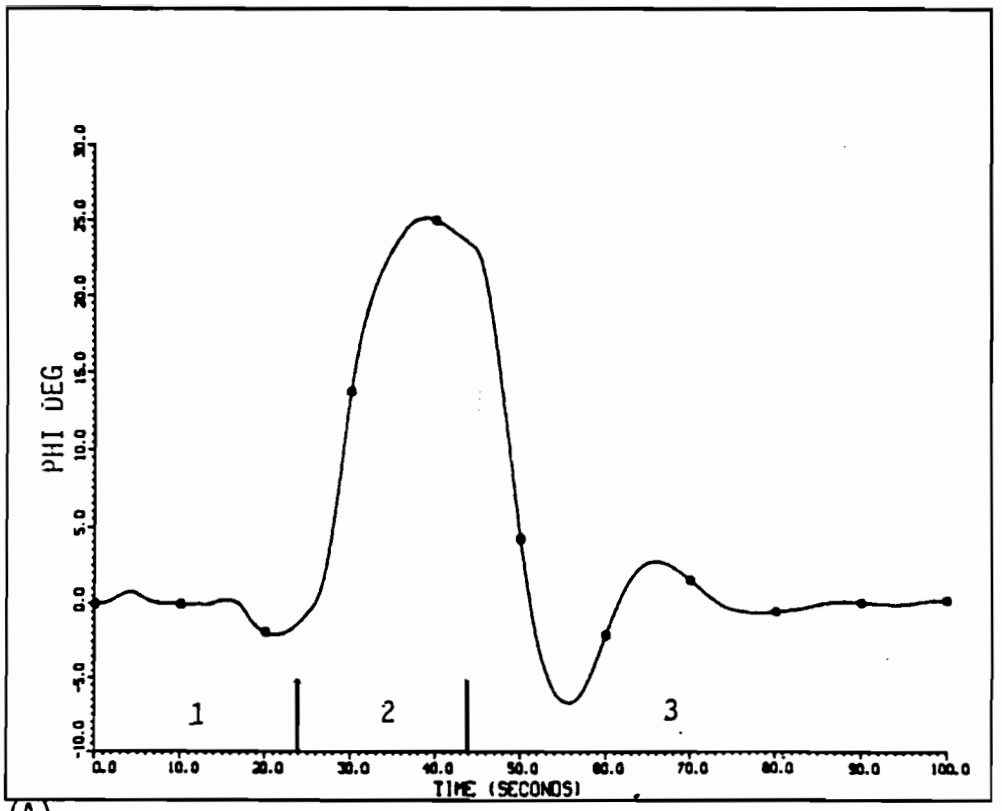

(A)

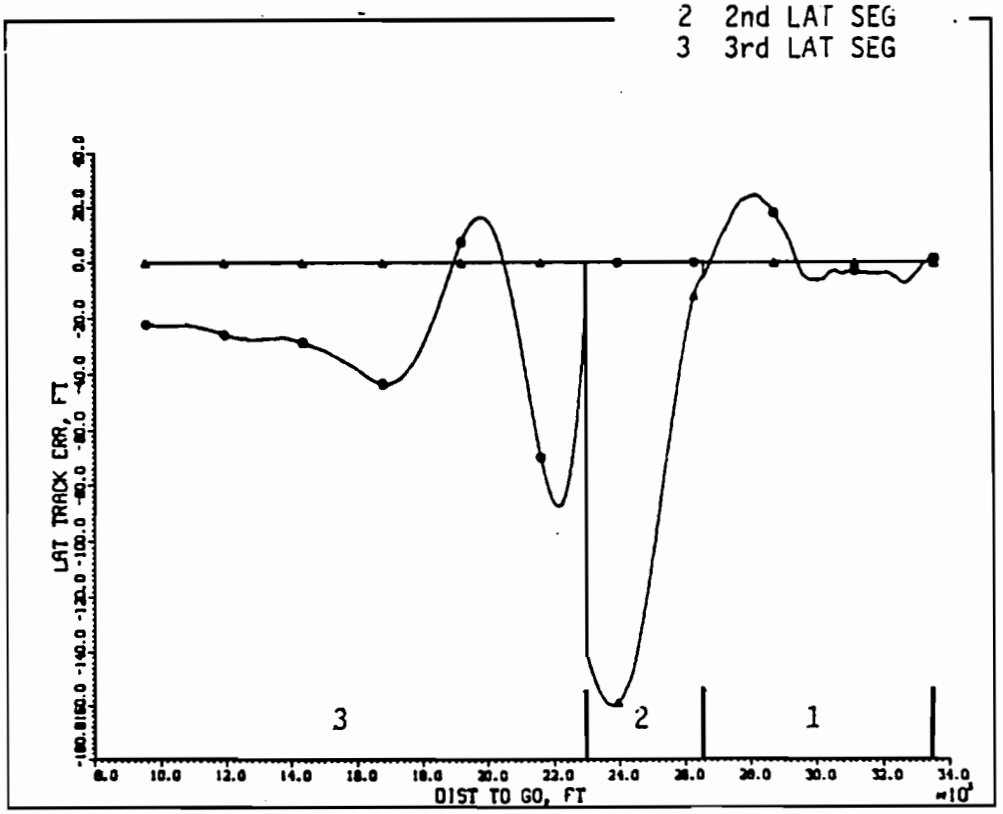

FIGURE 41 - BANK ANGLE AND LATERAL TRACKING ERROR FOR LATERALLY SEGMENTED FINAL (CASE 10)

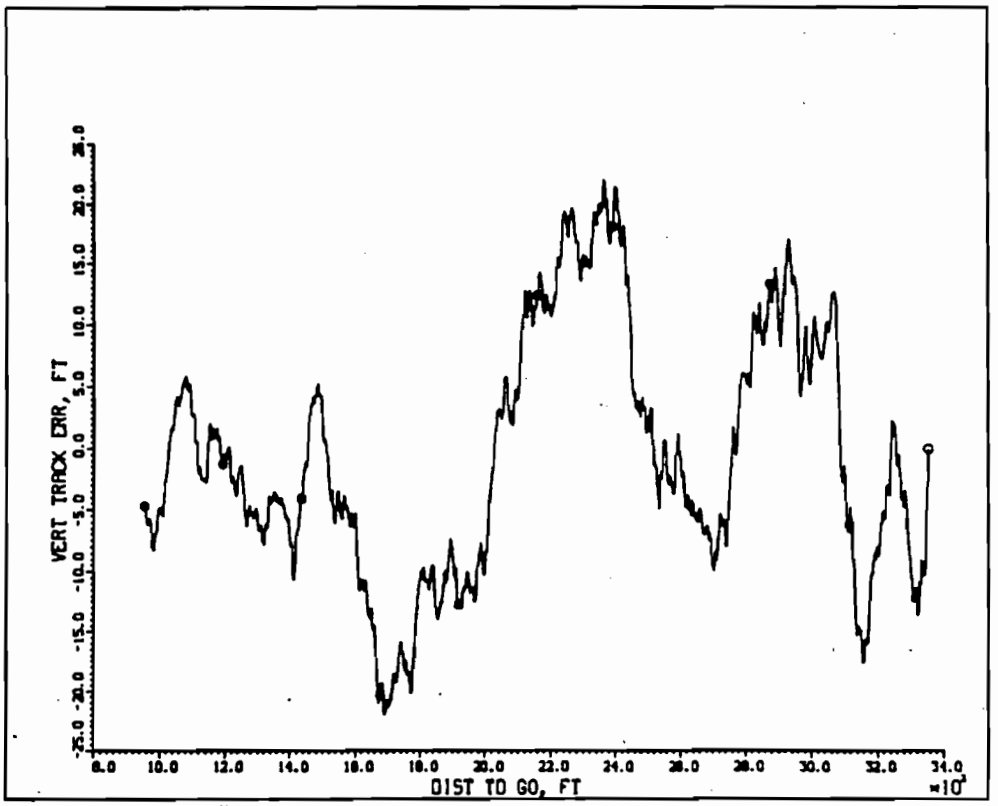

FIGURE 42 - VERTICAL TRACKING FOR LATERALLY SEGMENTED FINAL (CASE 10)

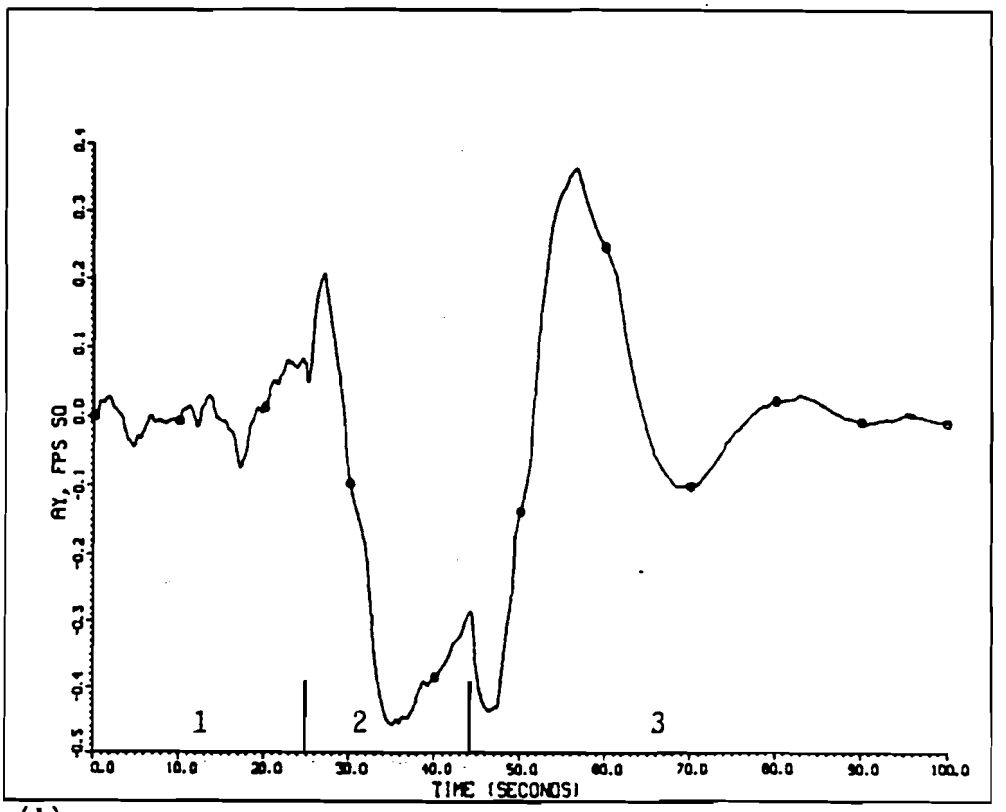

(A)

LEGEND

1 1st LAT SEG
2 2nd LAT SEG
3 3rd LAT SEG

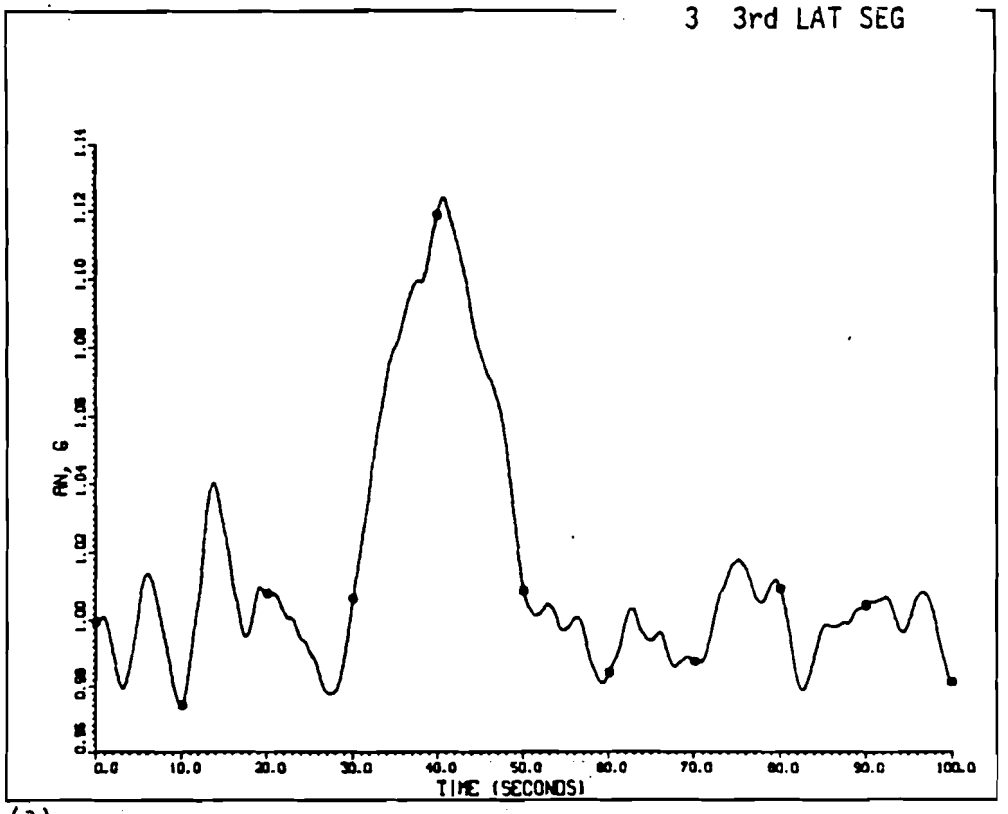

(B)

FIGURE 43 - LATERAL AND NORMAL ACCELERATIONS FOR LATERALLY SEGMENTED FINAL (CASE 10)

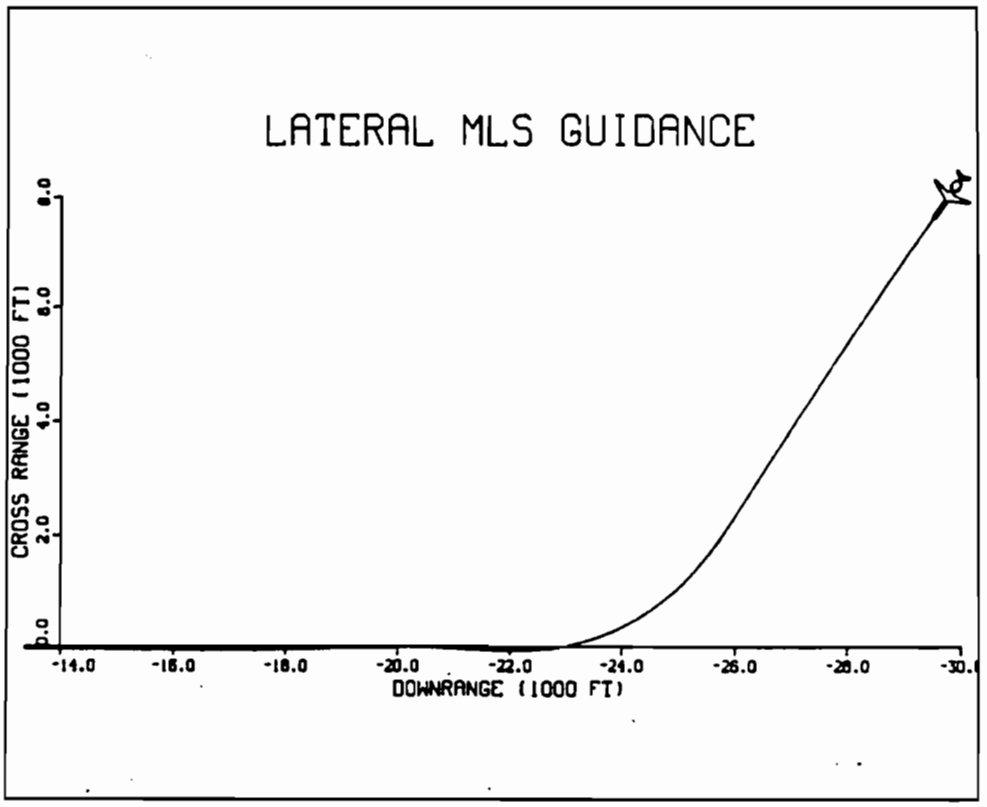

FIGURE 44 - GROUND TRACK FOR LATERALLY SEGMENTED FINAL (CASE 10)

Standard Bibliographic Page

1. Report No.	2. Government Accession No.	3. Recipient's Catalog No.
NASA CR-178030		

4. Title and Subtitle	5. Report Date
GUIDANCE STUDIES FOR CURVED, DESCENDING APPROACHES USING THE MICROWAVE LANDING SYSTEM (MLS)	MAY 1986
	6. Performing Organization Code
7. Author(s)	8. Performing Organization Report No.
J. B. FEATHER	
9. Performing Organization Name and Address	10. Work Unit No.
DOUGLAS AIRCRAFT COMPANY 3855 LAKEWOOD BLVD. LONG BEACH, CA. 90846	11. Contract or Grant No. NAS1-16202
12. Sponsoring Agency Name and Address	13. Type of Report and Period Covered CONTRACTOR REPORT
NATIONAL AERONAUTICS AND SPACE ADMINSTRATION, WASHINGTON DC 20546	14. Sponsoring Agency Code 505-45-33-56

15. Supplementary Notes

LANGLEY TECHNICAL MONITOR: C. R. SPIZER

FAA TECHNICAL MONITOR: W. F. WHITE

16. Abstract

This report documents results for MLS guidance algorithm development conducted by DAC for NASA under the Advance Transport Operating Systems (ATOPS) Technology Studies program (NAS1-16202). The study consisted of evaluating guidance laws for vertical and lateral path control, as well as speed control, for approaches not possible with present ILS equipment. Several specific approaches were simulated using the MD-80 aircraft simulation program, including curved, descending (segmented glide slope), and decelerating paths. Emphasis was placed on development of guidance algorithms specifically for approaches at Burbank, where proposed flight demonstrations are planned. Results of this simulation phase are suitable for use in future fixed-base simulator evaluations employing actual hardware (autopilot and a performance management system).

17. Key Words (Suggested by Authors(s))	18. Distribution Statement
MICROWAVE LANDING SYSTEM TERMINAL AREA GUIDANCE CURVED APPROACHES SEGMENTED GLIDESLOPE	UNCLASSIFIED - UNLIMITED Subject Category 04

19. Security Classif.(of this report)	20. Security Classif.(of this page)	21. No. of Pages	22. Price
UNCLASSIFIED	UNCLASSIFIED	87	A05

For sale by the National Technical Information Service, Springfield, Virginia 22161